RHEOLOGICAL, CHEMICAL AND MICROSTRUCTURAL CHARACTERIZATION OF ASPHALT BINDERS AGED AT DIFFERENT CONDITIONS AND EVALUATION OF THE USE OF ANTIOXIDANTS AND COPOLYMERS TO RETARD AGING

A Thesis

Presented in Partial Fulfillment of the Requirements for the

Degree of Master of Science

with a

Major in Civil Engineering

in the

College of Graduate Studies

University of Idaho

by

Mohammad Solaiman Khan

Major Professor: Emad Kassem, Ph.D.

Committee Members: Fouad M.S. Bayomy, Ph.D., P.E.; Armando McDonald, Ph.D.

Department Chair: Patricia J. S. Colberg, Ph.D., P.E.

May 2018

AUTHORIZATION TO SUBMIT THESIS

This thesis of Mohammad Solaiman Khan, submitted for the degree of Master of Science with a Major in Civil Engineering and titled "RHEOLOGICAL, CHEMICAL AND MICROSTRUCTURAL CHARACTERIZATION OF ASPHALT BINDERS AGED AT DIFFERENT CONDITIONS AND EVALUATION OF THE USE OF ANTIOXIDANTS AND COPOLYMERS TO RETARD AGING," has been reviewed in final form. Permission, as indicated by the signatures and dates below, is now granted to submit final copies to the College of Graduate Studies for approval.

Major Professor: Date:

Emad Kassem, Ph.D.

Committee Members: Date:

Fouad M.S. Bayomy, Ph.D. P.E.

Date:

Armando McDonald, Ph.D.

Department Chair: Date:

Patricia J. S. Colberg, Ph.D., P.E.

ABSTRACT

The rheological, chemical and microstructural properties of asphalt binders change with oxidative aging which is accelerated at elevated temperatures. Aging stiffens asphalt binders and increases the embrittlement of asphalt mixtures which would lead to fatigue cracking and eventually pavement failure under repetitive traffic loading. This study explored the feasibility of using antioxidant additives and copolymers with antioxidant agents to retard oxidative aging of asphalt binders. The performance of the additives was evaluated at the binder and mastic levels. The laboratory experiments included two unmodified binders, various antioxidant additives and copolymers, and three aggregate types. The fatigue characteristics of asphalt binders and mastic were determined before and after aging and an aging index was defined to evaluate the effect of the additives on aging. The results demonstrated that certain antioxidants and copolymers such as Redicote AP, Solprene, and Calprene may retard the aging and improve the rheological properties of the asphalt binders. In addition, the results of mastic testing confirmed the favorable effect of certain antioxidants on improving the resistance to fatigue cracking. Furthermore, the type of aggregate was found to influence the rate of aging of asphalt mixtures.

Based on the rheological and fracture test results on asphalt binders and mastic, the effect of antioxidants was further investigated and validated at spectroscopic, chemical and microstructural level using Fourier-transform infrared spectroscopy (FTIR), Gel-permeation chromatography (GPC) and Atomic Force Microscopy (AFM), respectively. The spectroscopic analysis with FTIR supported the efficacy of the additives in retarding aging by reducing the carbonyl growth in aged binders. The chemical analysis with GPC confirmed that both Redicote and Solprene were capable of reducing the large molecular size fraction in binders subjected to long-term aging. The image analysis with AFM provided insight on the spatial distribution, surface roughness parameters and micromechanical properties (i.e., adhesion, stiffness) of various phases and the effect of aging on the micro-rheology of antioxidant-modified binders.

The last part of this study examined the effect of aging on the viscoelastic response of asphalt mixture using the Prony series representation and a newly developed parameter called aging state variable *'A'*. The dynamic modulus test data was used for the analysis. The aging state

variable *'A'* was found to capture the effect of aging temperature and duration of aging on the viscoelastic properties of asphalt mixtures.

Keywords: Binder aging, antioxidants, FAM, gabbro, FTIR, AFM, GPC.

ACKNOWLEDGEMENTS

To my advisor, Dr. Emad Kassem, I am heartily grateful for the inspiration, encouragement, motivation and support he provided me throughout my thesis and graduate studies. Working with him was an opportunity of great learning experience. The patience he had for explaining complex concepts related to this research is greatly appreciated. Without his help and continuous support this work would not have been possible.

My sincere and profound thanks are due to Dr. Fouad Bayomy and Dr. Armando McDonald for serving as members of my thesis reviewing committee.

I would also like to thank Dr. Eric Aston for the help he provided during the testing of binder samples using AFM. Also thanks to Mr. Don Parks for his technical support when needed. This work would not have been possible without their support as well.

My cordial gratitude to Qatar National Research Fund (a member of Qatar Foundation) for their research grant (NPRP 6-773-2-320), because of which this work was made possible.

Acknowledgement is also due to the University of Idaho for the support given to this research through its facilities and for granting me the opportunity to pursue my graduate studies with financial support. I would once again like to thank the University of Idaho for having such a great atmosphere on campus for International students. At the University of Idaho, I never felt like away from home.

DEDICATION

To my parents for their prayers and continuous support

To my wife for believing in me

TABLE OF CONTENTS

LIST OF TABLES

LIST OF FIGURES

CHAPTER 1 INTRODUCTION

1.1 Problem Statement

Asphalt pavement is the most common and major type of pavements in the United States. Asphalt mixture is composed of approximately 95% aggregate and 5% asphalt binder by weight. The long-term performance of asphalt pavement greatly depends on the quality of the materials used, environmental conditions, and traffic level, and strength of the underlying layers. The rheological properties of asphalt binders change with oxidative aging which is accelerated at elevated temperatures. Aging stiffens asphalt binders and increases the embrittlement of asphalt mixtures which would lead to fatigue cracking and eventually pavement failure under repetitive traffic loading (Glover *et al.* 2009; Apeagyei 2011). Binder oxidation, loss of volatiles in the binder, and thixotropy or steric hardening cause binder aging (Masson *et al.* 2005; Swiertz 2010). The oxidative aging occurs due to the reaction between the hydrocarbons of asphalt and natural oxygen that causes irreversible chemical and rheological changes in the asphalt. The rate of oxidative aging is affected by the environmental conditions (i.e., temperature) (Bell 1989).

Antioxidants are chemicals that inhibit oxidation of molecules (Lü *et al.* 2010). Various polymers and copolymers are used as antioxidants. This study focused on the latest antioxidants available on the market and shortlisted the best possible combination based on the literature and investigated the potentiality of antioxidants and copolymers in retarding oxidative aging in terms of both SHRP and newly developed rheological parameters (Glover *et al.* 2005) at binder and mastic levels.

To verify the rheological results, this study also investigated the performance of the best antioxidants at spectroscopic, chemical and microstructural level using Fourier-transform infrared spectroscopy (FTIR), Gel-permeation chromatography (GPC) and Atomic Force Microscopy (AFM), respectively (Lu and Isacsson 2002; Jäger *et al.* 2004). This advanced characterization of both laboratory-aged antioxidant modified binders and field-aged binders

would help to understand the chemical and micro-rheological changes in asphalt binder at the molecular level when mixed with antioxidant additives.

Lastly, evaluating the effect of long-term aging on the viscoelastic properties of asphalt mixtures provides needed parameters in constitutive relationships to predict the performance of asphalt pavement over its service life. The study examined the effect of aging on the viscoelastic response of asphalt mixture using the Prony series representation and a newly developed parameter called aging state variable *'A'* (Rahmani *et al.* 2017).

1.2 Research Objectives

The main objectives of this study are:

- Evaluate the effect of antioxidant additives on rheological properties of asphalt binder including the SHRP rheological parameter $G^*sin\delta$ and other newly developed rheological parameters such as Glover-Rowe and Kandhal's ductility.
- Evaluate the effect of antioxidant additives on mechanical properties (i.e., fracture energy, flexibility index) of asphalt mixtures modified with antioxidant additives and copolymers.
- Perform FTIR analysis on laboratory-aged binder at different conditions and field-aged extracted binders to assess the rate of oxidation through the change in carbonyl compound and other functional group in asphalt binders.
- Perform GPC analysis to quantify the change in molecular weight distribution of asphalt binder due to aging.
- Investigate the effect of long-term aging condition on the microstructural properties of asphalt such as adhesion, stiffness and surface roughness parameters using AFM.
- Investigate the effect of aging on the viscoelastic properties of asphalt mixtures using a newly developed parameter called the aging-state variable *'A'*.

1.3 Organization of the Study

This thesis consists of six chapters. Chapter 1 presents an overview of this study. It includes the problem statement, objectives, and study organization.

Chapter 2 documents the main findings from a literature review on the use of antioxidant additives and copolymers to retard oxidative aging of asphalt binders. It also summarizes some of the plethora of studies performed to characterize the long-term aging of asphalt binder using spectroscopy tests such as FTIR, chemical analysis such as GPC/SEC and micro-mechanical testing with AFM.

Chapter 3 describes the various antioxidants used in this study and their performance in retarding aging of asphalt binders. The performance of antioxidants was assessed using the latest rheological parameters such as $G^*(\cos\delta)^2/\sin\delta$, Glover-Rowe parameter and Kandhal's ductility in addition to the SHRP parameter $G^*\sin\delta$. To evaluate the effect of antioxidants in terms of mastic aging characteristics, this chapter describes two inter-dependent mechanical parameters: fracture energy and flexibility index and associated load-displacement curves, obtained from the semi-circular bending (SCB) test at intermediate temperature.

Chapter 4 describes the asphalt sample preparation and test setup and explains the experimental procedure performed with the following equipment: FTIR, GPC and AFM. These tests yielded data on the spectroscopic, chemical and microstructural characteristics of both field-aged and laboratory-aged asphalt binders under different conditions and discusses the associated findings.

Chapter 5 investigates the effect of aging on the viscoelastic response of asphalt mixture using the Prony series representation and a newly developed parameter called aging state variable *'A'* as an indicator of age-induced viscoelastic response of asphalt mixtures.

Chapter 6 summarizes the main findings of this study and offers recommendations for future research.

CHAPTER 2 LITERATURE REVIEW

2.1 Introduction

This chapter summarizes results of a literature review on the use of antioxidant additives and copolymers to retard oxidative aging of asphalt at the binder, mastic and mixture levels. It also reviews previous research on fracture energy and flexibility indices for evaluating the effect of aging on mastic and full mixtures. In addition, this chapter summarizes some of the plethora of studies performed to characterize the long-term aging of asphalt binder using spectroscopic tests such as Fourier Transform Infrared Spectroscopy (FTIR), chemical analysis such as Gel Permeation Chromatography or Size Exclusion Chromatography (GPC/SEC), and micro-mechanical testing with Atomic Force Microscopy (AFM).

2.2 Review on Oxidative Aging of Asphaltic Material and Use of Antioxidant Additives and Copolymers in Retarding Aging

Asphalt is a dark-colored semi-solid material whose properties change with temperature and traffic loading conditions (e.g., frequency) due to its nonlinear viscoelastic nature and susceptibility to plastic deformation and rate-dependent damage (Rahmani *et al.* 2017). Due to its capability to bind or hold aggregates together, almost 95% of the produced asphalt binders are used in paving worldwide (Lesueur 2009). Typically, about 5% of asphalt binder, by weight of the mix, is heated up to around 160°C to decrease its viscosity and mixed with 95% aggregates, by weight of the mix, to produce hot mix asphalt (HMA). Asphaltic material had been used for building roads as early as 625 BC by Nabopolassar, King of Babylon (Abraham 1960); however, it was not until the early 1960s when pavement engineers first observed the detrimental effects of temperature and environmental factors on the service life and overall performance of flexible pavement (Abraham 1960; Bell 1989).

Since the term ‘aging’ has multiple interpretations in the asphalt industry, the chemical and subsequent rheological changes in asphalt binder due to the effects of temperature and time are referred to as ‘asphalt aging’ or ‘age-hardening’ in this study. Hardening of asphaltic materials occurs both during the production phase and throughout the service life of a

pavement (Bell *et al.* 1994; Roberts *et al.* 1996; Glover *et al.* 2009; Apeagyei 2011). The first stage of asphalt hardening is known as short-term aging which occurs very rapidly during the mixing of aggregate with asphalt. The asphalt is exposed to oxidation at high temperature and results in increased stiffness and viscosity (Roberts *et al.* 1996). The second stage takes a long time, almost 7-10 years of exposure to the environmental factors when the road is in service. Glover et al. (2009) predicted the hardening response of asphalt as presented in Figure 2.1. A rapid increase in viscosity can be seen at Region A during the stage of short-term aging, while an increase in the viscosity at a slow but constant rate is observed in Region B (long-term aging).

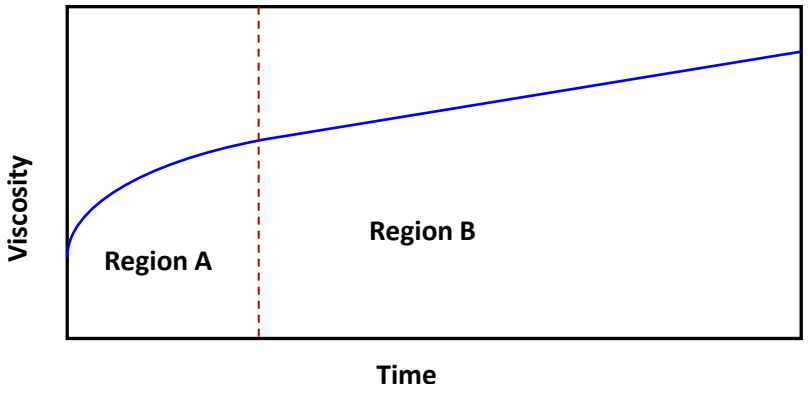

Figure 2.1 Typical hardening response for asphalt binder (Glover *et al.* 2009)

Factors affecting the degree of aging include mixing temperature during construction; climatic factors such as temperature, rainfall, ultraviolet exposure; and certain mixture properties such as asphalt and aggregate type, percent air void, moisture diffusion and binder content (Traxler 1963; Lee 1973; Lau *et al.* 1992; Ala *et al.* 2002; Kandhal and Chakraborty 1996; Morian *et al.* 2013). Aging causes significant reduction in penetration and ductility with an increase in softening point, ignition temperature, viscosity and stiffness of the binder (Siddiqui and Ali 1999; Rojas *et al.* 2012; Ala *et al.* 2002; Airey *et al.* 2004; Al-Azri *et al.* 2006), which leads to embrittlement of the asphalt mixture, early structural failure of pavement due to cracking (Vallerga 1981; Bell *et al.* 1995), and lower resistance to wear and moisture susceptibility (Barth 1962).

2.2.1 Asphalt Chemistry and Aging Mechanisms

Due to the wide variation in the petroleum source and distillation process, asphalt binder has a complex elemental composition. Almost 90% of asphalt binder is comprised of hydrocarbon, and the remaining portions include heteroatoms such as nitrogen (0-2%), oxygen (0-2%) and sulphur (0-9%) and metal atoms such as nickel, vanadium and iron in trace quantities (Mortazavi and Moulthrop 1993). Heteroatoms are responsible for the unique physical and chemical properties of asphalt.

Corbett's method identified the following distinct fractions in asphalt binder: asphaltenes, saturates, naphthalene and polar aromatics (resins) (Corbett 1969). All of these components together exhibit complex chemical-physical characteristics in asphalt binder (Hveem *et al.* 1959; Petersen 1984a; Pan *et al.* 2012). These chemical and physical properties of asphalt change with time due to various climatic and environmental factors and include oxidation, volatilization, thixotropy (steric hardening) and polymerization (Traxler 1961; Petersen 1984a; Bell 1989; Bell *et al.* 1994) among which the first three are considered significant factors in asphalt hardening (Bell *et al.* 1994; Apeagyei 2011).

Several researchers have demonstrated that the oxidative aging of asphalt, which is an irreversible chemical reaction between oxygen molecules and the distinct fractions of asphalt, generate polar chemical groups (Lau *et al.* 1992; Petersen *et al.* 1993; Glover *et al.* 2009; Pan *et al.* 2012). The asphalt hardening well below the wearing course was examined extensively by Glover (2005) and Al-Azri *et al*. (2006), who examined a large number of binders extracted from cores in Texas.

Some researchers have concluded that aromatic components decrease with an increase in the asphaltenes due to aging, resulting in the formation of certain chemical functional groups such as carbonyl and sulfoxide groups (Lesueur 2009). Liu *et al.* (1998) correlated carbonyl area (CA) with rate of oxidation, while Glover et al. (2009) described the carbonyl reaction rate with Equation 2.1.

$$\frac{dCA}{dt} = r_{CA} = AP^{\propto}e^{-E/RT} \tag{2.1}$$

where, $\frac{dCA}{dt}$ = carbonyl reaction rate, A = frequency factor, P = pressure, $\propto$ = reaction order, E = activation energy, R = gas constant, and T = absolute temperature. Studies show that the values of A, E, and $\propto$ differ for different asphalt types.

Volatilization and steric hardening are two significant mechanisms of asphalt hardening. In the process of volatilization, the lighter molecular weight fractions or the oil-like compounds such as the aromatics evaporate at higher mixing temperatures (i.e., 150°C) resulting in an increase in asphaltene content (Farcas 1996), stiffness and viscosity (Bell 1989; Christensen and Anderson 1992). At low temperatures, steric hardening occurs over time where the molecular structure of asphalt affects the viscoelastic properties of asphalt by increasing its viscosity and overall hardening (Masson *et al.* 2005; Traxler 1961). Steric hardening is reversible through re-heating (Swiertz 2010).

2.2.2 *Laboratory Accelerated Aging and Evaluation Methods*

A significant amount of research has been performed to simulate the aging of asphalt binders in the laboratory through application of extended heat and pressure. After laboratory aging, material properties such as viscosity, penetration, ductility, weight loss and stiffness modulus are compared with that of the unaged binders. The overall simulation process is mainly divided into the following two categories: asphalt binder and asphalt mixture as discussed in this section.

Accelerated aging of asphalt binders

To simulate the aging of asphalt binder in production, mixing, construction and during service life of roadway, researchers have developed several methods and aging protocols including 1) Rolling Thin-Film Oven (RTFO) (AASHTO T 240) to smiluate the short-term aging, and 2) Pressure Aging Vessel (PAV) (AASHTO R 28) to simulate the long-term aging. As per the current SuperPave specifications, asphalt binder should be subjected to short-term aging at 163°C for 85 minutes in RTFO followed by a long-term aging at 100°C for 20 hours at 2.07 MPa pressure in PAV to simulate several years of field aging (Anderson *et al.* 1994). PAV generally simulates aging of 8-10 years of pavement service life (Fernández-Gómez 2013).

Accelerated aging of asphalt mixtures

Between 1960 and 1990, little research was done to simulate the aging of asphalt mixtures compared to asphalt binder. Starting in the 1990s, several researchers performed research to simulate asphalt mixture aging subjected to various aging conditions and measured the physical properties of aged mixtures (Bell *et al.* 1994; Sias and Richard 2001). Currently, AASHTO R 30 standard procedure recommends to condition asphalt mixtures as per following three methods:

- mixture conditioning for volumetric mix design.
- short-term conditioning to simulate aging during asphalt and aggregate mixing and placement.
- long-term conditioning to simulate aging that occurs over the service life of pavement.

A forced-draft oven is used to condition the mixtures at different durations and temperatures, as presented in Table 2.1.

Table 2.1 Temperature and Time Duration for Different Conditioning Types

Conditioning Type	**Temperature**	**Time**
Conditioning for mixture design	Varies*	2 hours
Short-term aging	135 °C	4 hours
Long-term aging	85 °C	5 days

* Mixture's specified compaction temperature

This standard protocol does not account for different environmental conditions or mix properties. Thus, the applicability of these protocols to hot climatic conditions as in the Middle East is questionable without field validation (Sirin *et al.* 2017a). Roadways experience extreme climatic conditions at higher temperatures (often exceeding 40°C during the summer) in this region. There is almost no rainfall during the summer and very little during the rest of the year. These elevated temperatures increase the rate of binder oxidation resulting in fatigue cracking and ultimately pavement failure under heavy and repetitive traffic loading. Earlier research also demonstrated a need to develop an aging protocol that considers climatic conditions such as maximum/minimum air temperatures and average rainfall, in addition to traffic volume and mix properties (Bell *et al.* 1994; Houston *et al.* 2005; Said 2005; Baek *et al.* 2012). These studies

recommend to account for these changes during the design stage to improve the long-term performance of flexible pavements.

Bell et al. (1994) conducted a comprehensive research study to evaluate the short-term and long-term aging protocol of asphalt mixtures. As part of the Strategic Highway Research Program (SHRP), they investigated different accelerated performance tests to evaluate the effect of aging. Their study included different climate zones, and thus the aging was influenced by the environmental conditions. The results demonstrated that the AASHTO short-term aging protocol simulated asphalt mixture aging adequately well except few conservative predictions.

Houston et al. (2005) conducted a research study to verify and improve the procedures for long-term conditioning of asphalt mixtures. The researchers recovered field cores from three sites across the United States to represent different environmental conditions. Each one of these sites had multiple test sections constructed using different combinations of aggregates and binders. Loose mixtures were obtained from these sites and compacted in the laboratory and conditioned at multiple temperatures (80 °C, 85 °C, and 90 °C) for 5 days. The results show that, as expected, the dynamic modulus of laboratory specimens increased with the increase in conditioning temperature. Consequently, one would expect that warmer climates would cause more aging compared to cooler climates, which may contradict the current standard of long-term conditioning that specifies a single temperature (Houston *et al.* 2005), as shown in Table 2.1. The researchers observed high variability in the data from the selected sites, and due to this variability and inability to account for various variables such as environmental conditions and mix properties, the researchers were not able to develop a new procedure or revise the current one for long-term conditioning of asphalt mixtures. The researchers concluded that the current standard procedure is not sufficient to truly simulate and predict the long-term aging of asphalt mixtures in the field. Developing a new procedure that accounts for different environmental conditions and mix properties such as air void content is highly desirable. In addition, they recommended including different types of materials: unmodified binders, modified binders, rubber binders, and reclaimed asphalt pavement.

2.2.3 *Influence of Antioxidant Additives on Asphalt Mixture Aging*

Since oxidative aging was found to be the major cause of pavement hardening and subsequent failure due to cracking, researchers attempted to reduce the rate of oxidative aging using antioxidant additives. Chemicals that inhibit the oxidation reaction by trapping the free radicals responsible for reaction are called antioxidants (Lü *et al.* 2010). These chemicals, when mixed with asphalt binder, gets oxidized instead of the asphalt or react with the polar compounds or oxidation catalysts such as the metals in asphalt. Researchers used various antioxidant additives and evaluated their performance after aging when mixed with binder in respect to certain physical properties such as viscosity and ductility.

Mohamed (2007) evaluated the performance of CRABit (CR30 and CR50), a crumb rubber powder mixed with Zinc Dithiocarbamate and other accelerators, as antioxidants and applied in dense asphalt mixtures (ACW14). The study was performed in two stages. At the first stage, the authors tested the rheological properties of the antioxidants using wet mix through DSR. In the second phase, they prepared control and CRABit modified ACW14 dry mixtures and tested the resilient modulus, indirect tensile, creep and fatigue resistance of aged and unaged samples. Results showed improved performance of mixtures modified with CR30 after long-term oven aging.

Apeagyei et al. (2008) evaluated the fracture potential of asphalt mixtures containing furfural (an aromatic aldehyde) and an antioxidant and thermal stabilizer (DLTDP). They evaluated the performance of these antioxidants after short and long-term aging. The percentage of antioxidants were from 0.2% to 10% by weight of the binder. The mixing temperature was 125°C up to 4 hours with an operating fan speed of 750 rpm. The effects of antioxidants were evaluated with the parameters of SuperPave binder test in addition to dynamic modulus, creep compliance, and tensile strength test, to measure the cracking behavior of antioxidant-modified asphalt mixtures. Although it was found that aging decreased the fatigue life of both unmodified and antioxidant-modified binders, the later performed better compared to the unmodified one.

In addition to the previous study, Apeagyei (2011) evaluated several other additives including Irgafos P-EPQ, vitamin E, Carbon Black, hydrated lime, DLTDP/furfural and Irganox 1010. The antioxidant-modified binders were subjected to both short-term and long-term aging. The rheological parameters of both treated and untreated binders were measured after and before aging with a DSR. An index called aging index developed to compare the results in respect to the control unmodified base binder. The combination of furfural and DLTDP provided the lowest aging index after long-term aging. However, the antioxidant-modified binders showed lower stiffness when compared to unmodified binder, which is helpful in resisting cracking damage. The authors recommended further research on additional binders and antioxidants.

Pan at al. (2012) studied the aging and antioxidation mechanisms in atomic level by investigating chemical and physical bases of asphalt oxidation in addition to the coniferyl-alcohol lignin antioxidation strategy. They demonstrated that asphalt molecules displayed high reactivity with atmospheric oxygen by breaking the long hydrocarbon chains and the oxidation rate decreased with time. The results also demonstrated that the coniferyl-alcohol lignin to be a viable antioxidant additive for asphalt binder.

At the University of Illinois at Urbana-Champaign, a group of researchers developed an antioxidant called AOXADUR by mixing following three additives: aldehyde, thioester and a catalyst (Dempsey 2006). The aldehyde of AOXADUR causes a condensation reaction with asphalt and forms Novolacs which can reduce the growth of polar aromatics in the binder. The thioester limits the oxidative degeneration of hydrocarbons. AXADUR was found to reduce the aging index after long-term aging, increase the high-temperature stiffness and decrease the low-temperature stiffness. Thus the use of AXADUR is expected to improve the overall properties of asphalt mixtures.

2.3 Effect of Aging on the Viscoelastic Response of Asphalt Mixture with Prony Series Representation

The Prony series method, initially developed by Gaspard Riche de Prony in 1795, can be used to analyze the viscoelastic properties of a material subjected to constant stress. Thus, the strain-recovery function can be interpreted as a mechanical element model similar to the generalized Maxwell or Kelvin-Voigt model. This method is a widely popular function to fit the viscoelastic creep-recovery behavior of asphalt binder. Many researchers used the recovery part of a multiple creep-recovery test to obtain the nonlinear parameters of the viscoelastic reponse of asphalt binder (Rahmani *et al.* 2013; Rahmani *et al.* 2017; Park and Kim 2001; Kim *et al.* 2007; Huang *et al.* 2007; You *et al.* 2014) and identified the Prony coefficients through the Prony representation of transient creep compliance (*ΔD*) as given in Equation 2.2.

$$\Delta D = \sum_{n-1}^{N} D_n[1 - e^{-\lambda_n \psi^t}] \tag{2.2}$$

where, N = no. of Prony series coefficients

λ_n = *n*th retardation time

D_n = *n*th compliance associated with the *n*th retardation time

ψ^t = reduced time

Rahmani et al. (2013) investigated the effect of confinement pressure on the nonlinear viscoelastic properties of asphalt concrete and found that the confinement pressure significantly effects these properties. They related the nonlinear viscoelastic properties to the triaxiality ratio with an equation. In order to characterize the time dependent nonlinear viscoelastic response of asphalt, they used Schapery's nonlinear viscoelastic model (Equation 2.3) (Schapery 1969).

$$\varepsilon^t = g_0 D_0 \sigma^t + g_1 \int_0^t \Delta D(\psi^t - \psi^\tau) \frac{d(g_2 \sigma^\tau)}{d\tau} d\tau \tag{2.3}$$

where, *ε* = strain response

σ = stress response

D_0 = instantaneous creep compliance

ΔD = transient creep compliance

t and τ correspond to responses at specific time

g_0, g_1, and g_2 = nonlinear stress dependent parameters

ψ = reduced time (function of time–temperature shift factor)

Moreover, g_0 and g_1 define the effect of stress on D_0 and ΔD respectively whereas g_2 manages the effect of loading rate on ε. Rahmani et al. (2017) applied the Prony series to express the transient creep compliance ΔD as presented in Equation 2.2. To identify the Prony series coefficients and time–temperature shift factor, they performed strain controlled dynamic modulus test at different temperatures and frequencies. To calculate the Prony coefficients, they determined the storage and loss modulus from the complex modulus and phase angle data and applied inter-conversion relationships (Park and Schapery 1999). To minimize the error between experimental and predicted model, the researchers applied the nonlinear Generalized Reduced Gradient (GRG) method. They investigated the effect of oxidative aging on the viscoelastic response of asphalt binder by including the aged material properties with a superscript '*A*' in Schapery's general form of viscoelastic constitutive relationship as:

$$(\varepsilon^{\eta\, ve,t})^A = g_0 D_0^A \sigma^t + g_1 \int_0^{\psi} \Delta D^A (\psi^t - \psi^\tau) \frac{d(g_2 \sigma^t)}{d\tau} d\tau \qquad (2.4)$$

where, $(\varepsilon^{\eta\, ve,t})^A$ the viscoelastic nonlinear strain response of aged binder.

The corresponding instantaneous creep compliance and transient creep compliance are denoted as D_0^A and ΔD^A, respectively. Similarly, the Prony representation of the ΔD^A with n^{th} compliance (λ_n^A) and n^{th} retardation time (D_n^A) is presented in Equation 2.5.

$$\Delta D^A = \sum_{n-1}^{N} D_n^A [1 - e^{-\lambda_n^A \psi^t}] \qquad (2.5)$$

The Prony coefficients were extracted from the dynamic modulus test data of unaged and aged full mix. The long-term aging durations selected were 3 and 6 months at 60°C. Seven Prony parameters were considered and the effect of aging was evaluated by comparing the unaged and aged Prony parameters, i.e. retardation time and compliance terms. Figure 2.2 shows the decrease of both compliance and retardation terms due to aging and it was found that the aged and unaged terms follow a power-law relationship.

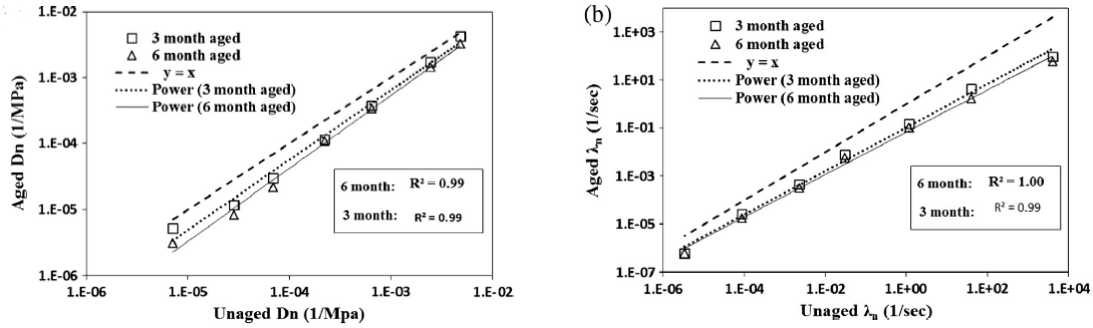

(a) (b)

Figure 2.2 Relationship between aged and unaged Prony series coefficients, (a) compliance term, (b) retardation time (Rahmani *et al.* 2017)

Both the compliance (D_n) and retardation time (λ_n) were found to be affected by level of aging although the effect was not significant. They proposed a new parameter called oxidative-aging state variable "A" to relate aged and unaged viscoelastic properties. The relationships are presented in Equation 2.6.

$$D_n^A = (1-A)^k D_n; \lambda_n^A = (1-A)^k \lambda_n \quad (2.6)$$

The aging state variable was found to increase with long-term aging as shown in Figure 2.3.

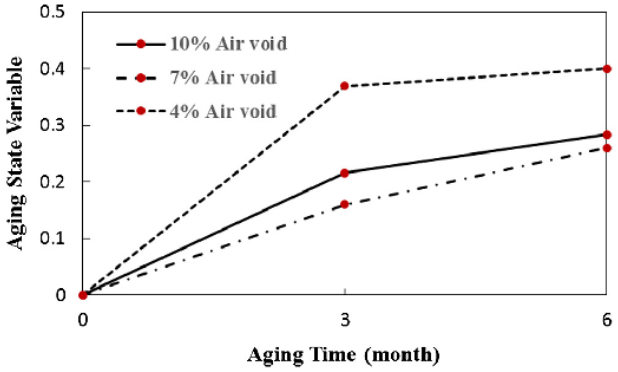

Figure 2.3 Aging state variable (A) vs. aging time at different air void % (Rahmani *et al.* 2017)

2.4 Characterization of Oxidative Aging of Asphalt Binder with Infrared Spectroscopy

The Infrared (IR) spectroscopy has been widely used for material-based spectroscopic analysis in the laboratories for almost over seventy years. Fourier Transform Infrared (FTIR) is one of the methods of IR spectroscopy where an infrared radiation is passed through a test specimen (Thermo Nicolet 2001). Part of the IR radiation is absorbed by the specimen and some of it is transmitted through the sample. The resulting spectrum describes the amount of IR absorbed and transmitted. The absorption peak of the spectrum is directly related to the vibration frequencies between the bonds of the atoms/molecules of that material which is known as stretching and bending of covalent bonds. Since each chemical compound are unique combination of atoms and molecules, each of them exhibit unique IR spectrum, which is like a fingerprint of that specimen. Also, the size of the peaks in a spectrum is a direct indication of the amount of material in that specimen. This feature of IR spectroscopy is useful in identifying the presence of an unknown component in a specimen (qualitative analysis), its amount (quantitative analysis) and the overall consistency of the sample.

2.4.1 *Theory of FTIR Technology*

Modern FTIR spectrometer comes with interferometer, an optical device that can produce a unique signal with all the IR frequencies encoded into it (Stuart 2004; King *et al.* 2004). The interferometer is comprised of a beam-splitter (i.e., Michelson interferometer) that divides the incoming IR beam into two optical beams of wavelength λ (Figure 2.4). One of the beam gets reflected by a fixed flat mirror while the other one gets reflected from a mirror movable over a distance Δl. So, one beam travels a fixed distance whereas the other beam changes the length of its travel path constantly which is a function of the mirror position. The difference in the path lengths is called the optical path difference or retardation (δ). The resultant beam, combination of the two interfering beams and thus known as the interferogram, is recaptured by the beam-splitter and sent through detector into the computer for decoding by means of Fourier transformation to get the spectral information (a frequency spectrum). Due to each position of the moving mirror, the signal of interferogram has information on all the IR frequency coming from the source. By measuring the interferogram, all the frequencies are measured at the same time which reduces the scanning time.

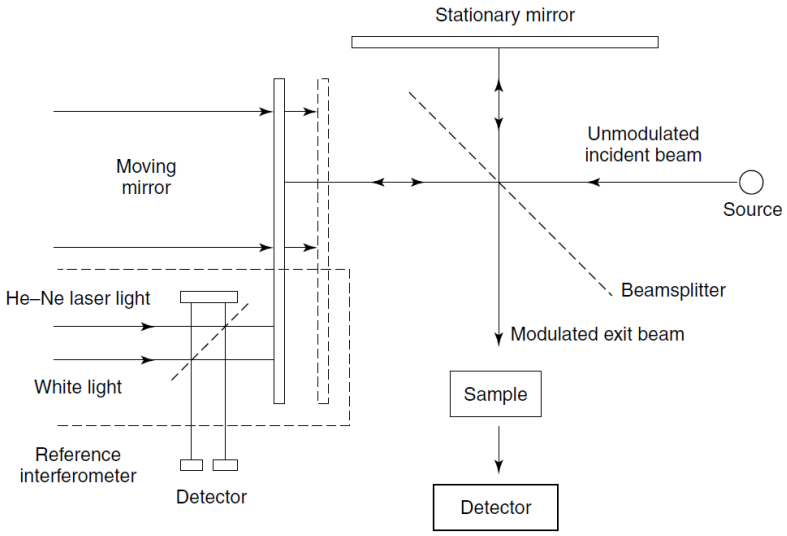

Figure 2.4 Schematic of a Michelson interferometer (Stuart 2004).

The signal or IR wave can be written as the following function of distance or retardation (δ) and wave number (λ) (Griffiths 1983),

$$I(\delta) = B(\bar{\nu}) \cos\left(2\pi \frac{\delta}{\lambda}\right) = B(\bar{\nu}) \cos(2\pi \bar{\nu} \delta) \tag{2.7}$$

where, B($\bar{\nu}$) is the intensity of the source at wavenumber $\bar{\nu}$.

Equation 2.7 can be written in the following Fourier transform equation (The Power of the Fourier Transform for Spectroscopists 2014) by exchanging $\bar{\nu}$ with f and δ with t:

$$\phi(\bar{\nu}) = \int_{-\infty}^{\infty} F(\delta) e^{-i2\pi\bar{\nu}\delta} d\delta \tag{2.8}$$

The usual range of IR spectrum is between 4000 cm^{-1} to 400 cm^{-1}. The energy of IR is less than that of visible light due to the inverse relationship between energy and wavelength. Bending and stretching are the two primary modes of vibration. Typically, stretching exhibits higher energy than bending and can be divided into symmetric and asymmetric stretch where the symmetric stretch is commonly of lower energy. The energy of the stretch decreases with the increase in atomic mass. FTIR spectroscopy is preferred over dispersive or filter methods because it is a non-destructive test (NDT) method with higher optical throughput and requires

no external calibration by the user (Thermo Nicolet 2001). The detectors used are more sensitive and thus lower the noise level. It is mechanically simple with only one moving mirror which reduces the possibility of mechanical failure.

2.4.2 *Previous Studies on Characterization of Asphalt Binders using FTIR*

FTIR has been used widely in characterizing the properties of asphalt binder and addressing its chemical changes due to various conditions such as oxidative aging, loss of volatiles, polymer modification etc. Peaks in the spectral data can be used to detect the chemical functional groups that contain oxygen including carbonyl and sulfoxides. Wei et al. (1996) studied the alteration of chemical composition of asphalt binders using FTIR and conducted research on developing protocol for fingerprinting asphalt binders. According to Wei et al. (1996), a combination of GPC and FTIR is an excellent tool for quality control of straight and polymer modified binders. Specially, FTIR can be used to examine unaged, aged and modified binder to characterize chemical functional groups that absorb IR light. Wei et al. (1996) prepared the samples by evaporating a Tetrahydrofuran (THF) solution on a KBr salt pellet and making a thin film of the test specimen. The absorption peaks for CH_3, CH_2, aromatic carbon and carboxyl groups were found 1375, 1450, 1600 and 1700 cm^{-1}, respectively. A calibration curve is required each time for different materials.

Lu and Isacsson (2002) observed the effect of aging on asphalt binder chemistry using an FTIR spectrometer, Infinity 60AR (Mattson, resolution 0.125 cm^{-1}). The binders (5% binder content by weight) were dissolved in carbon disulfide. Circular sealed cells (Zinc Selenide windows and 1 mm thickness) were used to scan solvent and samples. The test wavenumber ranged between 1900 cm^{-1} to 500 cm^{-1} and 32 scans were performed with iris of 5% resolution of 4 cm^{-1} to obtain the spectra. Lu and Isacsson (2002) confirmed the formation of carbonyl and sulfoxide compounds and an increase in the quantity of large molecules and in molecular weight distributions resulting in changes in the chemical and mechanical properties of asphalt binder (Figure 2.5) and formation of solid-like bitumen due to aging. It was found that carbonyl compounds (i.e., anhydrides, ketones and carboxylic acids) exhibited absorption at wavenumber of 1705 cm^{-1} (due to stretching of C=O bond) and the sulfoxides had peaks in the spectra around 1030 cm^{-1} (due to stretching in S=O bond).

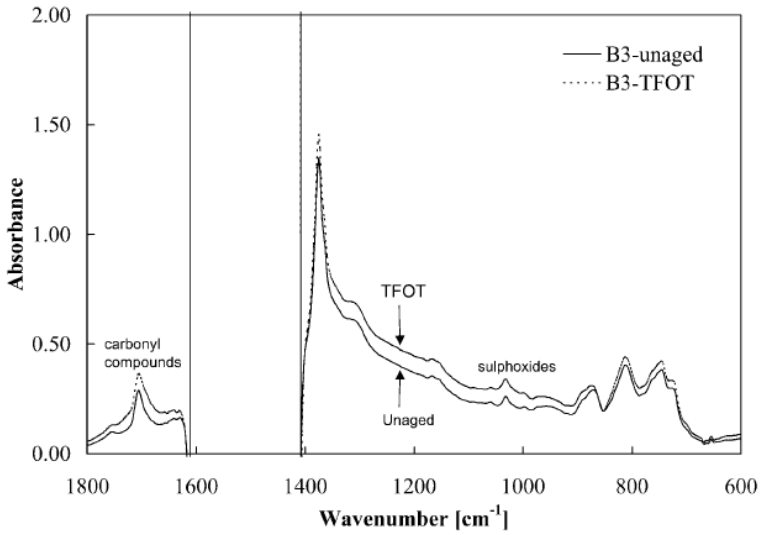

Figure 2.5 Effect of aging on bitumen FTIR spectrogram (Lu and Isacsson 2002)

Lamontagne et al. (2001) used FTIR spectroscopy to compare samples from field aging with RTFOT and PAV aged samples. They conducted research on bitumen samples by dissolving them in dichloromethane (30 g l^{-1} of CH_2Cl_2) and putting on KBr thin plate at a rate of 25-µl. To avoid interference in the spectra, nitrogen was flowed to evaporate the solvent which is known as the dry-plate technique. The FTIR results showed characteristic absorption bands areas from which the functional indices were calculated in order to incorporate several vibrations of the same type (for example the C=O ester, acid and ketone vibrations between 1753 and 1635 cm^{-1}). They have demonstrated that 1 hour of cell oxidation simulates 2 years of field aging. To calculate the spectrometric indices, they measured each of the band areas from valley to valley (Figure 2.6) instead of band heights because several vibrations of the same type of functional group was concurrently taken into account. For example, ester, carboxylic acids and ketone exhibit the vibration of the same functional group which is the carbonyl group C=O (usually between wavenumber of 1753 to 1635 cm^{-1}). To determine the band area ratio, the entire band was distributed into following indices:

- Aromatic index = A_{1600} / ∑A
- Aliphatic indices = (A_{1460} + A_{1376})/ ∑A, for branched- A_{1376}/ (A_{1460} + A_{1376}), for long chains- A_{724}/ (A_{1460} + A_{1376})
- Carbonyl index = A_{1700}/ ∑A; Sulfoxide index= A_{1030}/ ∑A,

where, $\sum A = A_{1700} + A_{1600} + A_{1460} + A_{1376} + A_{1030} + A_{864} + A_{814} + A_{743} + A_{724} + A_{(2953,2923,2862)}$.

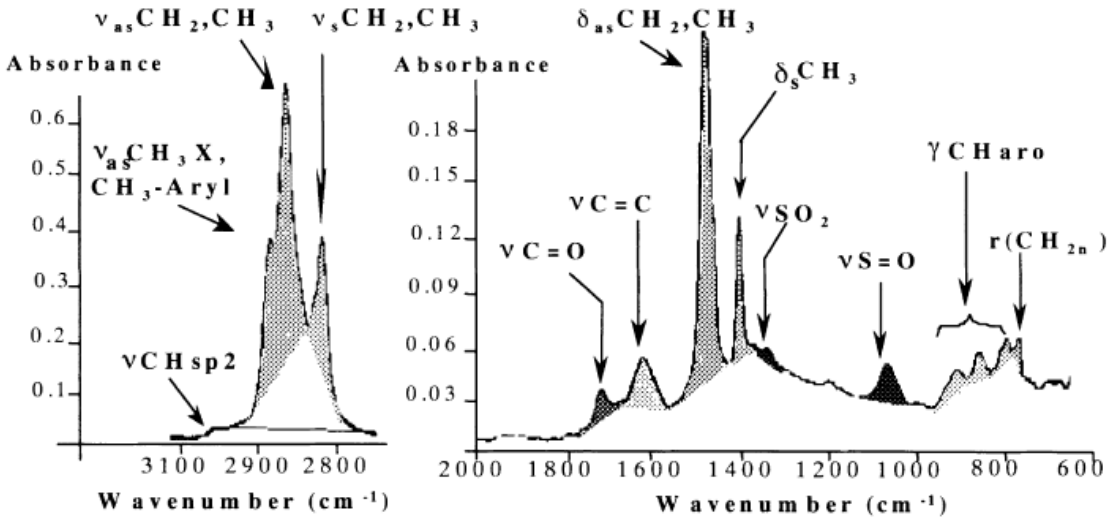

Figure 2.6 FTIR spectrum of a 4000-400 cm^{-1} original bitumen. Visualization of valley to valley area integration (Lamontagne *et al.* 2001)

To calculate the carbonyl area (CA), this valley to valley approach of calculating area under the curve of each band and dividing by the sum of area under all asphalt's characteristic bands was followed by several studies such as Zhang et al. (2011) and Ghavibazoo et al. (2015).

In a study performed by Zhang et al. (2011), the structural evolution of control and SBS modified asphalt binder under different aging modes were characterized by calculating the right aging index with the help of FTIR spectra and changes were found in carbonyl indexes. Similar to previous studies, carbon disulfide was used to dissolve asphalt binder (weight concentration of 5%) and KBr plate was used to perform FTIR analysis after the samples were dried. It was observed that, after aging, there was declination in the ethylene index which confirmed the degradation of SBS polymer in the binder. The increase in polar asphalt components of higher molecular size was associated with the increase of the carbonyl index. For the sulfoxide index, a mixed pattern of change was observed. An increase in sulfoxide index was found after short-term TFOT aging but decomposition of sulfoxide compound was observed after long-term aging at higher temperature (Figure 2.7). This observation led to confusion of using sulfoxide index as a parameter of measuring aging index. This similar observation was verified by both previous and later studies (Ouyang *et al.* 2006a; Yao *et al.*

2013) and thus the sulfoxide index is not considered as an aging index parameter of asphalt binder. The characteristic bands of the carbonyl functional group C=O was found to be centered on 1700 cm^{-1} while the sulfoxide group S=O was centered on 1030 cm^{-1}. The structural indices were calculated by considering the area of the functional bands with the help of following equations:

$$I_{C=O} = \frac{Area\ of\ the\ carbonyl\ band\ centered\ around\ 1700\ cm^{-1}}{\sum Area\ of\ the\ spectral\ bands\ between\ 2000\ cm^{-1}\ and\ 600\ cm^{-1}} \quad (2.9)$$

$$I_{S=O} = \frac{Area\ of\ the\ sulfoxide\ band\ centered\ around\ 1030\ cm^{-1}}{\sum Area\ of\ the\ spectral\ bands\ between\ 2000\ cm^{-1}\ and\ 600\ cm^{-1}} \quad (2.10)$$

$$I_{CH=CH} = \frac{Area\ of\ the\ ethylene\ band\ centered\ around\ 966\ cm^{-1}}{\sum Area\ of\ the\ spectral\ bands\ between\ 2000\ cm^{-1}\ and\ 600\ cm^{-1}} \quad (2.11)$$

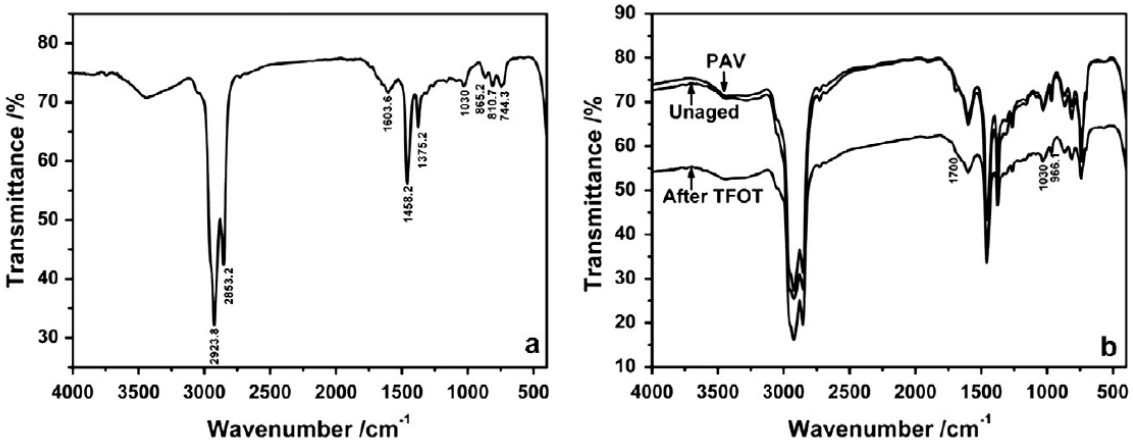

Figure 2.7 FTIR spectra of modified asphalts before and after aging and base asphalt: (a) Base asphalt (b) Modified asphalt (Zhang, Yu, *et al.* 2011)

In addition, Zhang at al. (2011) also used Tb-Layer Chromatography with Flame Ionization Detection (TLC-FID) on the four generic fractions of control asphalt binder (saturates, aromatics, resins and asphaltenes) before and after aging and found that the asphaltene and resin components increased after both short-term and long-term aging whereas the saturates and aromatics decreased. Specifically, the asphaltene content almost doubled after long-term aging which was found to be one of the prime reasons behind the change in rheological and thermodynamic properties of asphalt binder after long-term aging.

According to Shea (1998), almost all the carbonyl C=O stretching bands occur within 1870 to 1550 cm^{-1}. Ketones, esters and carboxylic acids commonly show IR absorption at 1750 to 1650 cm^{-1}. According to Han (Han 2011), the degree of the oxidation reaction in asphalt binders, thus the presence of functional groups containing oxygen such as the carbonyls is typically found at a wavenumber of about 1700 cm^{-1} (between 1650 cm^{-1} to 1820 cm^{-1}) and the content is measured as area under absorption band of this wavenumber. The changes in the concentration level of carbonyl and sulfoxide can be linked with aging index parameters to measure the oxygen uptake in binder level.

Petersen (2009) established a linear relationship between the increases in log viscosity with the carbonyl formation during asphalt oxidation. The presence of ketone compounds are another indication of the carbonyl IR absorption region because ketone can change the polarity of the accompanying aromatic ring components leading to an increase in the asphaltene portion and thus increasing the viscosity (Petersen 2009; Petersen and Glaser 2011). Another major oxidation product, sulfoxide, can also be identified with FTIR spectroscopy. In the past, sulfoxide was given less importance because it thermally decomposes at high temperature and thus making the whole analysis unreliable but Petersen and Glaser (2011) showed that for high sulfur asphalts, alcohol groups are formed due to oxidation that can have similar effects to that of ketones and increase the viscosity of asphalt binder. The amount of ketones and sulfoxides produced through oxidation depends on the source of the binder.

Yao et al. (2013) observed the change in amount of aromatics and aliphatics, in addition to the change in carbonyl and sulfoxide component, while performing FTIR analysis on the rheological properties of nanoclay and carbon microfiber modified asphalt binder. In this study, the spectral performance of the aliphatic, aromatic, ethylene, sulfoxide and carbonyl bands were investigated and the change in the ratio compared. DSR and FTIR tests were employed on unaged, RTFO aged and PAV aged control binder and binder mixed with polymer modified nanoclay to evaluate macro and micro-properties of modified asphalt binders. Yao et al. (2013) used same ratio as Zhang et al. (2011) to calculate sulfoxide and ethylene band but considered 1690 cm^{-1} as center for carbonyl band. The rest of the ratios were as follows:

$$I_{C-H\ of\ CH_3} = \frac{Area\ of\ the\ aliphatic\ branched\ band\ centered\ around\ 1376\ cm^{-1}}{\sum Area\ of\ the\ spectral\ bands\ between\ 2000\ cm^{-1}\ and\ 600\ cm^{-1}} \quad (2.12)$$

$$I_{C-H\ of-(CH_2)n-} = \frac{Area\ of\ the\ aliphatic\ index\ band\ centered\ around\ 1460\ cm^{-1}}{\sum Area\ of\ the\ spectral\ bands\ between\ 2000\ cm^{-1}\ and\ 600\ cm^{-1}} \quad (2.13)$$

$$I_{C=C} = \frac{Area\ of\ the\ aromatic\ band\ centered\ around\ 1600\ cm^{-1}}{\sum Area\ of\ the\ spectral\ bands\ between\ 2000\ cm^{-1}\ and\ 600\ cm^{-1}} \quad (2.14)$$

This research also confirmed carbonyl index as an aging parameter of asphalt binder since it increased significantly after PAV aging due to the oxidation reaction between oxygen from the air and the hydrocarbon of asphalt. The asphaltenes and the resins of asphalt binder form aromatic hydrocarbon by reacting with the oxygen through the aging process decreasing the ratio of asphaltenes and resin index. The difference between aromatic and aliphatic hydrocarbon is that aromatic exists with a planar structure stacking over each other and could have double or single bonds between carbon rings whereas aliphatic exists as a non-planar structure (Tang and Isacsson 2006; Leontaritis and Ali Mansoori 1988; Ali Mansoori 1997). The researchers found a decrease in aliphatic index ratio and an increase in aromatic index ratio after aging in the modified asphalt binder in comparison to the control binder. This is due to the reaction of maltene faction of aliphatic hydrocarbon with oxygen which produce asphaltenes. These asphaltenes again hydrogenate into aromatic hydrocarbon resulting in an increase of aromatic index ratio. The wavenumber of relevant characteristic main bands followed by Yao et al. (2012) are presented in Table 2.2.

Table 2.2 Assignations of the main bands of the FT-IR spectra (Larsen *et al.* 2009)

Wavenumber (cm^{-1})	**Assignations***
3594, 3735	νO-H
2924, 2853	νC-H aliphatic
1735	νC=O
1700	νC=O conjugated
1600	νC=C aromatic
1460	δC-H of $-(CH_2)_\pi-$ (aliphatic index)
1376	δC-H of CH_3 (aliphatic branched)
1030	νS=O sulfoxide

*ν = Stretching, δ = bending.

In a recent study, Yao et al. (2015) observed the effect of aging on asphalt binder under the conditions of dry and sufficient oxygen and performed extensive analysis on the quantitative change in functional groups of asphalt binder containing carbonyl compound. After FTIR analysis, six functional groups (shown in Figure 2.8) responsible for aging were identified and related to the susceptibility of fatigue and rutting of asphalt mixtures.

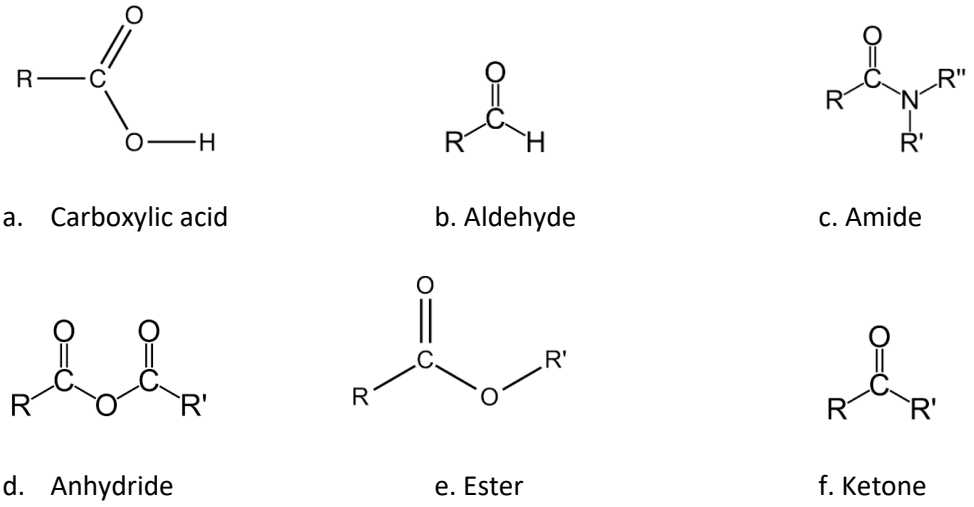

Figure 2.8 Six functional groups containing the carbonyl group (Yao *et al.* 2015)

Figure 2.9 displays the results of the ratio calculations of the control and nano-modified asphalt after PAV aging. The amount of carboxylic acid was found to be the largest among the carbonyl functional groups and increased after long-term aging. Ketones and amides also increased after PAV aging.

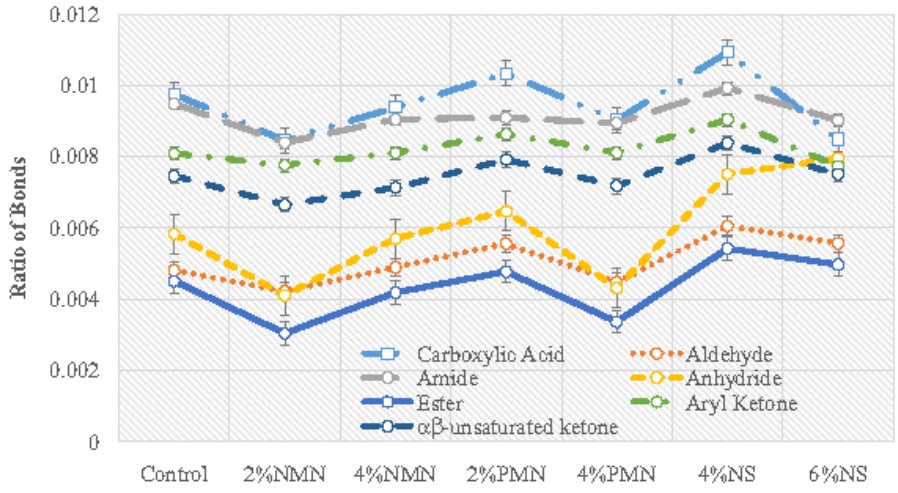

Figure 2.9 Ratio calculations of different bonds in the control and nano-modified asphalt after PAV aging (Yao *et al.* 2015)

2.5 Characterization of Oxidative Aging of Asphalt Binder using Gel Permeation Chromatography

Chromatography, a separation method invented by the Russian scientist Mikhail Tsvet (1901) (Agilent Technologies 2016), is one of the most useful analytical method since it can isolate mixtures in a sole step and measure the amount of every constituent and their relative quantities. Gel permeation chromatography (GPC)/size exclusion chromatography (SEC) is one type of liquid chromatography where the separation mechanism depends on the molecular size of the sample solution.

2.5.1 *Theory of GPC/SEC*

The fundamental mechanism of the GPC consists of two phases: the stationary phase and the mobile phase (Agilent Technologies 2016). The stationary phase inside the column consists of pores of beads in a stagnant gel like liquid. The mobile phase is the flow of the mixture of solvent with test material which goes inside and elutes from the column through the pores of the beads. The separation takes place inside the pores depending on the particle size of the sample. GPC/SEC has a pump that pushes the solvent through the apparatus. There is an injection port which introduces the test specimen inside the column. As mentioned earlier, the column holds the stationary phase. The detectors identify the components when they exit

the column. The whole setup is connected with a computer and can be controlled with a software where the results can be viewed.

Typically, the test specimen is first dissolved in a solvent. Once dissolved, the long chain of hydrocarbon breaks and forms a coil like ball of string such as tiny spheres which are led into the mobile phase and flown through the GPC column. The size of the spheres is very important since larger sphere indicates higher molecular weight. When the dissolved molecules move through the beads of the GPC column, following processes take place (Agilent Technologies 2016):

i. Spherical coils larger than the biggest pores of the beads get carried by the mobile phase directly and get excluded from the column since they cannot enter any pores.
ii. Spheres slightly smaller than the largest pore enter those pores but not the smaller pores and thus occupy some of the stationary phase.
iii. Spheres smaller than smallest pores enter almost all of the pores and occupy the stationary phase.

The smaller spheres take a long time and exit the column slowly whereas the larger bodies take much less time to elute from the column. This entire process depends on both the molecular size of the sample and pore size of the beads. The process of elution and particle separation is presented in Figure 2.10.

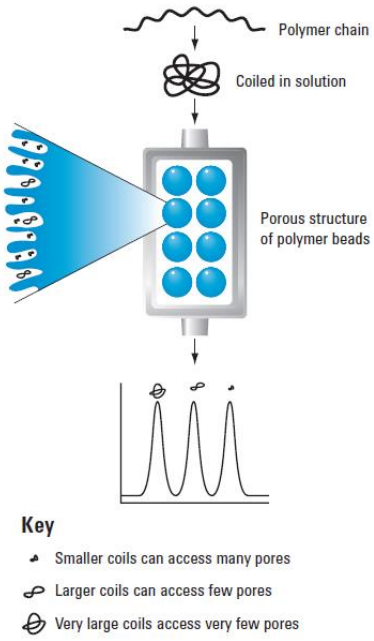

Figure 2.10 Separation of molecules based on their size in GPC (Agilent Technologies 2016)

A fraction of molecules (same size) may stay longer or lesser period of time in the column. This time required to elute is known as the retention time which is detected through various detectors and represented in the chromatogram as the amount of material eluted over time. The materials with large molecular weight elutes first and then the lower ones. The chromatogram data is compared with calibration graph consisting of elution behavior of standard samples with known molecular weight. This helps to calculate the molecular weight distribution of the target specimen and predict its performance. It should be noted that the separation mechanism in GPC is entirely based on molecular size which is a physical property of the sample, not any chemical property.

GPC is primarily used to:

i. characterize different types of compounds and isolate mixtures into distinct fractions,
ii. avoid damage in delicate compounds during testing in chromatography by using low pump pressure.

2.5.2 *Calculation of Molecular Weights in GPC/SEC*

There are some abbreviations used to define the molecular weight distribution, such as the M_n, M_w, M_z and M_p (see Figure 2.11). M_n is known as the 'Number-Average Molecular Weight' which is the calculated average of the weight distribution. M_n defines the value at which there are equal numbers of molecules on each side, at both lower and higher molecular weights. M_n affects the thermodynamic properties of the molecule (Equation 2.15) (PolyAnalytik 2016).

$$M_n = \frac{\sum c_i}{\sum c_i / M_i} \tag{2.15}$$

where, c_i and M_i are the concentration and molecular weight of an arbitrary fraction *i,* respectively.

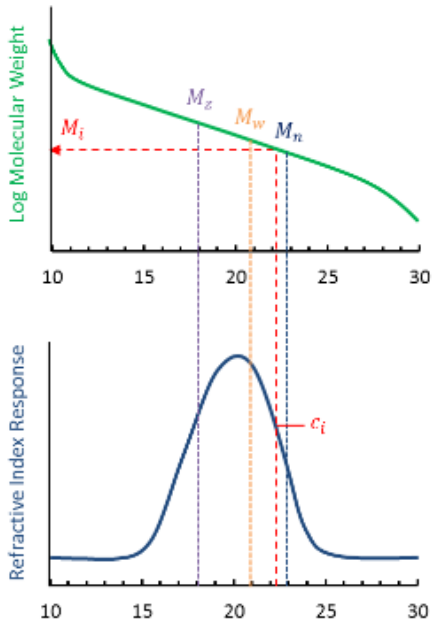

Figure 2.11 Molecular weight parameters in terms of a symmetrical distribution (PolyAnalytik 2016)

M_w, the 'Weight-Average Molecular Weight', defines the value at which there are equal masses of molecules on each side, at higher and lower molecular weight. M_w is sensitive to large molecules and influences the toughness of the material (Equation 2.16).

$$M_w = \frac{\sum M_i c_i}{\sum c_i} \tag{2.16}$$

M_z, the 'Z-Average Molecular Weight', takes into account the higher molecular weight components of the sample. M_z is sensitive to molecules with larger size and influences viscoelasticity of the material (Equation 2.17).

$$M_z = \frac{\sum M_i^2 c_i}{\sum M_i c_i} \tag{2.17}$$

Nonetheless, these parameters cannot be measured directly because standard GPC detectors are not able to count the number of molecules that get excluded from the column (Agilent Technologies 2016). So, the weight averages are calculated by measuring the concentration of molecules in respect to weight or volume by means of a concentration detector. Molecular weights are often expressed in the form of logarithm since values can be very large.

2.5.3 *Findings of Previous Research Studies*

As the values of the molecular weight of a material affect certain properties such as elasticity, toughness and brittleness, GPC has been widely used to characterize oxidative aging of asphalt binder by measuring the change in molecular weight distribution of chemical functional groups containing oxygen. It has been observed that small alterations in these values might cause major differences in the chemical and physical behavior of asphalt material.

Lu and Isacsson (2002) used the high performance GPC to measure the change in amount of fraction (large molecules) of molecular weight of bitumen due to aging in TFOT and RTFOT. Waters 515 HPLC pump fitted with Waters 410 differential refractometer was used in the analysis. Columns were filled with ultra-styragel and three columns were used pore sizes of 100, 500 and 500 A°. The system temperature was 35°C. The solution was prepared by mixing asphalt binder (5% by weight) with tetrahydrofuran. The injector delivered 50 µl sample solution into the column at a time. The pump maintained the flow rate of the THF mobile phase at 1 ml/min. Series of polystyrene standards were used to calibrate the system before testing.

Figure 2.12 demonstrates a comparative change in molecular weight and amount of unaged and TFOT aged bitumen. The particles with large molecular size elutes first and then the smaller one. The Fraction-I in the Figure 2.12 corresponds to large particles and Fraction-II

corresponds to smaller molecular size. Due to aging, the content of Fraction-I (the large molecules) increased while Fraction-II decreased by oxidation. This change of Fraction I and II content due to aging influences the increment of molecular weight and polydispersity (Mw/Mn) in asphalt binder. Hattingh (1984) and Dukatz *et al.* (1984) also confirmed the contribution of smaller particles (Fraction II) in the increase in fraction content of larger molecular size (Fraction I). This is also an indicator of the formation of polar functional groups in asphalt binder through oxidative aging. The GPC results of a test binder are summarized in Table 2.3.

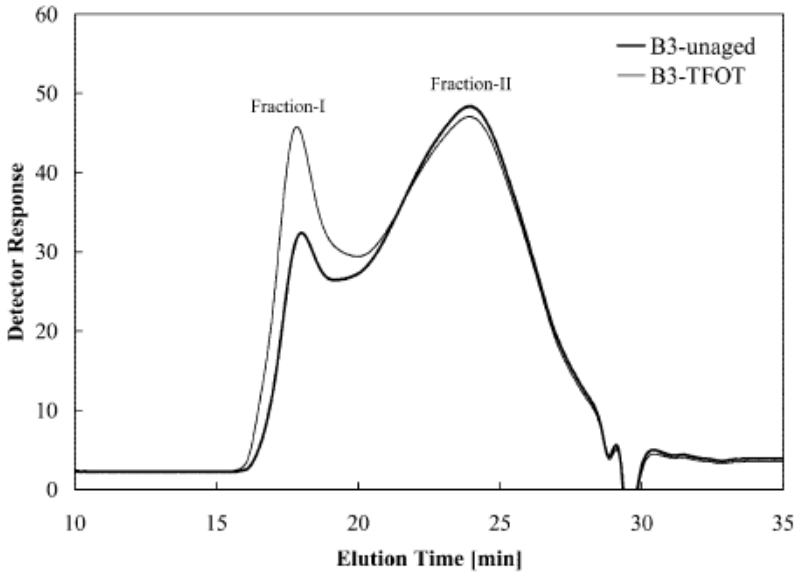

Figure 2.12 Effect of aging on asphalt GPC chromatogram (Lu and Isacsson 2002)

Table 2.3 Effect of aging on bitumen GPC parameters (Lu and Isacsson 2002)

Bitumens	Mn	Mw	Mw/Mn	Mn-I	Mn-II	Mw-I	Mw-II	I-%	II-%
B3-unaged	670	3320	4.95	10000	547	12300	1340	18	82
B3-TFOT	742	4430	5.97	8940	526	12200	1170	29.4	70.6
B3-RTFOT	753	4580	6.08	8810	526	12200	1140	30.9	69.1

Lee at al. (2008) conducted research on the effect of aging by RTFOT and STOA methods using the GPC on nine asphalt binders. The GPC test results showed that STOA method had more aging effect on asphalt mixtures compared to RTFOT method. The GPC was found effective in

evaluating the asphalt binders modified with rubber. Previous studies showed that the increase in the large molecular size (LMS) affects the viscosity and stiffness of asphalt binder and resulting in an increase in both of the parameters (Jennings 1980; Kim and Burati 1993). Lee at al. (2008) analyzed both RTFO aged and short-term field aged binders to measure the molecular weight distribution using the Waters GPC equipment equipped with a Waters 410 DRI meter as a detector and Waters 3 and HR 4E columns connected in series for separating the elements of asphalt binder by molecular size. The specifications of the columns used are shown in Table 2.4. To keep the temperature constant, the columns were kept inside an oven at 35^{o}C.

Table 2.4 Effective molecular weight range with pore sizes (Lee *et al.* 2008)

Column	**External length (cm)**	**Pore size (Angstrom)**	**Effective molecular weight range (ps)**
Styragel HR 3	30	1000	500-30,000
Styragel HR 4E	30	Mixed bed	50-100,000

The mixture for the mobile phase was prepared by dissolving the binder at a concentration rate of 0.5% by weight in tetrahydrofuran and filtered through a 0.45 µm syringe before injecting into the system. It required almost 30 minutes to perform each test and elution time was found from 11 to 21 minutes. Large molecular size (LMS) data was calculated from three test replicates. Figure 2.13 shows a typical chromatogram of control unaged and short-term aged binder. The area under the curve of the chromatogram profile was divided into 13 slices (Figure 2.13) as follows:

i. Slice 1 to 5: large molecular size (LMS)
ii. Slice 6 to 9: medium molecular size (MMS)
iii. Slice 10-13: small molecular size (SMS)

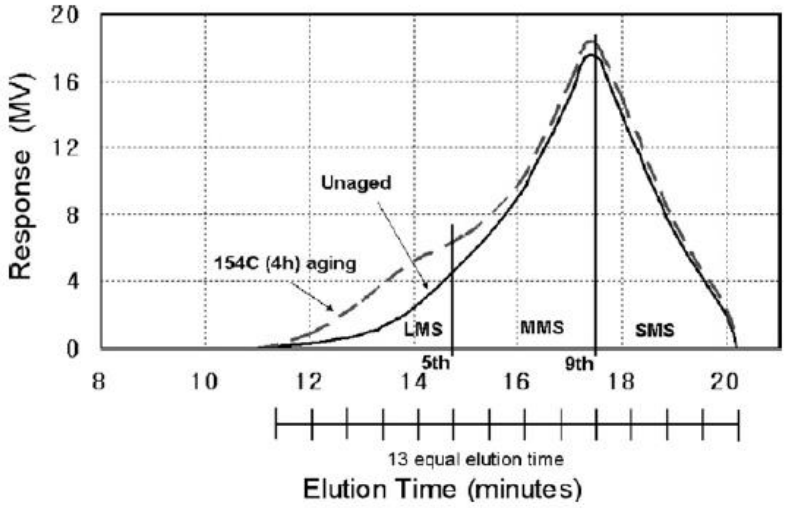

Figure 2.13 Typical chromatograms of a virgin binder (unaged) and a short term aged binder (Lee *et al.* 2008)

Ding et al. (2016) investigated the effect of intermolecular interaction between the unaged and aged binders using GPC to characterize the change in molecular association. Since asphalt binder is in the form of colloid, molecular association between different types of binder impact the properties of the mixed binder (Gray *et al.* 2011). GPC was used to study the molecular association since GPC chromatograms are affected by the molecular association of the different particles present in asphalt binder (Branthaver 1993; Herrington and Ball 1996). Ding et al. (2016) evaluated the effect of blending Reclaimed Asphalt Pavement (RAP) and Reclaimed Asphalt Shingles (RAS) with control binder and measured the degree of intermolecular interaction during mixing. It was found that different factors such as the percent binder content of aged binder, chemical composition of both unaged and aged binder and the large molecular size obtained from GPC test affect the degree of interaction. When difference in the chemical composition between unaged and aged binder is higher, more intermolecular interaction is found. Also, the large molecules were more active in terms of intermolecular interaction. For both RAP and RAS, in the LMS and MMS region, linear relationship was found between the mean signed difference and the aged asphalt binder content.

Sheng at al. (2016) developed a testing procedure to evaluate the effect of Warm Mix Asphalt (WMA) in mixing RAP/RAS with virgin binder using GPC. The WMA additives improves the compaction of asphalt mixtures by reducing the overall viscosity of the blend and reduces the rate of aging by lowering the mixing temperature. Since GPC was found to characterize the blend of WMA with RAP/RAS in terms of their LMS (%), Sheng et al. (2014), proposed the use of GPC in the asphalt blending process. The effect of WMA on the mixing of used RAP/RAS mixtures with fresh binder was evaluated by analyzing their LMS (%) and calculating the respective blending ratio.

2.6 Effect of Aging on Asphalt Binder Microstructure using Atomic Force Microscope

Due to the limited understanding of the micromechanical behavior of asphalt, it is often difficult to predict the service life of HMA. The varying chemical and structural compositions of crude oil source and the complex rheological and thermoplastic behavior of asphalt add more complexity. Advanced microscopy techniques such as Scanning Electron Microscopy (SEM), Atomic Force Microscopy (AFM), transmission electron microscopy and phase contrast microscopy are used to study the surface topography and physical properties of asphalt binders.

2.6.1 *Theory and Mechanism of AFM*

Conventional microscopes such as the optical and electron microscopes can generate image in 2D only. The vertical dimension of the surface irregularities cannot be measured with these microscopes. With a sharp tip that probes upon the surface, AFM can not only scan the surface topography with high magnification factor (up to 1,000,000X) but also measure the Z-dimension, with higher resolution than X-Y plane. Since it is a mechanical imaging instrument, it can measure physical properties of the sample in addition to imaging. This is the reason why AFM is a widely used tool in the study of asphalt microstructure. It can be used in surface topography, phase separation and mechanical properties such as adhesion and stiffness at the Nano scale.

Figure 2.14 shows a basic set-up diagram of an AFM. It has the following components (West 2006):

a. Piezoelectric Transducers: The purpose of the piezoelectric transducer is to convert the electric potential to mechanical motion. This controls the motion of the probe when moving across the sample surface. The transducers are typically crystalline or amorphous which changes geometry when subjected to potential difference at the two ends. The amount of change in shape depends on the type of the piezoelectric material and the magnitude of electric potential applied. If the expansion coefficient of a piezoelectric material is 0.1 nm, then the material will expand 0.1 nm if a potential of one volt is applied.

b. Force Transducers: The purpose of the force transducer is to measure the force between the sample surface and the probe. If the probe touches the sample surface, the force transducer gives an electrical signal which is amplified with an amplifier. The signal increases monotonically with the increase in force between the sample surface and the probe. Typical capability of a force transducer is up to 10 Pico Newton.

c. Feedback Control: Feedback controller continuously monitors the force between the sample surface and the probe tip and wheels the piezoelectric ceramic responsible for the relative distance between the sample surface and the probe tip.

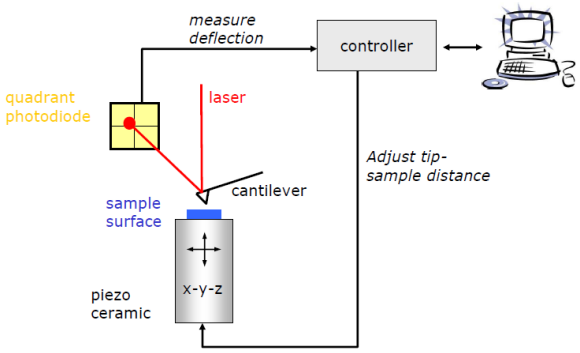

Figure 2.14 Basic AFM set-up (Kronenberger 2006)

These three components of an AFM help to put an image together. The force transducer measures the force between the sample surface and the probe tip, the feedback controller retains a fixed force by regulating the height of the Z piezoelectric transducer and the X-Y piezoelectric ceramic moves the probe in the horizontal plane upon the sample surface. The electric potential from the Z piezoelectric ceramic is then converted into an image.

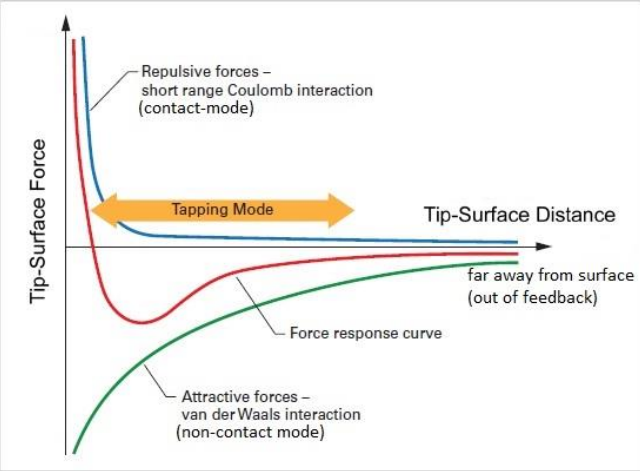

Figure 2.15 Atomic Interaction (force-separation curve) (West 2006; Zang 2016)

When the probe tip and the sample surface are not in contact, following forces (Figure 2.15) tend to occur (Zang 2016):

a. Repulsion: When the sample surface and the probe tip are very near (within a few Angstroms), an exchange interaction occurs among the atoms of the sample and the tip since their electronic orbitals overlap at such atomic distance. This short-range Coulomb interaction creates an intense repulsive force between the tip and sample surface.
b. Attraction (Van der Waals): Due to the intermolecular Van der Waals forces, resulting from the polarization interaction of nearby particles, an attractive force occurs between the tip and sample surface.

An AFM can be operated in the following modes: contact mode (CM), non-contact mode (NCM) and spectroscopy mode (SM) (Zang 2016). Each of the mode has their advantages and condition for appliance. In SM mode, the micromechanical properties of a sample can be obtained by moving the probe tip vertically, in respect to the test surface. NCM mode is useful for examining elastic or soft samples like asphalt binder since the force exerted is much less than CM mode. Despite its multi-faceted capability, AFM has some limitations and problems. A common problem when measuring with AFM is artifacts in images. The four primary sources of artifacts are the probe tip, piezo-scanners, image processing or feedback and vibrations (West and Starostina 2009). To minimize the likelihood of probe artifacts, the probe geometry

should be much smaller than the features of the images being measured. Using a probe that is not the optimal size for the application can result in features on a surface appearing too large, features in an image appearing too small, strangely shaped objects or repeating strange patterns in an image (West and Starostina 2009).

2.6.2 *Previous Research on AFM Analysis*

Several factors affect the mechanical properties of asphalt including temperature, repetitive loading, time/rate of loading and aging. Various distresses in HMA are directly dependent upon the mechanical behavior of asphalt binder. It is required to make sure that the asphalt binder used in the mix should be able to resist fatigue or temperature cracking, rutting and other distresses. To improve the quality of asphalt binder during either the process of refining or by applying additives, proper understanding of the chemical components of asphalt is required.

About 82 to 88 % of asphalt is carbon and 8 to 11 % is hydrogen. However, there are presence of heteroatoms of oxygen, sulfur and nitrogen which are responsible for the polarity in asphalt (Lesueur 2009; Petersen 1984b). Based on the source of crude oil and the refining process, the chemical components vary from binder to binder. Since the amount of each chemical component in asphalt binder is extremely diverse, it is sensible to categorize the components of asphalt binder based on their different characteristics rather than modeling the engineering properties of each of the component. Among the common characteristics such as polarity, ionic character and molecular size distribution, polarity is more suitable in relating asphalt binder rheological properties with the chemical properties.

The Saturate, Aromatic, Resin and Asphaltene (SARA) analysis divides the asphaltenes and maltenes of asphalt into four polar fractions commonly known as the Saturates, Aromatics, Resins and Asphaltenes where the Asphaltenes are the most polar and the Saturates are the least polar. Several researchers strained to relate the amount of polar fractions present in asphalt with their engineering properties. Corbett (1969) confirmed that the presence of more aromatics and saturates soften the asphalt, but asphaltenes and resins increase the stiffness. Dealy (1979) showed that the asphalt becomes more viscous if the asphaltene quantity is

increased and vice versa for maltenes. After analyzing binder chemistry at molecular level, Robertson et al. (1991) found that polar molecules affect the elastic part of asphalt's viscoelastic behavior whereas the non-polar part affects the viscous part. However, after investigating physical and chemical properties of asphalt binder from two different sources, Michalica et al.(2008) found that the binder that had lower asphaltene content exhibited more stiffness than that with higher asphaltene content. This finding confirms that stiffness of the binder cannot be directly related to the SARA fractions since the mechanical and physical properties of these components vary from source to source. In addition, it is not wise to conclude that an asphalt binder could have higher stiffness just because the asphaltene content is high. These finding led to the study of asphalt microstructure to better explain and relate the chemical and physical properties of asphalt with microscopic tools like AFM.

Researchers frequently observed the "bee" like structures in the dispersed phase of aged binder with AFM and proposed their presence as a correlation between increased amount of asphaltene and consecutive higher stiffness of the binder (LOEBER *et al.* 1996; Pauli *et al.* 2001). In later work, Pauli et al. (2011) hypothesized the presence of bee structures in asphalt as a result of aliphatic chains. Jäger et al. (2004) used AFM in non-contact mode (NCM) and spectroscopy mode (SM) to provide insight into surface topography and mechanical properties of two asphalt binders at room temperature. They also observed the randomly distributed "bee-shaped" structures in the topography images in both types of asphalt (Figure 2.16c). In the surface topography, the alternating lower and higher elevations form the bees. They did not find any association with the change in topography with alternating asphalts. However, they identified four subdomains from the analysis of surface topography, each having different mechanical properties. The areas of the surface with higher stiffness exhibited lower adhesion and vice versa.

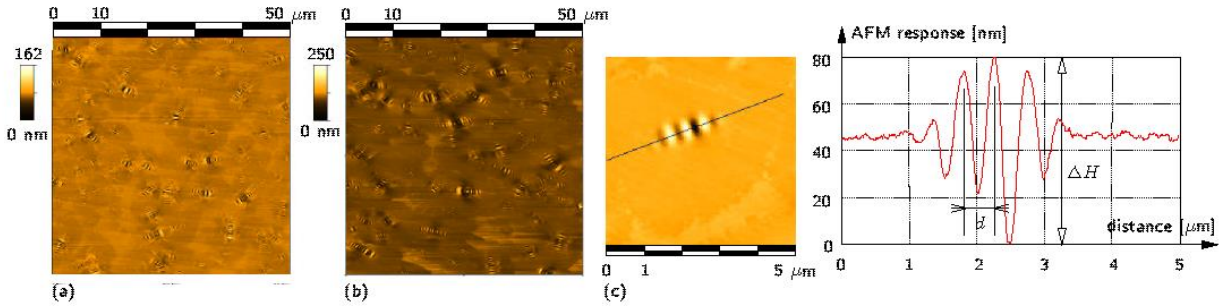

Figure 2.16 Topographic image of (a) B50/70; (b) B160/220 binders; (c) characteristic dimensions, *d* (nm) and *ΔH* (nm) of a bee (Jäger *et al.* 2004)

To understand the stiffness behavior of the four subdomains, the relative stiffness was measured by averaging the stiffness value from specific locations of the associated plots. The bee structures were found to be surrounded by hard-matrix phases of higher stiffness areas.

Masson et al. (2006) investigated 13 bulk specimens of asphalt binder. They prepared each sample to test in AFM by heat-casting method. This method ensures the solid-state structure of asphalt since in solid-state of asphalt, the rheological properties are dominant. Masson et al. (2006) used phase detection microscopy (PDM), an intermittent contact AFM mode, to obtain phase-lag and topographic images at room temperature (Figure 2.17a). The AFM was a JEOL JSPM-5200 machine. MikroMasch probes with beam-shaped cantilevers were used. The tip radius, spring constant and free resonance frequency of the probe were 10 nm, 40 Nm^{-1} and 160 kHz, respectively. Images were taken at several locations of the surface of each sample. Similar “bee structures” were observed. However, previously unseen morphologies of the binders were classified into three groups. The first group exhibited a fine dispersion (0.1–0.7 µm) in a homogenous matrix. The second group displayed domains of about 1 µm. The third group revealed up to four different phases termed as ‘catana’, ‘peri’, ‘para’ and ‘sal’ phases, which were found of vastly different sizes. Masson et al. (2005) also performed the topographic profile analysis on the catana phase, i.e., bee structures found in the PDM images.

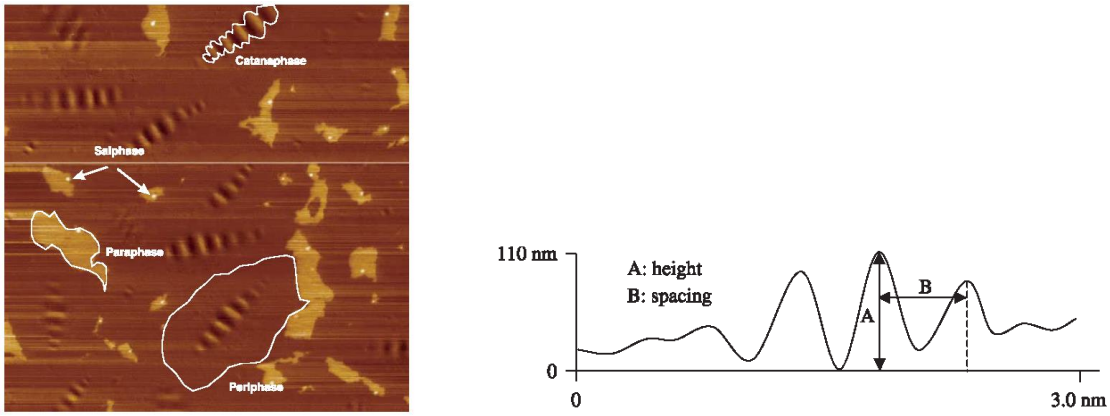

(a) (b)

Figure 2.17 (a) PDM image of a typical binder (15 µm × 15 µm) with all the identified phases, (b) Typical line profile from topographic image (Masson *et al.* 2006)

They also performed the elemental analysis in each bitumen type and correlated the metal content (in parts per million, ppm) with the % area of catana phase. The area was calculated with an image analysis software (Clemex SPM). The saturate (S), polar aromatic (PA), asphaltene (As) and naphthene aromatic (NA) compositions did not show any correlation with the PDM morphology. However, this research showed a good correlation between the area of the "bees" from PDM images and the elements in asphalt such as vanadium and nickel (Figure 2.18). This indicates that binder morphology and molecular arrangement seem to be partly governed by the polarity of the metallic cations.

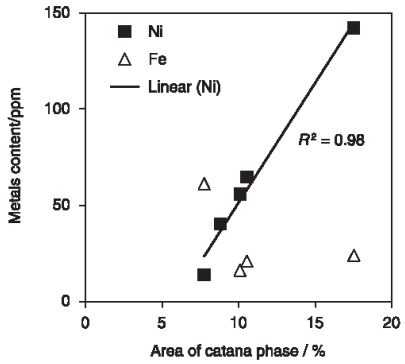

Figure 2.18 Correlation between the nickel and iron contents and the area of the catana phase in PDM (Masson *et al.* 2006)

Allen et al. (2012) studied the micro-rheology of these phases using AFM before and after oxidative aging upon six SHRP designated binders and presented differences between the

properties amongst the various microstructures within test asphalt binders. In addition, they evaluated the influence of oxidative aging on the properties of test binders. Nano-indentation creep measurements of each phase-separated regions showed heterogeneous domains in asphalt with different mechanical properties. Oxidative aging caused considerable microstructural changes within these domains, including variations in phase structure, properties and distribution. Clustering, phase dispersion and materialization (bee structure) are the three typical microstructural changes observed in this study. Prior to aging, asphalts AAB, AAD and ABD each consisted of two distinctive phases: dispersed and continuous. Aging increases the percentage of higher stiffness components in asphalt binder which is the prime reason for increase in stiffness after aging. In addition, the dispersed and continuous phase also showed an increase in stiffness.

The Agilent 5400 AFM system was operated in NCM for phase imaging and SM for nanoscale indentation to estimate the micro-mechanical properties of asphalt. The testing was performed with a Silicon Nitride tip mounted on the free end of a conical shaped PPP-NCL cantilevers. The average resonant frequency of the cantilever was 175 kHz and a force constant ranging from 21 to 98 Nm^{-1}.

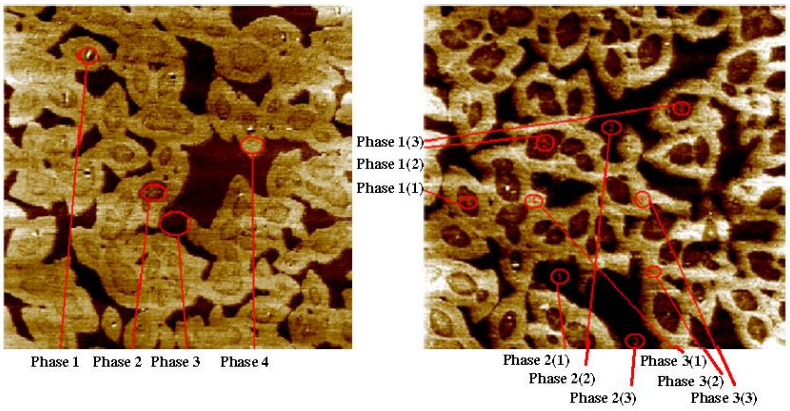

Figure 2.19 Phase images of binder AAB and location of force measurements (25 µm × 25 µm) (Allen *et al.* 2012)

Allen et al. (2012) identified the distribution of different phases in each asphalt types (Figure 2.19), compared the deflection in each type (Figure 2.20b), and observed the line profile (Figure 2.20c) to see variation in the surface of each phase. They conducted creep

measurements to differentiate the time-dependent creep-like deformation of each identified phases between unaged and aged binders.

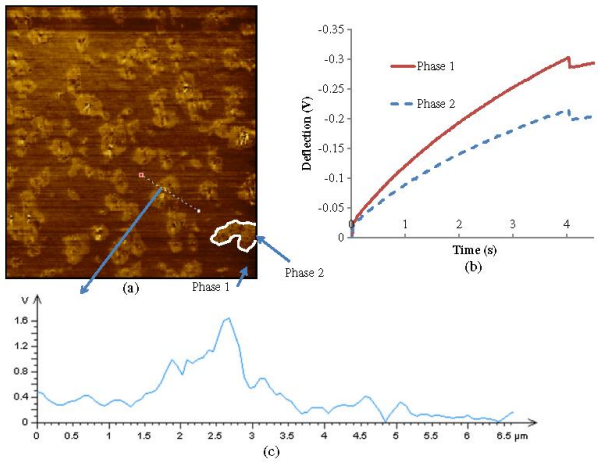

Figure 2.20 (a) Phase image; (b) creep measurements; (c) profile extraction for asphalt AAB (Allen *et al.* 2012)

Allen et al. (2012) also performed the statistical analysis (Table 2.5) of the surface texture, roughness and topography fluctuations to assess the microstructural phase differences of each asphalt types. A notable observation from the comparison of surface texture statistics is that S_p, S_v and S_z increased for each asphalt due to aging, which clearly shows that age-induced structural phase change is also accompanied by increased roughness.

Table 2.5 Comparison of Surface Texture Statistical Analysis (Allen *et al.* 2012)

Asphalt	Surface Texture Statistics						
	S_p (nm)	S_v (nm)	S_z (nm)	S_a (nm)	S_q (nm)	S_{sk}	S_{ku}
AAB	175	155	330	76.4	88.0	0.06	1.82
AAB-aged	186	181	367	72.7	84.2	-0.11	1.88
AAD	123	123	245	54.9	63.4	-0.04	1.83
AAD-aged	134	154	288	54.2	62.0	-0.23	1.87
ABD	74	83	157	35.3	40.8	-0.05	1.31
ABD-aged	152	175	327	63.7	74.6	-0.13	2.02

Allen et al. (2014) evaluated these phases for asphalt binders with varying concentrations of the different polar fractions. They observed that oxidative aging increased the area of 'catana' phase. This finding was consistent with the results from previous studies (Lin and Meier 1995;

Petersen 1984b). Allen et al. (2014) also reported that the concentration of different polar fractions and chemical parameters present in the binder had a significant and consistent influence on the size, distribution and micro-rheology of the different phases. In addition to the imaging mode, in this study, the AFM was also operated in spectroscopy (SM) mode. The SM mode helps to measure the adhesion (pull-off force) of soft materials such as asphalt binders by moving the tip vertically with respect to the sample surface. In order to obtain qualitative pull-off force measurements in the units (nN) reported in this paper, the detected tip-deflection data, reported in least significant bits (LSB) units, were converted to units of volts (V). The data values reported in volts are then converted to nanometers, D_{max} (nm), where D_{max} is the maximum vertical raw deflection of the cantilever tip given in the respective units. Finally, the pull-off force can be computed from the following equation:

$$F_{pull-off}(nN) = D_{max}(nm)\ X\ k\ (\frac{nN}{nm}) \tag{2.18}$$

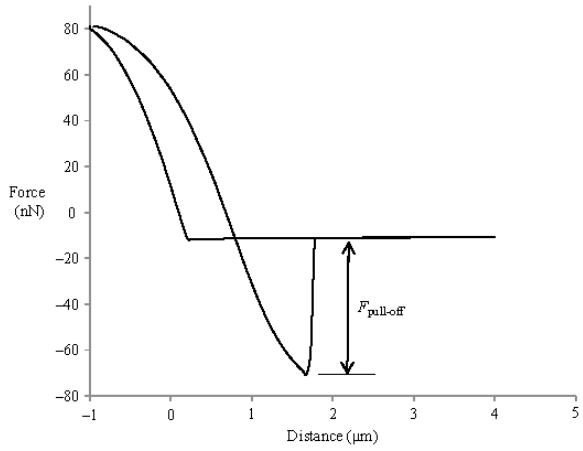

Figure 2.21 Typical force–distance plot depicting the pull-off force, $F_{Pull-off}$, between the AFM tip and asphalt surface (Allen *et al.* 2014)

The pull-off (adhesion) forces were obtained via force–distance curves by initiating an approach of the AFM tip into the asphalt followed by retraction of the tip from the asphalt. During the retraction phase of the test, the force required to remove the tip from the material surface transitions from a maximum negative force to a near-zero force, thus revealing the pull-off force of the tip-surface interaction as noted in Figure 2.21. By allowing the tips to interact with each phase of the two different asphalts, i.e. continuous, dispersed, 'bee'

structure and 'bee' casing phases, the microstructural adhesion measurements were obtained. Six measurements were extracted from each phase to perform statistical analysis of the adhesion measurements.

A study conducted by Jahangir at al. (2015) evaluates the microstructural change in asphalt binder resulting from RTFO and PAV aging. In this study, creep indentation technique was applied on asphalt binder using AFM. The creep test data was used to determine the viscoelastic properties of the various phases detected in asphalt samples from two different sources. The effect of these changes on the evolution of damage in asphalt binder subject to tensile deformation was also investigated. Numerical simulations were performed with these data to compare the effect of tensile strains on the internal stress distribution of the binder (i.e., the induced damage with the experimental results). A microloading apparatus, fabricated specifically to induce tensile strains in the binder, was used and the resulting damage was observed with AFM.

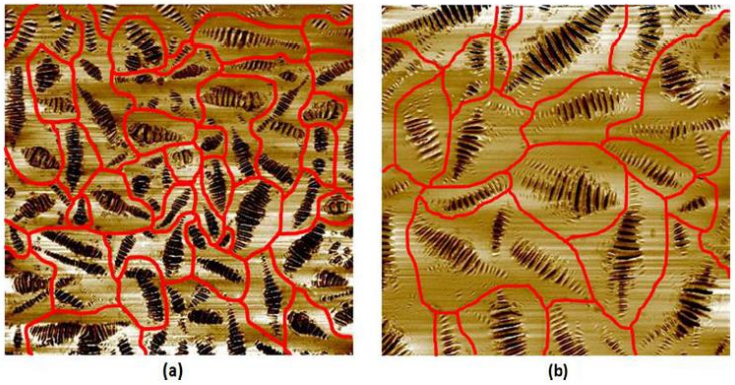

Figure 2.22 AFM phase image showing interstitial phase of asphalt binders (a) A and (b) B (50 X 50 μm^2) (Jahangir *et al.* 2015)

To quantitatively assess the changes in the microstructure due to the applied tensile strain, image analysis techniques were employed using the open source image analysis tool 'ImageJ'. Various geometric attributes were obtained and a comparison of these attributes was done before and after strain was applied to the test specimens. Due to phase separation and changes that occurred in the bee casing and interstitial phases (Figure 2.22), comparisons

were made based on the discrete bee phase. Table 2.6 compares the distribution of the bee structures before and after loading in binders A and B.

Table 2.6 Microstructural analysis of asphalt with ImageJ (Jahangir *et al.* 2015)

Strain level	Total count	Mean area (μm^2)	% Area
Before (binder A)	743	2.93	21.39
1% (binder A)	586	2.99	17.07
5% (binder A)	490	2.61	12.35
Before (binder B)	369	5.40	19.58
1% (binder B)	317	5.29	16.26
5% (binder B)	272	3.21	8.69

Both finite element modelling and test results showed that the applied strain induced a phase separation concentrated in the interstitial zone between adjacent bee structures. This phenomenon was defined as the load-induced phase separation. This study proposed that at each of the domains within asphalt microstructure, the regions with high stress intensity act as a center for damage formation. The findings of this study demonstrated that that evaluating the asphalt microstructure and micro-rheology is vital in perceiving how the damage formulates in asphalt binder and it can be better engineered to increase the overall durability.

In a recent study, Troy et al. (2014) investigated the contact adherence energy of binder thin films with AFM force-displacement mechanism. This technique utilizes ultra-thin bitumen films (500–800 nm) as test sample and a glass micro-bead cantilever tip as the test probe. The mechanism involves applying direct tension between the bitumen and glass tip when they are in contact, and consecutively fracturing and creating the adherence. The work required to fracture the contact is measured in respect to temperature and rate of separation between the tip and binder. These studies were performed to measure surface energy of asphalt binder as it relates to the fatigue properties and self-healing behavior of asphalt binder. Adhesive properties were found to be a function of separation rate and test temperature by exhibiting the transition behavior from viscous to viscoelastic nature. In this paper, adherence energy is quantified and interpreted in terms of the Derjaguin, Muller and Toporov (DMT) model (Derjaguin *et al.* 1975). Several test results also showed that at higher temperature (i.e, above the ambient temperature), the adherence energy diminishes, and the surface energy prevails.

Previous studies strongly support the notion that the amount and characteristics of different chemical components significantly affect the rheological and micromechanical properties of asphalt. However, there is a need for more research on the effect of aging on the micro-mechanical behavior of asphalt binders and the use of antioxidant additives and copolymers to retard the aging affects.

CHAPTER 3 RETARDING AGING OF ASPHALT BINDERS USING ANTIOXIDANT ADDITIVES AND COPOLYMERS*

3.1 Introduction

The United States has more than 92% of the roads paved with asphalt (NAPA-EAPA 2011). Asphalt binder gets stiffer with time which is termed as age hardening or aging. Two types of aging can occur; short-term aging and long-term aging. Short-term aging is related to the hardening occurred while mixing and compaction of asphalt mixtures, while long-term aging takes place after the pavement is laid for operation (Bell 1989). There are several causes of binder aging including loss of oily components due to volatility, oxidation and thixotropic effects or steric hardening (Bell et al. 1994). The aging of asphalt is commonly associated with changes in the mixture mechanical response. The loss of oily components of asphalt binder through evaporation increases its viscosity thus stiffening the mixture. In addition, the oxidation leads to increased amounts of chemical compounds like ketones and sulfoxides which causes the mixture to become more brittle. The embrittlement of asphalt mixtures increases the susceptibility to fatigue cracking. The fatigue parameter G*Sinδ was proposed during the SHRP research as an indicator for susceptibility of asphalt binders to fatigue damage and therefore it was included in the SuperPave Performance Grade (PG) specification. A limit value specified as per SuperPave procedures is 5000 kPa.

The viscosity of the asphalt binder when it undergoes short-term aging increases rapidly as it is mostly related to the loss of volatiles, whereas long-term aging is comparatively slower mainly because it is predominantly dictated by oxidation.

---

*Reprinted with the permission from "Retarding Aging of Asphalt Mixtures using Anti-Oxidant Additives," by Kassem, E., Khan, M. S., Katukuri, S., Okan, S., Muftah, A., Bayomy, F. (2017). *International Journal of Pavement Engineering* (IJPE), DOI: 10.1080/10298436.2017.1394098

Another cause of asphalt aging is due to steric hardening, also known as physical hardening. While the volatilization and oxidative aging change the chemical composition and molecular structure of asphalt and are irreversible, steric hardening, caused by the structural reorganization of asphalt molecules in the room temperature over time, can be reversible. Researchers found a good correlation between the ordering of asphaltenes with steric hardening (Masson et al. 2005).

A few studies were conducted to evaluate the applicability of using antioxidant additives to retard the aging of asphalt binders. Earlier studies showed that antioxidant additives provide resistance to oxidative hardening of asphalt binders. These studies involved evaluating the antioxidants using the basic physical properties like ductility and viscosity (Beitchman 1960; Martin 1968; Januszke 1971). Apeagyei (2008 and 2011) examined the effects of several antioxidant additives like Irganox 1010, Vitamin E, Hydrated lime, Carbon Black, DLTDP, and Furfural on aging of asphalt binders. In general, the results of these studies demonstrated that these antioxidants help in retarding the aging of asphalt by getting oxidized instead of asphalt binders. The most promising results were found with a combination of Furfural and DLTDP (thioester antioxidant). Furfural was first made to react with asphalt in presence of a strong acid and DLTDP was added at a later stage. According to Apeagyei (2008) and Apeagyei et al. (2008 and 2011), this combination resulted in retarding the aging of asphalt by about 43%. This combination also increased the high temperature stiffness of the asphalt binder. Apeagyei (2008 and 2011) and Apeagyei et al. (2008) used a short-term aging index as a screening tool to evaluate the effect of various additives to retard the aging of the test asphalt binders.

Williams (2008) showed that lignin, which contains ethanol co-products, can be an effective antioxidant in retarding the aging of asphalt binder. The research involved using four different asphalt binders with four different co-products. The dynamic shear rheometer and bending beam rheometer were used to assess the effectiveness of the selected antioxidant additives. The results showed that lignin had a favorable antioxidant action. In addition, Pan et al. (2012) showed that the coniferyl-alcohol lignin is a viable antioxidant for petroleum asphalt.

Reyes (2012) assessed the potential of using vitamin E as an antioxidant modifier to slow the aging process in asphalt mixtures. Two binders were considered: unmodified (PG 64-22) and modified (PG 70-22). Vitamin E was used as an antioxidant additive, while two calcium-based additives were used as stabilization agents. The stabilization agents were used to increase the stiffness of the binder due to incorporating the vitamin E, which has low viscosity. The mixing of asphalt binders with the additives was conducted for one hour using a high shear mixer at 2100 rpm. The temperature was maintained at 160^{o}C using a heating plate. Temperature sweep tests were performed to analyze the effect of these antioxidants on the asphalt binders. The results of this study showed that the use of vitamin E reduced the viscosity of the binders, but using stabilization agents such as fly ash and hydrated lime improved the stiffness of the antioxidant vitamin E-modified binders. The modified binders with vitamin E had desirable characteristics that would resist fatigue cracking; however, there was a concern about rutting resistance. The antioxidant vitamin E-modified binder had reduced stiffness, reduced modulus, and increased phase angle. Reyes (2012) suggested that further experiments be conducted to determine optimum antioxidant and stabilization agent percentages to achieve better performance with aging.

Dessouky and Diaz (2015) evaluated the effect of co-polymers with enhanced antioxidant agents on the rheological properties of polymer modified binder PG 70-22 through temperature sweep tests. The co-polymers were Solution Ethylene-Butylene/Styrene (SEBS) and Solution Styrene-Butadiene Rubber (SSBR). The researchers defined an aging index to evaluate the effect of co-polymers in reducing the brittleness of the asphalt binder. The results showed that the co-polymers improved the rutting and moisture resistance of the modified asphalt mixtures, but they decreased the fatigue life compared to the control mixture.

3.2 Scope of Chapter 3

The State of Qatar is experiencing tremendous economic growth that requires improving the sustainability of its infrastructure. Almost all roads in Qatar are asphalt pavements that are subjected to heavy traffic loading at elevated temperatures. Permanent deformation (rutting), fatigue cracking, and potholes are common distresses in pavements. The state has a subtropical arid climate with high temperatures most of the year. The average temperature

often reaches or exceeds 40^{o}C during the summer months while the pavement surface temperature often exceeds 60^{o}C. These elevated temperatures increase binder oxidation significantly, which could lead to fatigue cracking and eventually pavement failure with heavy and repeated traffic loading. The main objective of this part of the study is to explore the feasibility of using antioxidant additives and co-polymers to retard the aging of asphalt binders and evaluate the effect of antioxidant additives on the performance of asphalt mixtures. Several antioxidant additives were selected based on the reported performance in the literature and their availability. Two asphalt binders from different crude sources were evaluated. In addition, this study evaluated the influence of antioxidant additives on the susceptibility of fine portion of asphalt mixtures (FAM) to fatigue cracking.

3.3 Experimental Setup and Testing Procedure

3.3.1 *Asphalt Binders and Antioxidant Additives*

The experimental plan consisted of testing the control binders and antioxidant modified binders using a dynamic shear rheometer. The asphalt binders selected for testing were PG 64-22 and PG 67-22. The PG 64-22 is from a Qatari source, while PG 67-22 is from a Venezuelan source. Various antioxidant additives were selected based on pervious performance reported in the literature. In addition, new additives were also included. The additives examined in this study included Irganox 1010, Hydrated lime, Carbon black, Dilauryl Thiodipropionate (DLTDP), Calprene 6120, Solprene 1205, Redicote AP, Furfural, and various combinations of these additives. Table 3.1 and Table 3.2 present the testing matrix of asphalt binders with different combinations of antioxidant additives. The researchers started with the PG 64-22 testing matrix (Table 3.1) and they identified the most promising additives to be further evaluated with PG 67-22 (Table 3.2).

The Irganox 1010 is a phenolic antioxidant with high long-term heat stability. The Irganox 1010 is reported to provide resistance to thermo oxidative degradation. It comes in a form of fine powder and its melting point in between 110°C to 125°C (Mayzo Antioxidants 2016). While, the active ingredient in Redicote AP is a modified amine surfactant.

The Solprene- 1025 is a Solution Styrene-Butadiene Rubber (SSBR), consists of styrene/butadiene co-polymer with 25% styrene content and 17.5% exist as a polystyrene block. Also, the Calprene-6120 is a 68/32 Solution Ethylene-Butylene/Styrene (SEBS) thermoplastic co-polymer, and it comes in a solid pellet form.

The Dilauryl Thiodipropionate (DLTDP) is a thioester antioxidant that provides protection for several petroleum products against deterioration. The melting range is from 39°C to 42°C.

The hydrated lime is proved to reduce chemical aging of asphalt. Sebaaly et al. (2006) found that the hydrated lime had favorable effects in retarding the oxidative aging. In addition, several studies showed that Carbon black can act as a good antioxidant to retard aging. It acts as a photo oxidative stabilizer. Apeagyei (2011) illustrated that the effectiveness of carbon black could be due to many surface groups such as the quinones, phenols, carboxyphenols on its structure.

Table 3.1 Testing matrix and rheological properties of PG 64-22 asphalt binder

Additive	Unaged (G*Sinδ at 25°C) (Pa)	Std. Deviation of unaged (G*Sinδ at 25°C) (Pa)	PAV (G*Sinδ at 25°C) (Pa)	Std. Deviation of PAV (G*Sinδ at 25°C) (Pa)	Aging Index	Percent Decrease
Control PG 64-22	768	18	3435	148	4.47	-
1% Irganox 1010	851	30	3050	42	3.59	19.82
2% Irganox 1010	849	12	3135	191	3.69	17.39
1% Hydrated Lime	789	17	2795	7	3.54	20.80
2% Hydrated Lime	845	8	2635	7	3.12	30.24
3% Hydrated Lime	852	11	2830	113	3.32	25.74
1.5% DLTDP	360	11	1910	170	5.31	-18.62
3% Solprene	1370	57	3195	49	2.33	47.86
3% Calprene	1356	150	3540	28	2.61	41.63
2% Solprene	1215	120	3340	170	2.75	38.54
2% Calprene	1141	226	3310	255	2.90	35.11
1% Redicote AP	600	24	2120	269	3.53	21.00
2% Vit E	597	3	3765	49	6.31	-41.00
2% Vit E + 2% Hyd. lime	563	7	3215	205	5.71	-27.68
3% Vit E + 2% Hyd. lime	471	14	3315	389	7.04	-57.36
2% Furfural + 1.1% Hcl+ 1% Redicote AP	563	17	2650	57	4.71	-5.24
1% Carbon Black	683	42	2970	99	4.35	2.78
2% Furfural + 1.1% Hcl	829	58	3485	21	4.20	6.01
2% Furfural + 1.5% Hcl	859	4	3785	92	4.41	1.48
2% Furfural + 1.2 Hcl% + 1.5 % DLTDP	370	35	2370	42	6.41	-43.21
2% Furfural + 2 Hcl + 1.5 % DLTDP	441	58	2425	78	5.50	-22.94
1% Irganox + 1% DLTDP	505	20	2215	106	4.39	1.93
1% DLTDP	502	14	2040	14	4.06	9.14

Table 3.2 Testing matrix and rheological properties of PG 67-22 asphalt binder

Additive	Unaged (G*Sinδ at 25°C) (Pa)	Std. Deviation of unaged (G*Sinδ at 25°C) (Pa)	PAV (G*Sinδ at 25°C) (Pa)	Std. Deviation of PAV (G*Sinδ at 25°C) (Pa)	Aging Index	Percent Decrease
Control PG 67-22	671	49	3785	191	5.64	-
1% Irganox 1010	662	27	2625	64	3.97	29.70
2% Irganox 1010	588	42	2650	42	4.51	20.04
1% Hydrated Lime	520	9	3075	49	5.92	-4.93
2% Hydrated Lime	623	23	3020	184	4.85	14.06
3% Hydrated Lime	558	18	2690	71	4.83	14.46
1.5% DLTDP	375	1	1830	184	4.88	13.49
3% Solprene	790	11	3260	71	4.13	26.80
3% Calprene	1075	64	3305	78	3.07	45.50
1% Redicote AP	503	18	2050	57	4.08	27.75
2% Furfural + 1.1% Hcl+ 1.5% DLTDP	500	13	2250	85	4.50	20.22

A high shear mixer Silverson L5M - A was used for mixing the antioxidant additives with asphalt binders (Figure 3.1). The speed of the mixer can be varied from 1 to 10,000 rpm. The aluminium beads in Figure 3.1a were used to maintain the temperature during mixing. The beads were kept in the oven at the mixing temperature for 4 hours before mixing. Then, it was placed on a heating plate maintained at the mixing temperature (Figure 3.1). The temperature was continuously monitored with the heating plate and kept constant during the whole period of mixing the antioxidant additives. The asphalt binder was mixed with the additives in quarter gallon cans (Figures 3.1c and 3.1d). The weight of the binder sample in the can was about 600 grams and the antioxidant additives were added to the binder sample by percent weight. Table 3.3 presents the mixing temperature, duration, and speed (rpm) for various additives tested in this study. The Solprene and Calprene additives needed longer mixing time compared to other additives as presented in Table 3.3. To assess the effect of the mixing time on the properties of asphalt binders, the researchers measured the viscosity of two PG 64-22 pure binder samples at 135°C; one was a reference sample while the other sample was heated for 6 hours. The researchers noticed a slight increase in viscosity of about 6%.

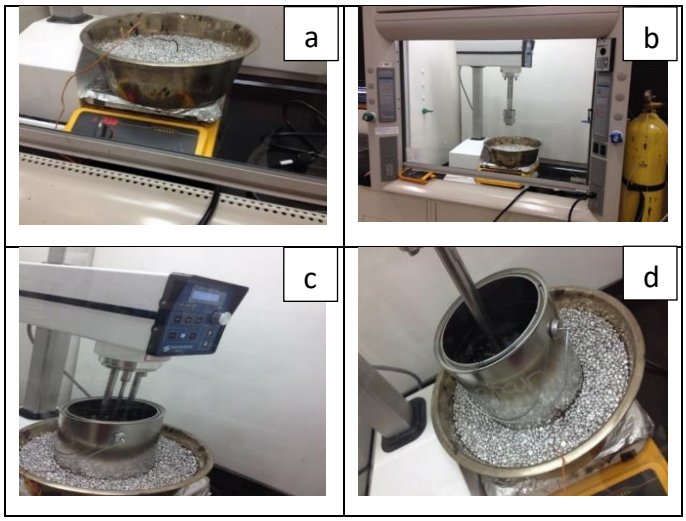

Figure 3.1 Mixing procedures with a High Shear Mixer

A dynamic shear rheometer (DSR) (Figure 3.2) was used to test asphalt binders to evaluate the effect of antioxidant additives on the change of their rheological properties. The researchers were mainly interested in the resistance to asphalt binders to fatigue since it is well established that aging affects the resistance of asphalt binders and mixtures to fatigue. Two asphalt binder samples were tested at each combination. The test was conducted at 25°C in accordance with AASHTO T 315. The complex shear modulus (G*) and phase angle (δ) were measured using the strain-controlled mode and the resistance of test asphalt binders to fatigue were evaluated by calculating G*sinδ. The G*sinδ increases with binder aging.

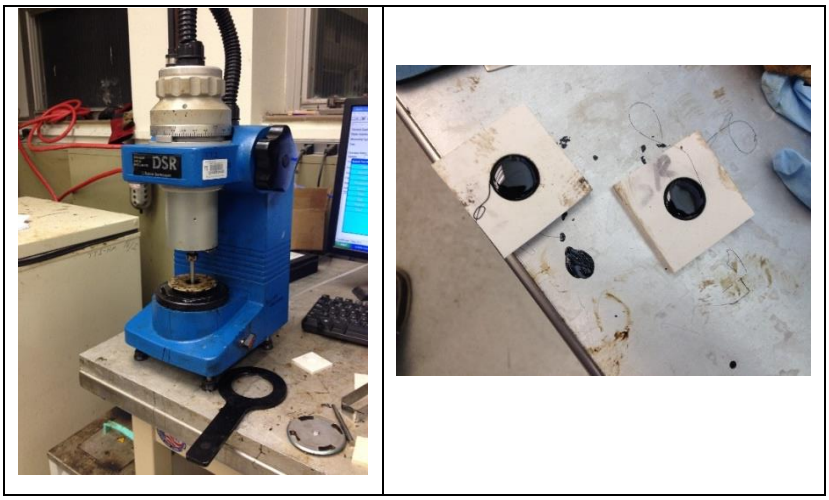

Figure 3.2 DSR and binder test samples

Table 3.3 Mixing temperature, time, and speed of various antioxidant additives

Antioxidant Additive	Mixing Temperature (°C)	Time	Speed (rpm)
Irganox 1010	125	30 minutes	750
Hydrated Lime	160	1 hour	1800-2000
DLTDP	125	45 minutes	1000-1200
Furfural	125	1-2 hours	1200-1500
Solprene 1205	170	4 – 5 hours	2100
Calprene 6120	170	7 - 8 hours	2100
Redicote AP	125	30 minutes	750-1000
Vit E	125	45 minutes	1000-1200
Vit E + Hyd. Lime	160	1 hour	1800-2000
Furfural + Hcl+ Redicote AP	125	2 - 3 hours	1500
Carbon Black	125	30 minutes – 1 hour	1000
Furfural + Hcl	125	2 - 3 hours	1000-1200
Furfural + Hcl + DLTDP	125	4 hours	1800-2000
Irganox + DLTDP	125	1 -2 hours	1000-1200

3.3.2 *Fine Asphalt Mixtures*

Fatigue cracking is a common distress in asphalt pavements and the susceptibility of asphalt mixture to fatigue cracking increases with aging. Recent work at Texas A&M University has demonstrated that the fatigue results of full asphalt mixtures are highly influenced by the heterogeneity of the internal structure of asphalt mixtures. Therefore, researchers recommend conducting fatigue testing on the fine portion of asphalt mixtures (FAM), which is more uniform and less heterogeneous before testing full asphalt mixtures (Masad et al. 2006; Masad et al. 2008). In this study, a semi-circular bending (SCB) test was conducted on FAM specimens to evaluate the effect of aging on the fracture energy and fatigue resistance. The FAM test specimens were prepared through mixing asphalt binder with the fine portion of the aggregate gradation [passing sieve No. 16 (1.18 mm)]. A SuperPave gyratory compactor (SGC) was used to compact FAM test samples with a diameter of 150 mm and a height of 58 mm, then these samples were trimmed to 44.5 mm height. Each sample was cut into two symmetric semicircular bend specimens. The notch size is 13 mm in length and 2 mm in width. One asphalt binder (PG 64-22) and two antioxidant additives (Redicote and Solprene), in addition three aggregates (gabbro, limestone and basalt) were used in the preparation of the

FAM samples as presented in Table 3.4. The limestone and gabbro aggregates, in addition to PG 64-22 binder are most common used in the road construction in Qatar. The antioxidant additives Redicote and Solprene were selected because they provided good performance with the PG 64-22 as discussed later in the paper. The binder content and aggregate gradation for the FAM mixtures were determined following the procedure proposed by Sousa et al. (2013). Figure 3.3 provides the gradation of the FAM mixtures and the binder content was calculated to be 10.5%, 7.3% and 9% by weight of mix for the limestone, gabbro and basalt mixtures, respectively.

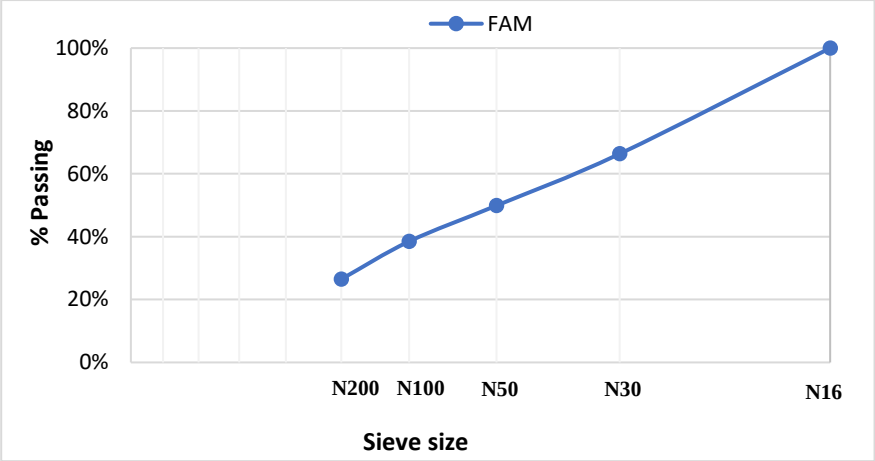

Figure 3.3 Gradation of FAM mixtures

Table 3.4 Testing matrix of FAM

Specimen Type	Aggregate	Binder Grade (PG)	Aging Condition	Asphalt Modifier/Polymers
FAM	Gabbro	PG 64-22	Unaged	Control (No modifier)
	Limestone		Aged	1% Redicote
	Basalt			3% Solprene

The SCB test was conducted according to AASHTO TP 105-13 using an asphalt mixture performance tester (AMPT). The SCB test was conducted at an intermediate temperature of 21.1°C, and performed by applying monotonic compressive loading at a rate of 0.3 mm/min. The test was terminated when the load dropped below 0.1 kN. During the test, the applied load and deformation were recorded, and the fracture energy was calculated upon

completion of the test. The fracture energy (G_f) is calculated by dividing the area under the load-deformation curve by the ligament area (Equation 3.1). It is considered as one of the indicator of asphalt mixtures ability to resist damage caused by cracking (Kim and Wen 2002; Kim et al. 2009). Another parameter called Flexibility Index (F.I.) can be also calculated from the SCB test (Al-Qadi et al. 2015). The F.I. describes the flexibility of asphalt mixtures. The flexibility increases as the F.I. increases and vice versa. Figure 3.4 shows the load-displacement curve of a typical gabbro FAM sample with the graphical representation of parameters used to calculate the F.I.

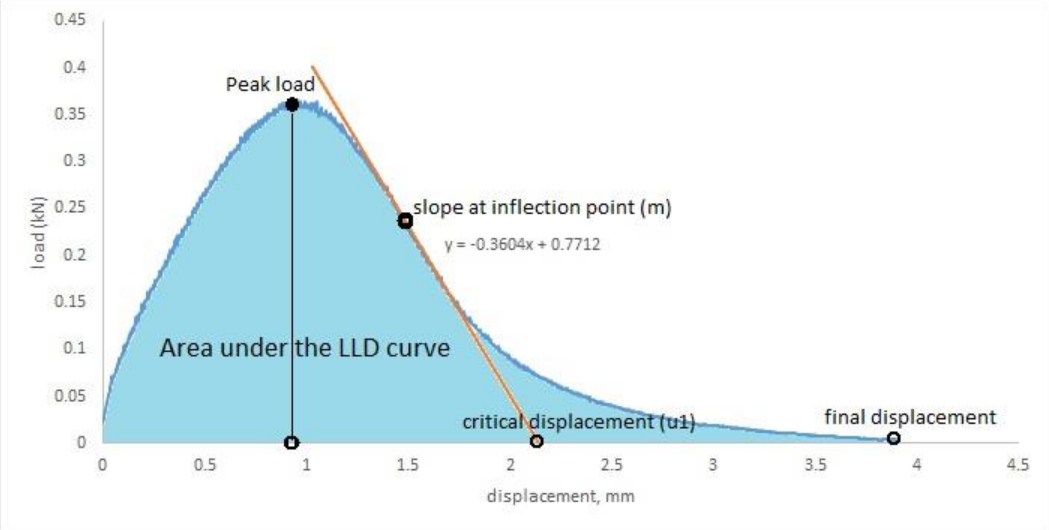

Figure 3.4 Calculation of fracture energy and flexibility index from SCB test

A study by Al-Qadi (Al-Qadi et al. 2015) on the correlation between F.I. of lab mixtures and field performance found that asphalt mixtures with F.I. less than 2 exhibited poor performance in the field whereas F.I. values of 2 to 6 exhibited intermediate performance. Samples with F.I. greater than 6 showed good results in the field. The fracture energy and the F.I. for FAM was calculated using Equation 3.1 and 3.2, respectively.

$$Fracture\ Energy, G_f = \frac{Work\ of\ fracture, W_f}{Area_{ligament}} \tag{3.1}$$

$$Flexibility\ Index = \frac{Fracture\ Energy, G_f}{absolute\ value\ of\ post-peak\ load\ slope, |m|}\ x\ 0.01 \tag{3.2}$$

where, Area of the ligament = thickness of the SCB sample x (radius – notch depth)

Work of fracture W_f = the work required to fracture a unit surface area of SCB specimen

Post-peak slope |m| = the slope of the tangent drawn at the first inflection point after the peak of the load-displacement curve

Figure 3.5 shows the SCB mastic sample after preparation and during testing using the AMPT.

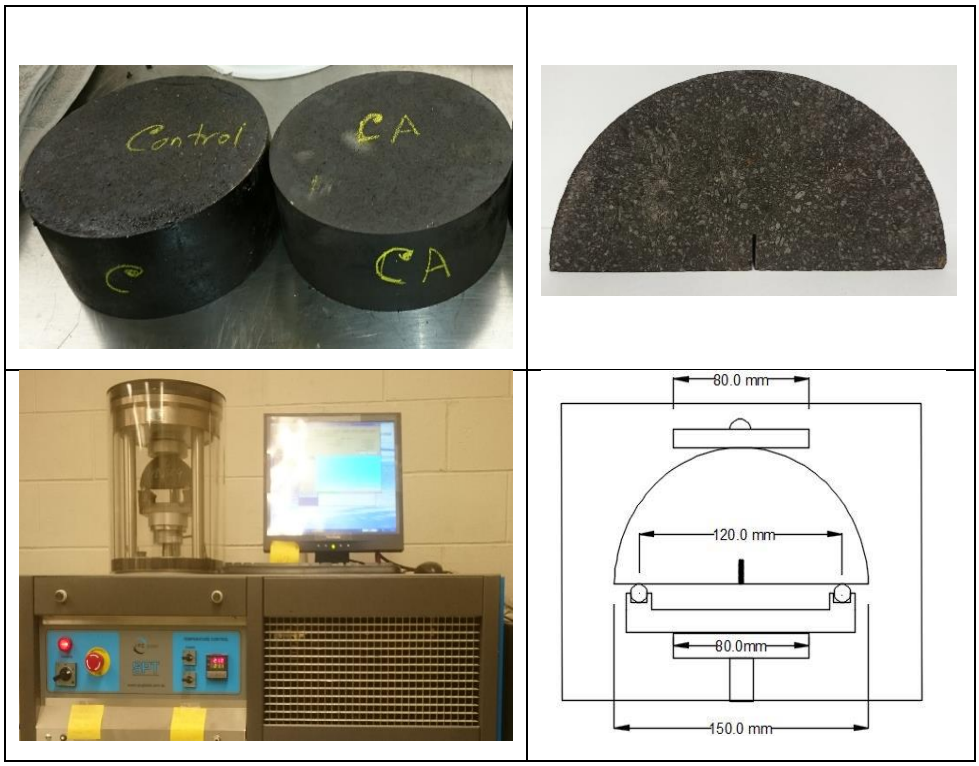

Figure 3.5 SCB mastic preparation and testing

3.3.3 *Simulating Long-Term Aging of Asphalt Binders and FAM*

in order to evaluate the effect of antioxidant additives to retard the aging, the asphalt binder test samples were subjected to short-term aging and then long-term aging. The short-term was performed using rolling thin film oven test (RTFOT) as per AASHTO T240 procedure. Then, the binder was placed in a pressure aging vessel (PAV) for long-term aging following AASHTO R 28 procedure. The RTFO test simulates aging during mixing and placement while the PAV test ages the material equivalent to approximately 7 to 10 years of field exposure (Pan and Tarefder 2016; Xiao *et al.* 2015). For the FAM, the loose mixes were conditioned in an oven at 135^{o}C for 2 hours to simulate the short-term aging, and then were kept in the same oven for 72 hours before compaction to study the effect of long-term aging.

3.3.4 *Quantifying the Effect of the Antioxidants on Aging Characteristics*

The aging index (AI) was used as a tool to analyze the effect of antioxidants on the test binders and FAM. For asphalt binder, the long-term aging index was defined as the ratio of the fatigue parameter of the PAV aged binder to the fatigue parameter of the original binder. The fatigue parameter (G*sinδ) increases as the aging increases. A lower AI compared to the control binder indicates favorable effect of the antioxidant to retard aging. For FAM, the long-term aging index was defined as the ratio of the fracture energy of unaged FAM to the fracture energy of aged FAM. The fracture energy of FAM decreases as the aging increases. A lower AI implies less aging occurred. The aging indices for binder and FAM were calculated using Equations 3.3 and 3.4, respectively.

$$Aging\ Index\ of\ Asphalt\ Binder = \frac{G*sin\delta\ of\ PAV\ aged\ asphalt}{G*sin\delta\ of\ unaged\ asphalt} \quad (3.3)$$

$$Aging\ Index\ of\ FAM = \frac{fracture\ energy\ of\ unaged\ FAM\ mix}{fracture\ energy\ of\ aged\ FAM\ mix} \quad (3.4)$$

3.4 Experimental Results, Data Analysis and Discussion

3.4.1 *Asphalt Binder Aging Characteristics*

Table 3.1 and 3.2 present the fatigue parameter (G*Sinδ) for the asphalt binder test samples before aging and after long-term aging, in addition to the aging index (AI) and percent decrease of AI compared to the AI of the control asphalt binder. Figures 3.6 and 3.7 show graphical illustrations of the AI for all the test binders. The percent decrease in both Table 3.1 and Table 3.2 indicates how much the AI decreased after mixing with antioxidant additives when compared to the AI of control binder. The following main observations can be made.

- The results showed that the hydrated lime increased the intermediate temperature stiffness of the unaged PG 64-22 binder. Also, it was found to improve the fatigue resistance of the aged binders. It lowered the G*Sinδ compared to the control binder after long-term aging. It decreased the fatigue parameter by 23% which is desired when cracking due to aging is a concern. The mixing was done at three percentages: 1%, 2% and 3%. The lowest aging index was found to be at 2% by weight of the binder. At this percentage, the decrease in long-term aging index was about 30%. The

hydrated lime was also tested with PG 67-22 binder. It was found to decrease the AI by about 14% at both 2% and 3% by weight of the binder.

- The Irganox 1010 was tested with both PG 64-22 and PG 67-22 binders at 1% and 2%. The results demonstrated that using Irganox 1010 had favorable effect on asphalt binders. It decreased the fatigue parameter after long-term aging and the decrease in the AI was about 19% and 17% at 1% and 2%, respectively. For the PG 67-22 binder, the AI was reduced by about 29% at 1% by weight of the binder. These results showed that the Irganox 1010 may have different effect with different asphalt binders.
- The carbon black was found to decrease the AI by approximately 3% for the PG 64-22 binder. Although, it could decrease the fatigue parameter after aging by 14%, it slightly altered the fatigue parameter of the unaged binder. No significant retarding of aging occurred at the percentage tested and therefore no further testing was performed with PG 67-22.
- The Redicote AP was mixed with the base binder at 1% by weight of the binder. At this percentage, the additive decreased the fatigue parameter of the PAV aged binder by almost 38%. In addition, the AI decreased by about 21% compared to base PG 64-22 binder. The Redicote was also tested with PG 67-22 at the same percentage. It decreased the AI by about 27% and decreased the fatigue parameter after PAV aging by almost 46%. The Redicote reduced the fatigue parameter of both binders before aging compared to base binders. These results demonstrated that the Redicote antioxidant is a viable antioxidant with the test binders in the research.
- The Solprene 1205 was mixed at two percentages: 2% and 3%. The optimum performance was found at 3% with PG 64-22 binder. The reduction in the AI was about 47%. Although the fatigue parameter did not decrease greatly after the long-term aging, it improved the original properties of the control binder. The intermediate temperature stiffness increased immensely thereby decreasing the AI. The Solprene 1205 when mixed with the PG 67-22 binder, it reduced the AI by approximately 27%. It increased the intermediate stiffness before aging and reduced the stiffness after long-term aging compared to control binder.

- The Calprene 6120 was tested at two percentages: 2% and 3%. The lowest AI was obtained at 3% by weight of the binder. The addition of this percentage of antioxidant resulted in 41% reduction in the AI. This additive was then selected to mix with PG 67-22 binder. The mixing resulted in a stiffer binder compared to the base one. The reduction in AI was about 45%. This co-polymer additive improved the intermediate temperature stiffness of both the binders and it was also helpful in reducing the fatigue parameter of PG 67-22 binder from 3785 kPa to 3305 kPa.
- The furfural was mixed with asphalt in presence of hydrochloric acid as catalyst. The results showed that, this combination tends to make the binder stiffer than original. This combination can be used with antioxidants that relatively soften the binder to get the desired stiffness.
- The DLTDP can act as a secondary antioxidant and provide synergistic effects when combined with primary antioxidants. Although it increased the fatigue resistance vastly, its drawback was in the changes that it made to the original binder. It made the base unaged binder very soft.

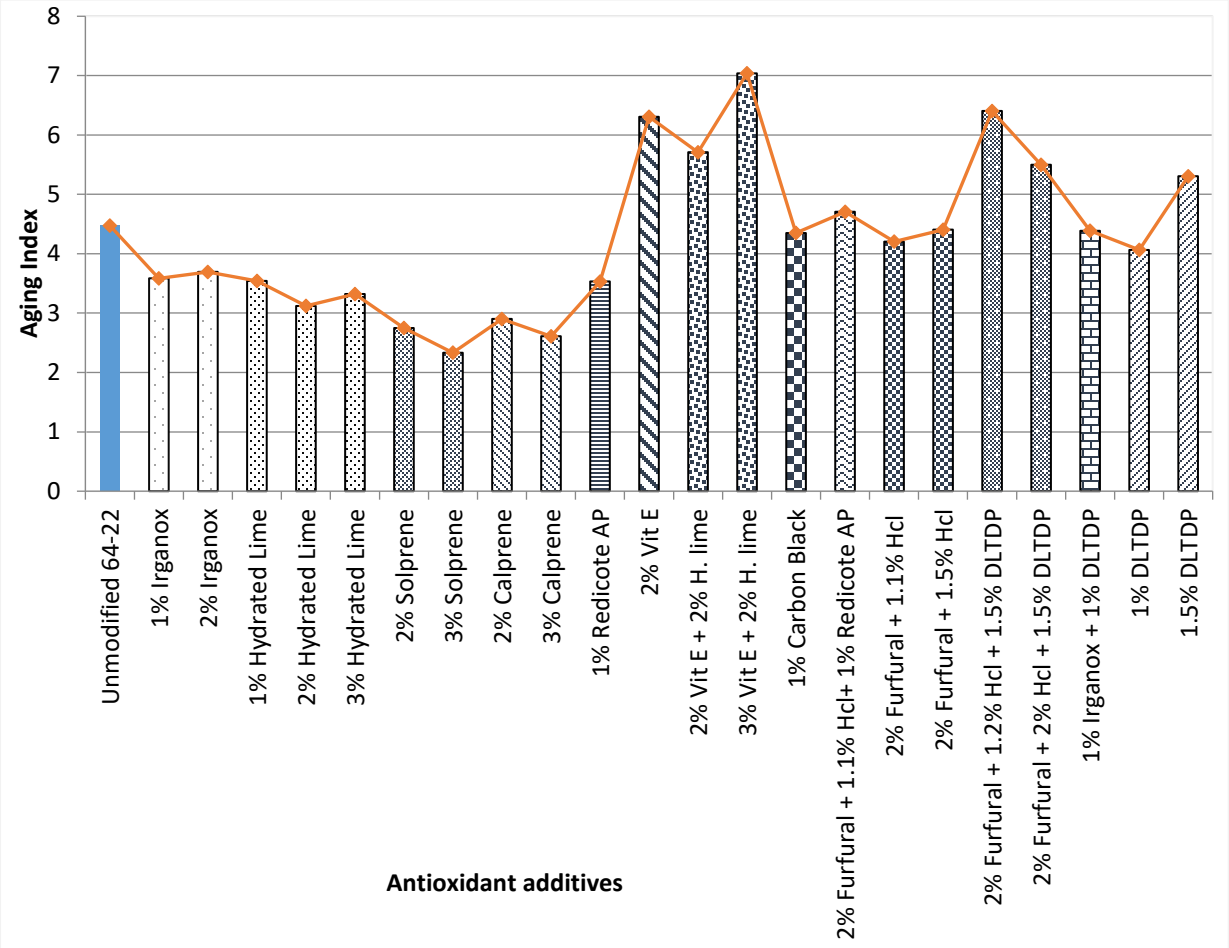

Figure 3.6 Aging Index of PG 64-22 asphalt binders (based on G*sinδ)

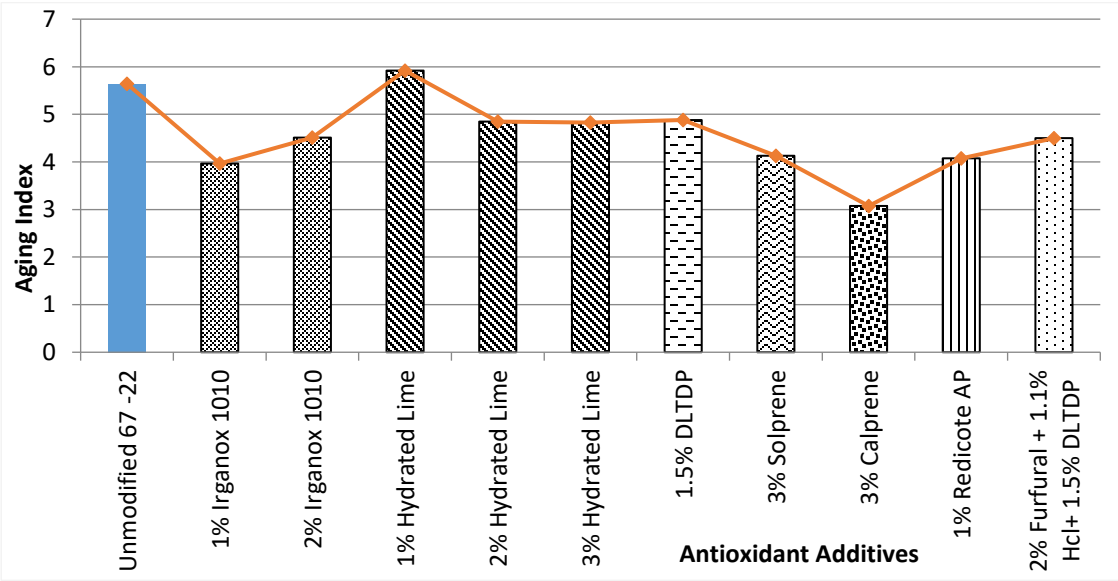

Figure 3.7 Aging Index of PG 67-22 asphalt binders (based on G*sinδ)

3.4.2 *Impact of Antioxidant Additives on Linear Viscoelastic Properties of Asphalt Binder*

The results from the screening process showed that the Redicote AP is one of the most promising antioxidant additives for both PG 64-22 and 67-22 binders. The other additives that showed great decrease in the AI were the Solprene 1205 and the Calprene 6120. The Solprene 1205 provided improved performance with the PG 64-22, while Calprene 6120 showed high reduction in aging with PG 67-22 binder. Frequency sweep tests were performed on the binders modified with these antioxidant additives to study the impact of these additives on the linear viscoelastic properties of the binders. The testing was performed on both unaged and PAV aged samples. The frequency sweep test was conducted at seven temperatures: 10, 20, 30, 40, 50, 60 and 70°C and 10 frequencies at each temperature. The frequencies selected were 37.5, 30, 25, 20, 15, 10, 5, 1, 0.5 and 0.1 Hz. An 8mm diameter plate was used to test the sample from 10 to 30°C at 1% strain and a 25mm diameter plate was used for temperatures greater than 30°C at 10% strain. A gap of 1mm between the parallel plates was maintained in all cases. All frequency sweep tests were performed as per the AASHTO T-315 procedure. From the frequency sweep test, the complex modulus of the asphalt binder at different frequencies (37.5 to 0.1 Hz) and temperatures (10 to 70°C) was measured. To construct a master curve, 20°C was considered as the reference temperature. The Williams-Landel-Ferry model (Williams et al. 1955) was used for the time-temperature shift factor function. The time-temperature shift factor (αT) for any temperature T (i.e. 10 to 70°C) was calculated as per Equation 3.5.

$$log\alpha T = \frac{C_1(T-T_R)}{C_2+(T-T_R)} \tag{3.5}$$

where, T_R = reference temperature (20°C), and C_1 and C_2 are fitting coefficients.

The reduced frequency at the reference temperature was calculated from the applied frequency, using the Equation 3.6 of time-temperature shift factor. The time-temperature shift factor can be expressed as follows:

$$\alpha T = \frac{\omega Tr}{\omega T} \tag{3.6}$$

where, αT = time-temperature shift factor,

ωT = frequency at given temperature,

ωTr = reduced frequency of ωT at the reference temperature.

The complex modulus (G*) was calculated according to Equation 3.7 and the master curve was constructed by using an extension of Christensen, Anderson and Marasteanu (CAM) model (Marasteanu and Anderson 1999).

$$|G*| = \frac{G_g}{\left(1+\left(\frac{\omega_c}{\omega_R}\right)^k\right)^{\frac{m_e}{k}}} \quad (3.7)$$

where, G_g = maximum shear Modulus (1 GPa), ω_R = reduced frequency, and ω_C, m_e, k are fitting coefficients. Initial values were assumed for the fitting parameters (i.e. ω_C, m_e, k, C_1 and C_2) and the CAM model was fitted by reducing the SSE (sum of squares error) between measured and predicted complex shear modulus. The reduction of SSE involved optimization of the fitting parameters with the Microsoft Excel Solver.

For PG 67-22, the results in Figure 3.8 showed that the Calprene-modified binder provided higher stiffness at all temperatures and frequencies compared to the base PG 67-22 binder. The master curve (Figure 3.8) demonstrated that the rheological properties of Calprene-modified binder highly differs from the control binder at the high temperature (low-reduced frequency) region. This is mainly due to the polymer modification. The Calprene-modified binder showed a large increase in high temperature stiffness compared to the control binder. This property is highly beneficial during the early stage of pavement construction. On the other hand, the Redicote-modified binder showed a slightly lesser stiffness compared to the control binder at all the temperatures and frequencies. However, the difference is very low and it can be concluded that the original properties remain intact. The master curve showed that the rheological properties of Redicote-modified binder do not differ vastly compared to the control. After PAV aging, the results in Figure 3.8 demonstrated that Redicote-modified binder provided lesser stiffness compared to the control binder. This property is highly desirable for aged binder to resist fatigue cracking.

For PG 64-22, the results in Figure 3.9 demonstrated that the Redicote-modified binder showed a slight decrease in the high temperature stiffness compared to control binder at all frequencies. On the other hand, being a copolymer, Solprene provided a high temperature stiffness which improves the resistance of asphalt binder to rutting at high temperature. The master curves in the Figure 3.9 demonstrated that Solprene-modified binder had different rheological properties compared to control binder and Redicote-modified binder especially at the low-reduced frequency region. The master curves also showed that the properties of both control and Redicote-modified binder are almost the same in both low- and high-reduced frequency regions. After PAV aging, the results in Figure 3.9 demonstrated that the rheological properties of the Solprene modified binder are different from the control binder and Redicote-modified binder at the low-reduced frequency region (high temperature). In the same low frequency region, the master curves showed that the properties of both control PAV aged and Redicote PAV aged are almost the same. This means that an antioxidant may work differently with different binders.

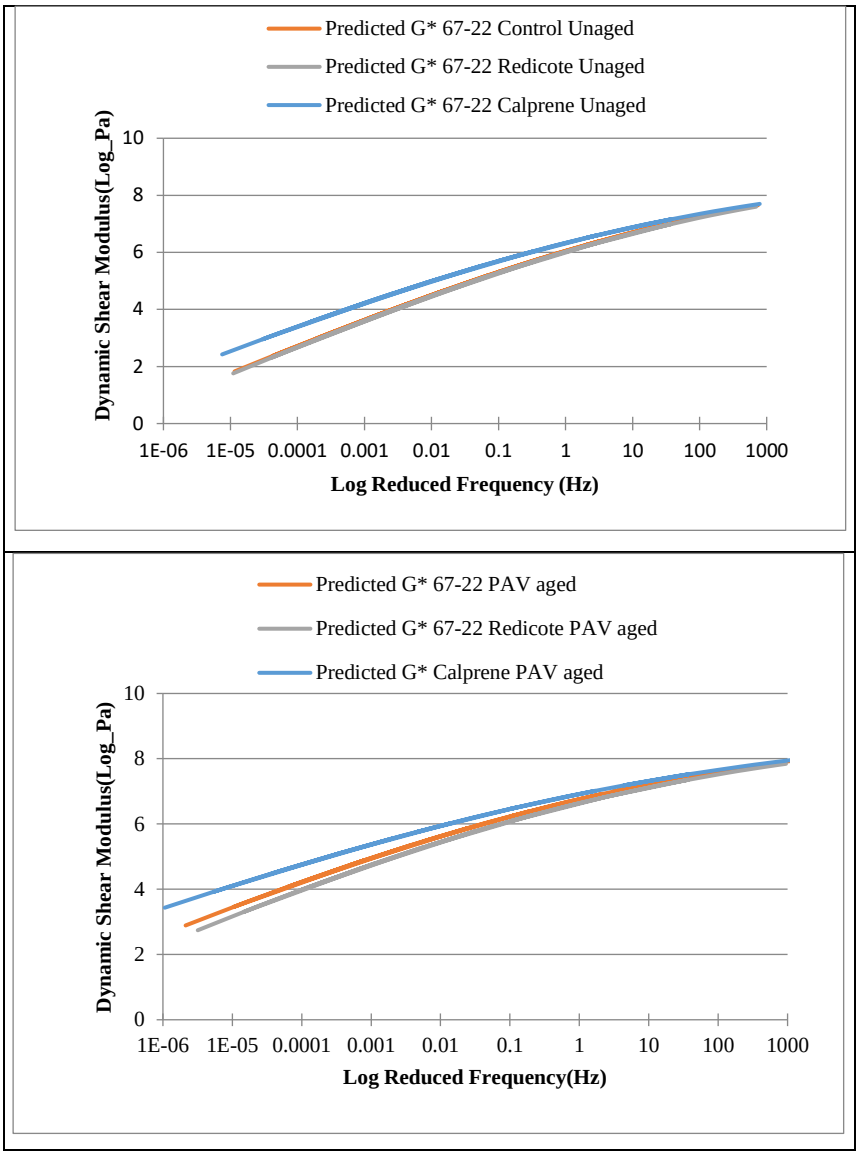

Figure 3.8 Dynamic shear modulus master curve for PG 67-22 asphalt binder with different antioxidants

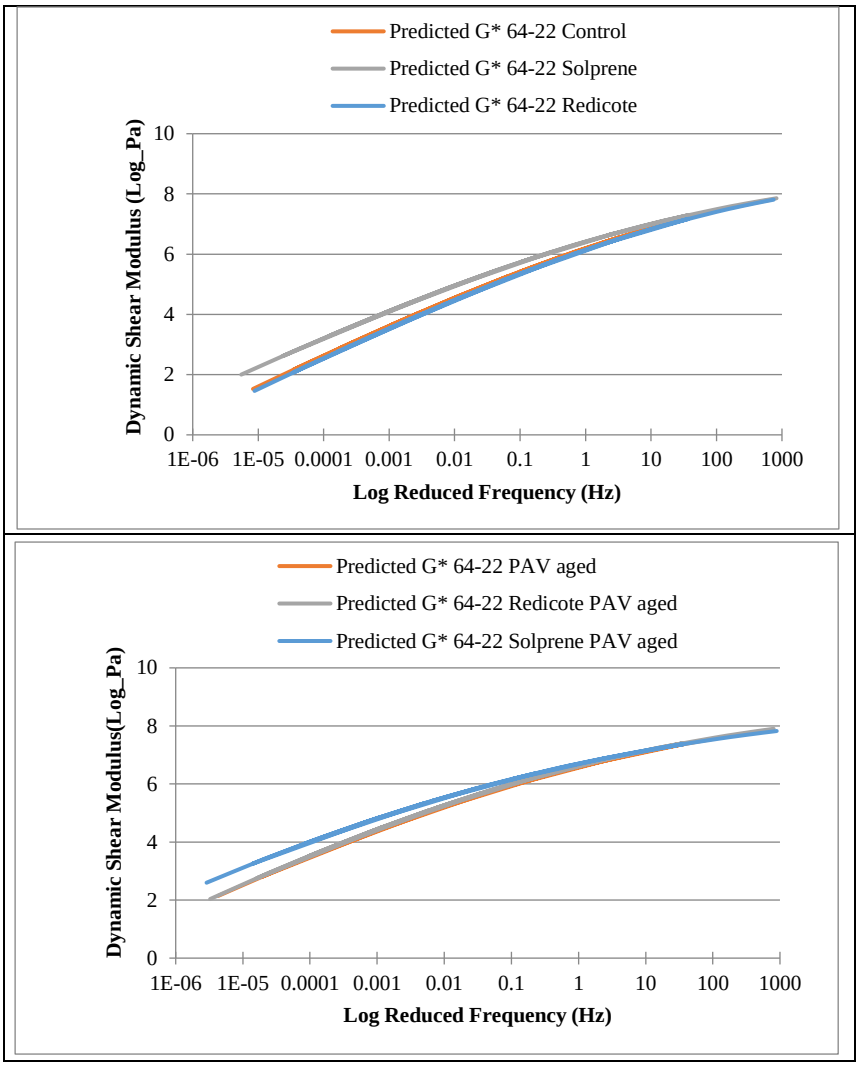

Figure 3.9 Dynamic shear modulus master curve for PG 64-22 asphalt binder with different antioxidants

The researchers investigated another a newly developed rheological parameter [G'/(η'/G')]. This parameter was initially proposed and used by Glover (Glover et al. 2005) to correlate Kandhal's (Kandhal 1977) ductility with age-induced cracking due to tensile failure. A good correlation was found when the long-term aged binders were tested in DSR at 15°C with an angular frequency of 0.005 rad/s. Glover (Glover et al. 2005) tested the G'/(η'/G') parameter on both unmodified and polymer-modified binders (PMB) and it was found that ductility decreased after oxidative aging with an increase in G'/(η'/G'). For the binders without any polymer modification (i.e. SBS, crumb rubber etc.), Equation 3.8 was proposed to predict age-induced asphalt hardening and consecutive fatigue cracking in terms of ductility (Glover et al. 2005):

$$\text{Ductility (cm)} = 0.23 * \{G'/(\eta'/G')\}^{-0.44} \quad (3.8)$$

where, G' = storage shear modulus,

η' = dynamic viscosity

Several other researchers (Anderson et al. 2011; King *et al.* 2012; Rowe et al. 2014) verified the Glover's parameter G'/(η'/G') with ductility and concluded with similar findings. Anderson et al. (2011) applied time-temperature superposition principle to test binders at 44.7°C and 10 rad/s, in order to simplify the testing procedure. In addition, they also performed frequency sweep test at different temperatures (5, 15 and 25°C) and frequencies (0.1 to 100 rad/s) to develop a master curve at the reference temperature of 15°C and predicted G'/(η'/G') at 15°C and 0.005 rad/s. They named this method as the master curve procedure and compared the same Glover's parameter derived with Texas A&M standard DSR method. The master curve procedure provided better correlation of predicted ductility with the measured one when compared to the standard DSR method. Rowe et al. (2011) reduced G'/(η'/G') into $G^*(\cos\delta)^2/\sin\delta$ keeping the frequency (ω) constant (0.005 rad/s) and renamed it Glover-Rowe (G-R) fatigue parameter. According to Rowe (2011), the G-R parameter was found to be a good indicator of fatigue cracking. Based on Kandhal's observation (Kandhal 1977) that cracking initiates when ductility falls below 5 cm in aged binder, King et al. (2012) suggested a limit for G-R parameter to predict damage onset (Equation 3.9).

$$G^*(\cos\delta)^2/\sin\delta \leq 180 \text{ kPa} \quad (3.9)$$

In this study, the master curve procedure was used and both the parameters (i.e., G'/(η'/G') and $G^*(\cos\delta)^2/\sin\delta$) were calculated from the master curves of Figure 3.8 and 3.9 at 15°C and 0.005 rad/s as presented in Table 3.5 and graphically in Figure 3.10. The AI in Table 3.5 is the ratio of 20 hours PAV aged G'/(η'/G') or $G^*(\cos\delta)^2/\sin\delta$ to that of the unaged one. Since the G-R fatigue parameter was actually derived from G'/(η'/G'), both the parameters exhibited equal AI. Both the parameters [(G'/(η'/G') and $G^*(\cos\delta)^2/\sin\delta$] increased with long term aging.

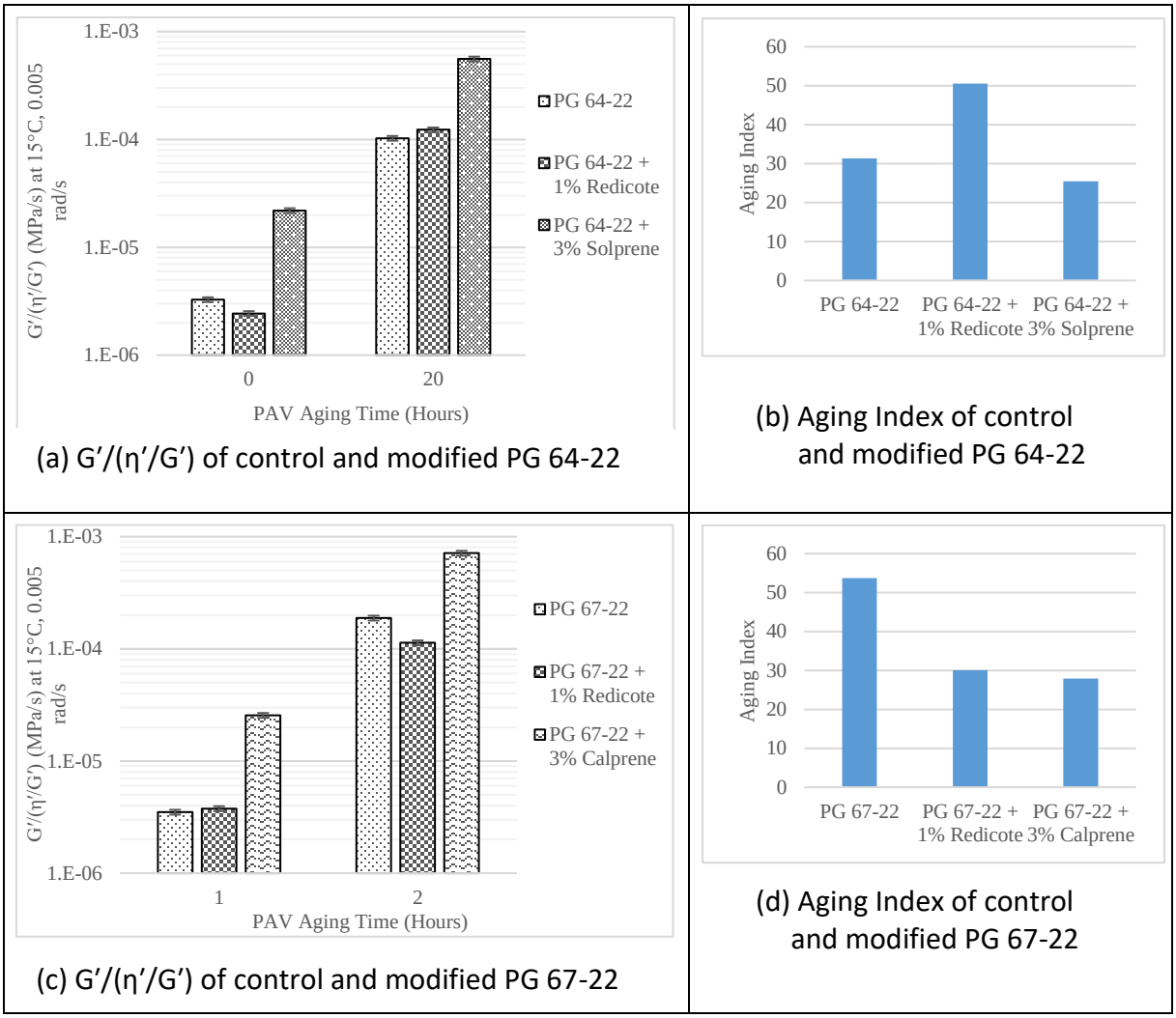

Figure 3.10 Predicted G'/(η'/G') (MPa/s) at 15°C, 0.005 rad/s and corresponding Aging Index (based on G-R parameter): (a) G'/(η'/G') of control and modified PG 64-22; (b) Aging Index of control and modified PG 64-22; (c) G'/(η'/G') of control and modified PG 67-22; (d) Aging Index of control and modified PG 67-22

Despite an immediate increase in G'/(η'/G') or G-R parameter after mixing the antioxidants, the rate of aging decreased significantly in all cases except PG 64-22 modified with 1% Redicote. In PG 67-22, the aging indices of binders modified with 1% Redicote and 3 % Solprene were 30.05 and 27.91, respectively, which is considerably lower than the AI of unmodified PG 67-22 (53.74). These results demonstrate that both the antioxidants showed satisfactory performance with PG 67-22 in terms of G'/(η'/G') or G-R fatigue parameter whereas with PG 64-22, it was 3% Solprene. The G-R parameter was calculated to check the degree of damage in respect to the damage onset of fatigue cracking and in all cases, it was

found much lesser than 180 kPa. Ductility was also predicted using Equation 3.8, and the results presented in Table 3.6 conformed with the findings of the fatigue parameter G'/(η'/G'). The data is presented in Table 3.6 and shown graphically in Figure 3.11. Mixing the antioxidants reduced the percent decrease in ductility compared to the unmodified binder and after long term aging, all the test samples satisfied Kandhal's minimum ductility limit of 5 cm.

Table 3.5 Predicted G'/(η'/G') (MPa/s) and G*(cosδ)^2/sinδ at 15 °C, 0.005 rad/s from Master Curve

a. G'/(η'/G') (MPa/s) at 15°C, 0.005 rad/s

Item	PG 64-22		PG 64-22 + 1% Redicote		PG 64-22 + 3% Solprene	
	PAV 0	PAV 20	PAV 0	PAV 20	PAV 0	PAV 20
Replicate 1 (MPa/s)	3.84E-06	1.02E-04	2.21E-06	1.29E-04	1.69E-05	5.61E-04
Replicate 2 (MPa/s)	2.71E-06	1.03E-04	2.66E-06	1.17E-04	2.69E-05	5.54E-04
Average (MPa/s)	**3.27E-06**	**1.03E-04**	**2.43E-06**	**1.23E-04**	**2.19E-05**	**5.58E-04**
Aging Index		**31.34**		**50.56**		**25.44**
Std. Dev. (MPa/s)	7.99E-07	2.32E-07	3.16E-07	9.00E-06	7.06E-06	4.73E-06
COV (%)	24.4%	0.2%	13.0%	7.3%	32.2%	0.8%

Item	PG 67-22		PG 67-22 + 1% Redicote		PG 67-22 + 3% Calprene	
	PAV 0	PAV 20	PAV 0	PAV 20	PAV 0	PAV 20
Replicate 1 (MPa/s)	3.38E-06	1.83E-04	3.17E-06	1.13E-04	2.62E-05	7.74E-04
Replicate 2 (MPa/s)	3.62E-06	1.93E-04	4.36E-06	1.13E-04	2.49E-05	6.52E-04
Average (MPa/s)	**3.50E-06**	**1.88E-04**	**3.77E-06**	**1.13E-04**	**2.55E-05**	**7.13E-04**
Aging Index		**53.74**		**30.05**		**27.91**
Std. Deviation	1.70E-07	7.41E-06	8.42E-07	2.93E-07	9.52E-07	8.63E-05
COV (%)	4.8%	3.9%	22.4%	0.3%	3.7%	12.1%

b. G*(Cosδ)^2/Sinδ (kPa) at 15°C, 0.005 rad/s

Item	PG 64-22		PG 64-22 + 1% Redicote		PG 64-22 + 3% Solprene	
	PAV 0	PAV 20	PAV 0	PAV 20	PAV 0	PAV 20
Replicate 1 (kPa)	0.77	20.48	0.44	25.88	3.39	112.19
Replicate 2 (kPa)	0.54	20.54	0.53	23.33	5.38	110.85
Average (kPa)	**0.65**	**20.51**	**0.49**	**24.60**	**4.38**	**111.52**
Aging Index		**31.34**		**50.56**		**25.44**
Std. Dev. (kPa)	0.16	0.05	0.06	1.80	1.41	0.95
COV (%)	24.4%	0.2%	13.0%	7.3%	32.2%	0.8%

Item	PG 67-22		PG 67-22 + 1% Redicote		PG 67-22 + 3% Calprene	
	PAV 0	PAV 20	PAV 0	PAV 20	PAV 0	PAV 20
Replicate 1 (kPa)	0.68	36.59	0.63	22.60	5.24	154.73
Replicate 2 (kPa)	0.72	38.69	0.87	22.69	4.97	130.32
Average (kPa)	**0.70**	**37.64**	**0.75**	**22.65**	**5.11**	**142.53**
Aging Index		**53.74**		**30.05**		**27.91**
Std. Dev. (kPa)	0.03	1.48	0.17	0.06	0.19	17.26
COV (%)	4.8%	3.9%	22.4%	0.3%	3.7%	12.1%

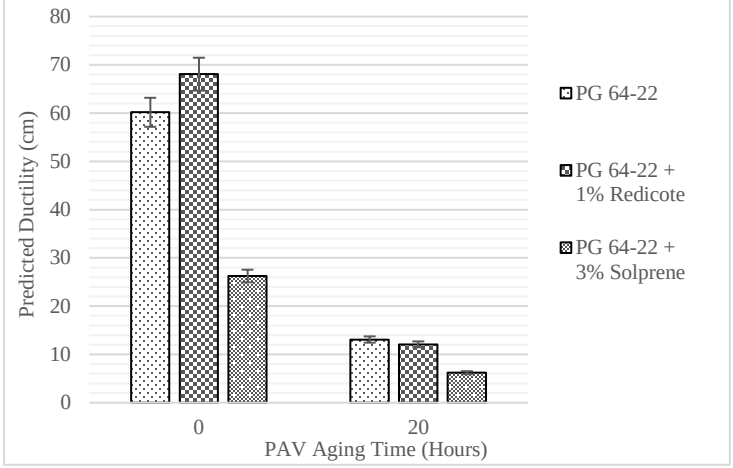

(a) Ductility of control and modified PG 64-22

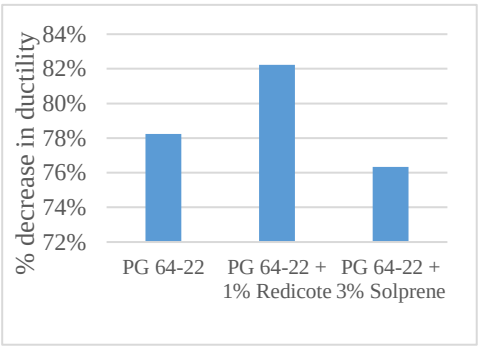

(b) Rate of decrease in Ductility after long-term aging (PG 64-22)

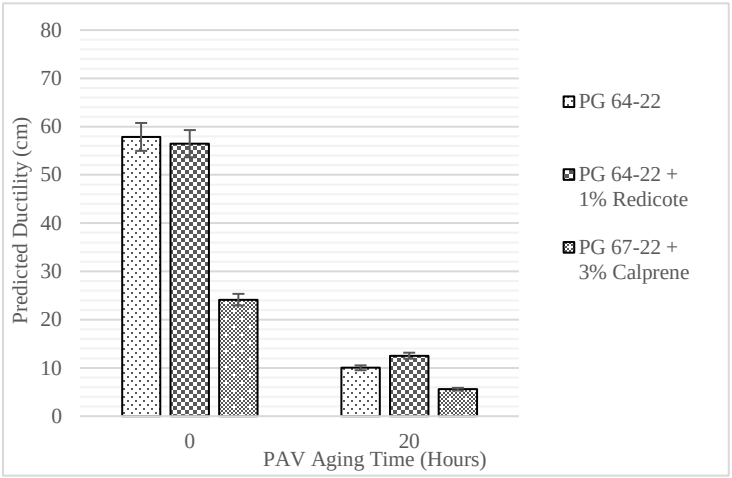

(c) Ductility of control and modified PG 67-22

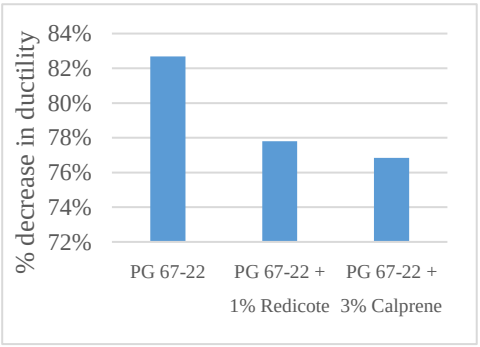

(d) Rate of decrease in Ductility after long-term aging (PG 67-22)

Figure 3.11 Predicted Ductility (cm) at 15°C, 0.005 rad/s and corresponding rate of decrease in Ductility (%): (a) Ductility of control and modified PG 64-22; (b) Rate of decrease in Ductility after long-term aging (PG 64-22); (c) Ductility of control and modified PG 67-22; (d) Rate of decrease in Ductility after long-term aging (PG 67-22)

Table 3.6 Predicted Ductility (cm) at 15°C, 0.005 rad/s using G'/(η'/G')

Item	PG 64-22		PG 64-22 + 1% Redicote		PG 64-22 + 3% Solprene	
	PAV 0	PAV 20	PAV 0	PAV 20	PAV 0	PAV 20
Replicate 1 (cm)	55.56	13.10	70.83	11.82	28.92	6.20
Replicate 2 (cm)	64.77	13.08	65.32	12.37	23.58	6.23
Average (cm)	**60.17**	**13.09**	**68.07**	**12.09**	**26.25**	**6.21**
% Decrease		**78.2%**		**82.2%**		**76.3%**
Std. Dev. (cm)	6.51	0.01	3.90	0.39	3.77	0.02
COV (%)	10.8%	0.1%	5.7%	3.2%	14.4%	0.4%
Item	PG 67-22		PG 67-22 + 1% Redicote		PG 67-22 + 3% Calprene	
	PAV 0	PAV 20	PAV 0	PAV 20	PAV 0	PAV 20
Replicate 1 (cm)	58.73	10.15	60.41	12.54	23.86	5.38
Replicate 2 (cm)	56.99	9.90	52.51	12.52	24.42	5.80
Average (cm)	**57.86**	**10.02**	**56.46**	**12.53**	**24.14**	**5.59**
% Decrease		**82.7%**		**77.8%**		**76.8%**
Std. Dev. (cm)	1.23	0.17	5.59	0.01	0.40	0.30
COV (%)	2.1%	1.7%	9.9%	0.1%	1.6%	5.3%

3.4.3 *FAM Aging Characteristics*

Table 3.7 presents the fracture energy of aged and unaged FAM mixtures evaluated in this study. The fracture energy is defined as the area under the load-deformation curve in the SCB test. It is clear that the fracture energy decreases with aging for all test FAM mixtures as shown in Figures 3.12, 3.13 and 3.14. The aged FAM specimens experienced higher peak, but lower displacement at failure as presented in Tables 3.8 and 3.9, respectively. Such behavior is expected as the aging causes the asphalt mixtures to be more brittle. The aging index (AI) of FAM shown in Figure 3.15 clearly demonstrated that both antioxidant additives have favorable effects on the gabbro and limestone FAM mixtures, but not in basalt FAM mixtures. Using Redicote and Solprene additives had slight effect on the fracture energy before aging for limestone and basalt FAM mixtures; however, gabbro and limestone, both had favorable effects after aging. The fracture energy of gabbro FAM mixtures modified with Redicote and Solprene had higher fracture energy compared to the control gabbro FAM after aging. Thus, the mixtures are expected to have better resistance to fatigue cracking. Both Redicote and

Solprene additives provided comparable AI of 1.17 and 1.16 for Redicote and Solprene, respectively. However, the Solprene provided higher fracture energy after aging compared to Redicote. The results showed that any of these additives may be viable to reduce aging when used with gabbro aggregate and PG 64-22 binder.

Table 3.7 Fracture energy of FAM SCB specimens

Aggregate	Mixture Type	Avg. Fracture Energy (J/m^2), unaged	SD of Fracture Energy (J/m^2), unaged	Avg. Fracture Energy (J/m^2), aged	SD of Fracture Energy (J/m^2), aged	Aging Index (AI)
Gabbro	Control	220.82	29.90	106.88	14.29	2.07
	1%Redicote	196.43	16.80	168.38	5.63	1.17
	3%Solprene	213.18	14.74	183.05	5.29	1.16
Limestone	Control	237.19	3.48	170.71	12.72	1.39
	1%Redicote	236.94	11.57	220.63	22.13	1.07
	3%Solprene	249.27	2.00	211.51	42.77	1.18
Basalt	Control	174.97	16.84	132.61	6.28	1.32
	1%Redicote	233.76	15.36	110.88	6.70	2.11
	3%Solprene	203.05	23.99	136.65	17.07	1.49

Table 3.8 Peak load of SCB test

Aggregate	Mixture Type	Avg. Peak Load (kN), unaged	Std. Deviation of Peak Load (kN), unaged	Avg. Peak Load (kN), aged	Std. Deviation of Peak Load (kN), aged
Gabbro	Control	0.422	0.080	0.992	0.010
	1%Redicote	0.334	0.018	0.965	0.021
	3%Solprene	0.433	0.011	0.885	0.061
Limestone	Control	0.358	0.001	1.103	0.164
	1%Redicote	0.344	0.016	0.965	0.117
	3%Solprene	0.446	0.031	1.015	0.078
Basalt	Control	0.264	0.030	0.614	0.035
	1%Redicote	0.304	0.000	1.050	0.063
	3%Solprene	0.308	0.042	1.200	0.152

Table 3.9 Displacement at failure of SCB test

Aggregate	Mixture Type	Avg. Displacement at Failure (mm), unaged	Std. Deviation of Displacement at Failure (mm), unaged	Avg. Displacement at Failure (mm), aged	Std. Deviation of Displacement at Failure (mm), aged
Gabbro	Control	1.973	0.031	0.551	0.019
	1%Redicote	2.033	0.140	0.835	0.069
	3%Solprene	1.918	0.068	1.013	0.037
Limestone	Control	1.068	0.016	0.473	0.027
	1%Redicote	1.064	0.000	0.617	0.008
	3%Solprene	1.155	0.153	0.628	0.132
Basalt	Control	1.131	0.062	0.480	0.012
	1%Redicote	1.445	0.046	0.427	0.014
	3%Solprene	1.232	0.049	0.474	0.020

The results also demonstrate that Redicote and Solprene increased the fracture energy of limestone FAM mixtures before aging as well as after aging. These results demonstrate that limestone FAM mixture modified with both Redicote and Solprene would have better fatigue resistant compared to control limestone mixtures. The AI for both Redicote and Solprene were 1.07 and 1.18, respectively. Based on these results, both additives can be used with limestone aggregates and PG 64-22 binder. However, the Redicote provided higher fracture energy after aging and less AI compared to Solprene.

Finally, the gabbro control FAM mixtures had higher AI (2.06) compared to limestone control FAM mixtures (1.12) and basalt control FAM mixtures (1.21). These results showed that aggregate type have a great influence of aging of asphalt mixtures. A recent study by the authors (Sirin *et al.* 2017b) showed that the aggregate type may influence the rate of aging of asphalt binders.

Table 3.10 presents the Flexibility Index (F.I.) of aged and unaged FAM mixtures evaluated in this study. The F.I. is defined as the ratio of fracture energy to post-peak slope of the load-deformation curve in the SCB test (Equation 3.6). It can be seen that F.I. decreased with aging

for all test FAM mixtures since the post-peak slope became steeper after aging as shown in Figures 3.12, 3.13 and 3.14.

Table 3.10 Flexibility Index of FAM SCB specimens

Aggregate	Mixture Type	Avg. Flexibility Index, unaged	SD of Flexibility Index, unaged	Avg. Flexibility Index, aged	SD of Flexibility Index, aged
Gabbro	Control	5.33	0.30	0.06	0.01
	1%Redicote	7.43	0.54	0.40	0.13
	3%Solprene	6.59	0.14	0.59	0.01
Limestone	Control	10.30	2.12	0.24	0.12
	1%Redicote	11.49	0.40	0.91	0.37
	3%Solprene	5.76	0.20	0.64	0.18
Basalt	Control	8.09	0.86	0.74	0.01
	1%Redicote	12.65	2.57	0.06	0.03
	3%Solprene	8.89	0.52	0.07	0.02

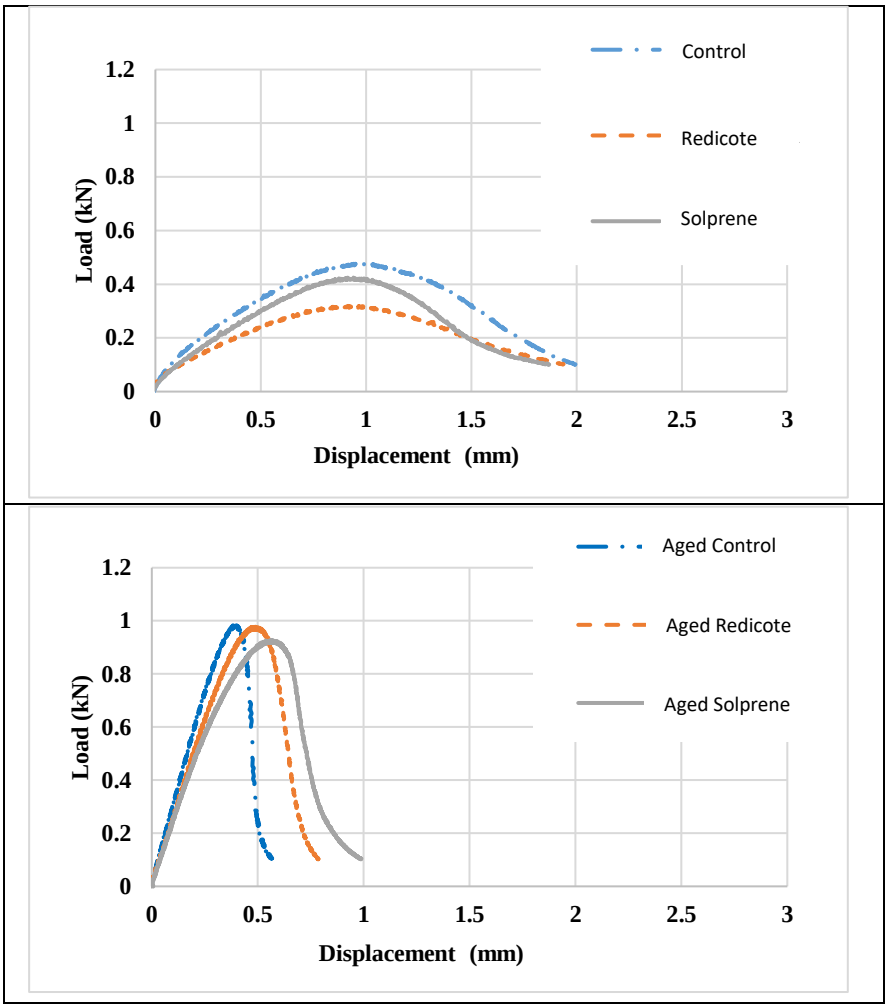

Figure 3.12 Example of Load vs. displacement for Gabbro FAM mixtures with different antioxidants

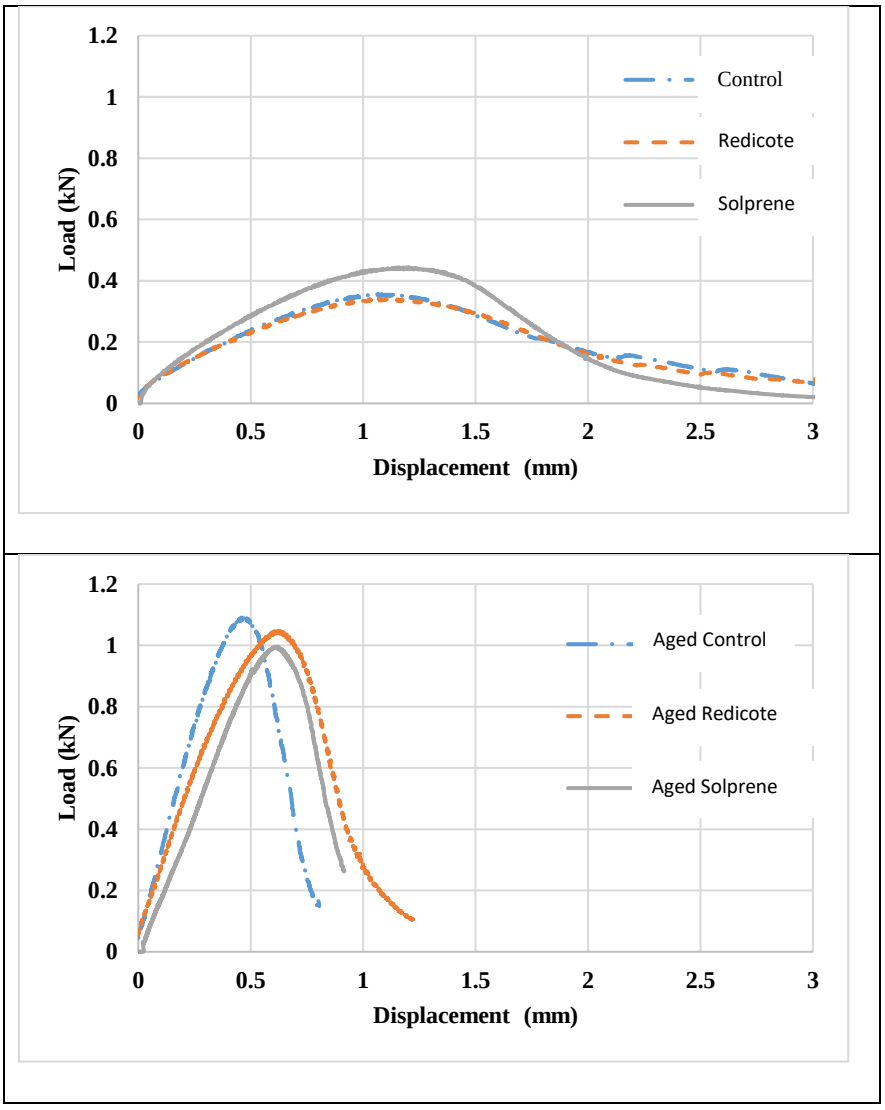

Figure 3.13 Example of Load vs. displacement for Limestone FAM mixtures with different antioxidants

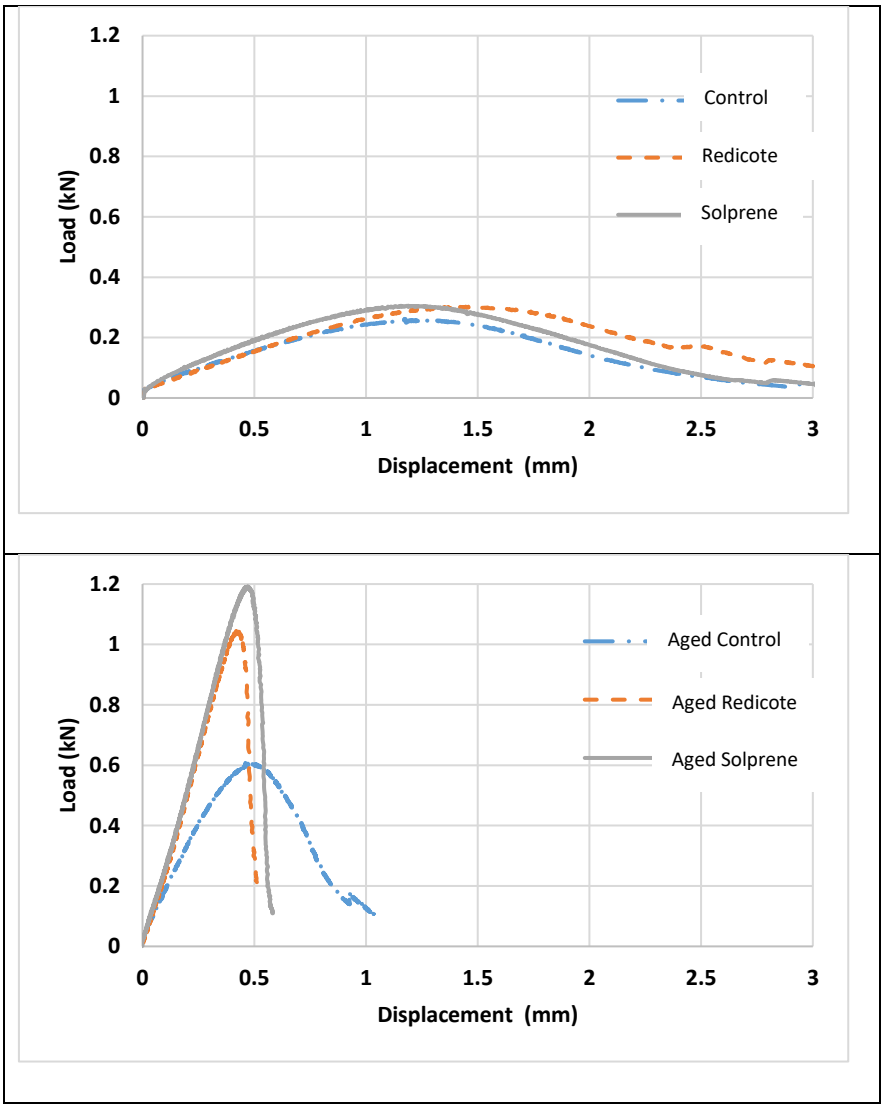

Figure 3.14 Example of Load vs. displacement for Basalt FAM mixtures with different antioxidants

The F.I. of FAM shown in Figure 3.16 clearly demonstrated that both antioxidant additives have favorable effects in the gabbro and limestone FAM mixtures after aging, but not in basalt FAM mixtures. These results are consistent with that of the fracture energy results. Samples with higher F.I. would have better resistance to cracking. Solprene provided the highest F.I. of 0.59 with gabbro after aging whereas for limestone it was Redicote (0.91). The results specify that both of the additives are viable to resist damage in the FAM mixtures when used with gabbro and limestone aggregate. Both the additives failed to provide satisfactorily results with basalt after aging in terms of F.I.

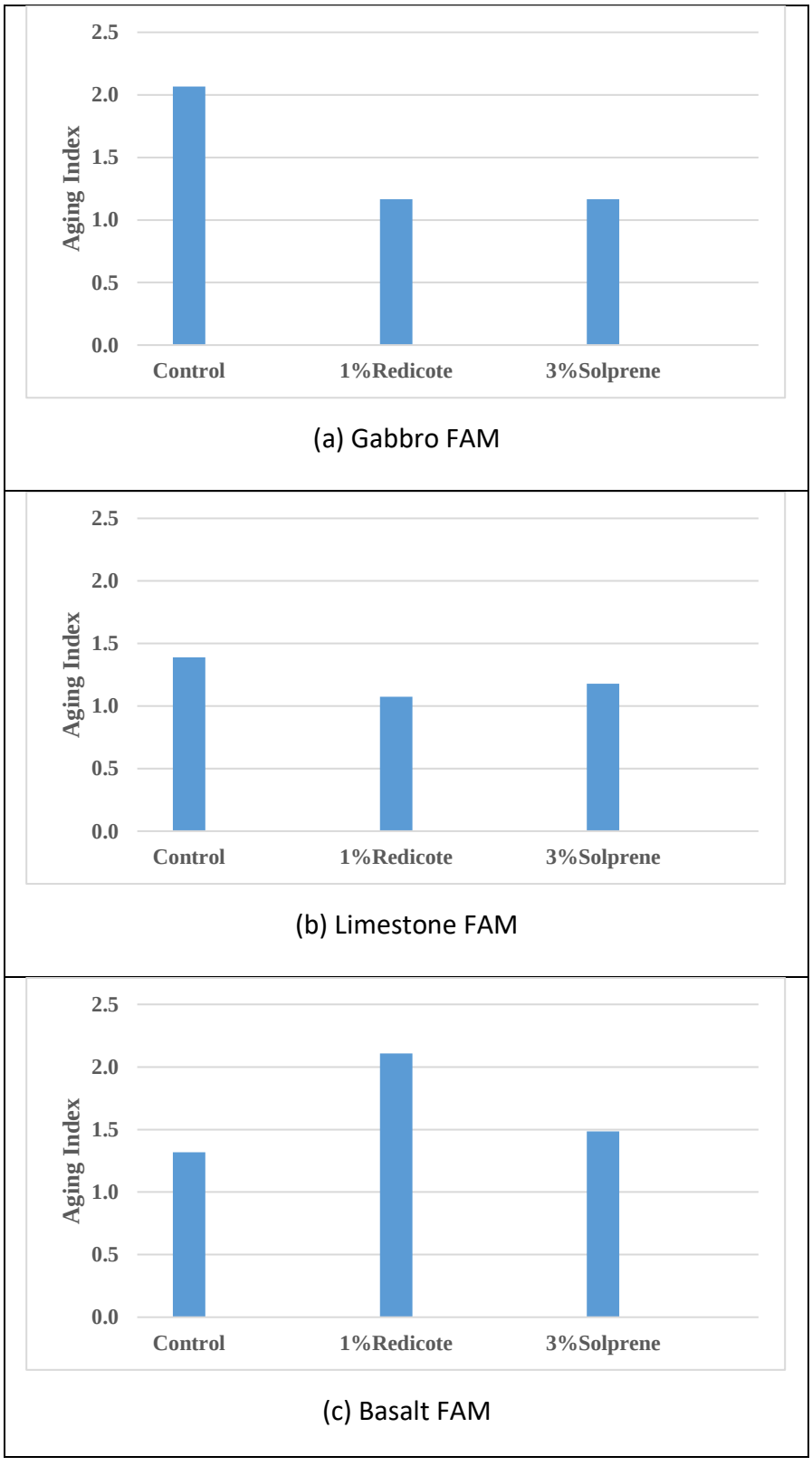

Figure 3.15 Aging index of FAM mixtures (based on Fracture Energy)

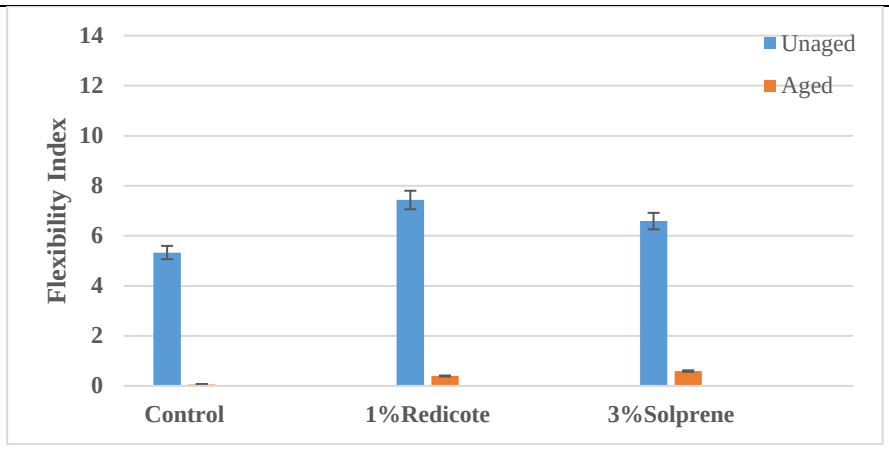

(a) Gabbro FAM

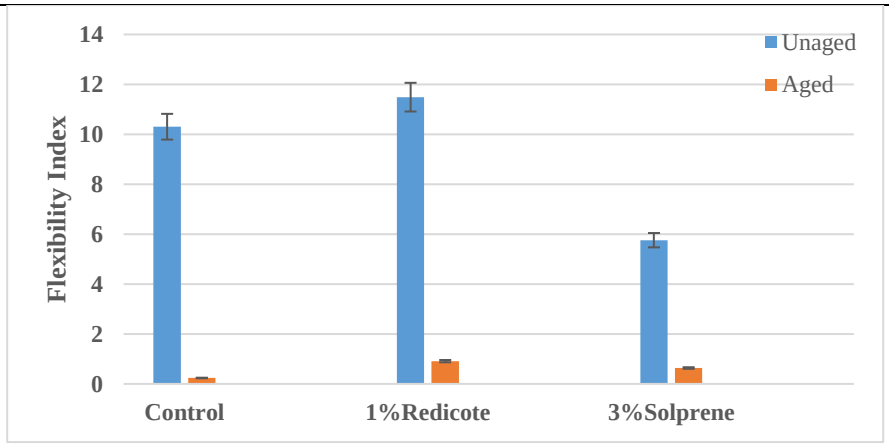

(b) Limestone FAM

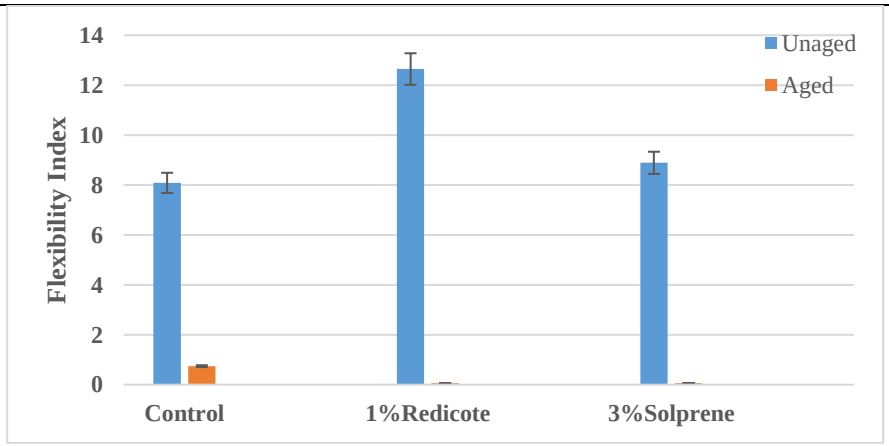

(c) Basalt FAM

Figure 3.16 Flexibility index of FAM mixtures

3.5 Statistical Analysis of the Findings

The purpose of mixing the antioxidant additives with asphalt binder is to retard the long term oxidative aging process. It was found that mixing the antioxidants altered the binder's mechanical properties and parameters such as the fracture energy and the G*sinδ (SHRP fatigue parameter). A statistical analysis using the effect size method was performed to quantify the difference between the unaged and aged condition in respect to these parameters by measuring the magnitude of the treatment effect of antioxidants (Table 3.11 and 3.12). The effect size method, also known as the Cohen's *d* (Cohen 1988), is a simple way of quantifying the difference between two variables that has many advantages over the use of tests of statistical significance alone. The major benefit is that effect size emphasizes the size of the difference rather than confounding this with sample size. This method is also important due to its simplified comparison of the magnitude of one experimental treatment with another (Thalheimer and Cook 2002). Mathematically, Cohen's *d* can be expressed with Equation 3.11 which is the difference between the treatment and control population mean divided by the standard deviation of the respective conditions (Cohen 1992).

$$d = \frac{\bar{x}_t - \bar{x}_c}{\sqrt{\frac{(n_t-1)s_t^2+(n_c-1)s_c^2}{n_t+n_c}}} \tag{3.11}$$

where, $\bar{x}_t$ = mean of the modified binder parameter (treatment group)

$\bar{x}_c$ = mean of the unmodified binder parameter (control group)

n_t = sample size of the modified binder parameter

n_c = sample size of the unmodified binder parameter

s_t = standard deviation of the treatment group

s_c = standard deviation of the control group

Table 3.11 Representation of Fracture Energy with Effect Size Method

Aggregate Type	Mixture	Avg. Fracture Energy of Unaged samples (J/m^2)	Avg. Fracture Energy of Aged samples (J/m^2)	Effect Size (Fracture Energy)
Gabbro	Control	220.82	106.88	4.86
	1% Redicote	196.43	168.38	2.23
	3% Solprene	213.18	183.05	2.72
Limestone	Control	237.19	170.71	7.12
	1% Redicote	236.94	220.63	0.92
	3% Solprene	249.27	211.51	1.24
Basalt	Control	174.97	132.61	3.33
	1% Redicote	233.76	110.88	10.36
	3% Solprene	203.05	136.65	3.18

The authors used this method because it is compatible with the type of testing performed in this study with small sample size (i.e., two replicates) since other tests for statistical significance such as the t-test might not be applicable (Bower et al. 2016). Higher effect size means there is a statistical significance in the difference between the unaged and aged samples due to the treatment of antioxidants. The mixture modified with antioxidants were compared with the control unmodified mixtures.

The effect size of fracture energy (Table 3.11) conforms to the findings of AI. The control unmodified FAM has higher effect size compared to FAM modified with 1% Redicote and 3% Solprene in both gabbro and limestone. It is an indicator of the satisfactory performance of the antioxidant additives in retarding aging since the reduction in fracture energy of unmodified FAM is more statistically significant than the modified FAM. In basalt, the reduction in fracture energy of FAM modified with 1% Redicote is more significant than the control one and the 3% Solprene is almost equal. This means the antioxidants did not perform well with basalt.

Table 3.12 Representation of G*sinδ at a reference temperature (20°C) from the master curve data in terms of Effect Size Method

Temp. (°C)	Frequency (Hz)	PG 64-22 (Effect Size)			PG 67-22 (Effect Size)		
		Control	1% Redicote	3% Solprene	Control	1% Redicote	3% Calprene
20	**37.5**	2.55	11.32	0.81	53.26	4.11	13.57
	30	2.99	12.50	1.57	51.57	4.18	13.45
	25	3.17	12.58	1.91	55.05	4.38	16.94
	20	3.34	13.56	2.86	55.87	6.97	15.39
	15	3.72	14.35	3.57	65.58	9.37	16.51
	10	4.11	14.95	5.93	71.12	11.15	17.16
	5	4.89	16.78	8.39	85.56	12.22	18.11
	1	6.50	17.47	13.88	125.49	6.07	19.43
	0.5	7.13	17.45	17.12	129.24	8.11	19.64
	0.1	8.05	16.55	23.90	151.62	19.87	19.19

The researchers examined the effect size of G* sin δ at a reference temperature of 20 °C from the master curve data as presented in Table 3.12. For PG 67-22, the effect size of G*sin δ of the unmodified control binder is higher than the binders modified with 1% Redicote and 3% Calprene in all frequencies. This indicates there is a significant difference between the unaged and aged unmodified PG 67-22 binder due to oxidative aging compared to the modified binders. Statistically, the antioxidants performed well with PG 67-22 in retarding aging. For PG 64-22, the effect size of 3% Solprene is less than the control one at medium to higher frequencies which is an indicator of better performance against fatigue cracking. Solprene performed well with PG 64-22 than Redicote in terms of statistical significance.

CHAPTER 4 COMPARATIVE CHARACTERIZATION OF FIELD AGED BINDER AND LAB AGED BINDER MODIFIED WITH ANTIOXIDANT ADDITIVES AND COPOLYMERS USING FTIR, GPC AND AFM

4.1 Introduction

This chapter describes the asphalt sample preparation, test setup and experimental procedure performed using various equipment including FTIR, GPC and AFM, to obtain the required data for spectroscopic, chemical and microstructural analysis. In addition, this chapter discusses the findings of the analysis. The laboratory PAV aging of the antioxidant modified binders were performed in the Advanced Characterization of Infrastructure Materials (ACIM) lab at the Department of Civil Engineering. The field-aged binders were extracted from six test sections from the State of Qatar. The FTIR and GPC sample preparation and testing were performed in the Department of Forest, Rangeland and Fire Sciences at the College of Natural Resources. The AFM imaging was performed at the Department of Chemical & Materials Engineering.

4.2 Experimental Setup and Testing Procedure using FTIR

4.2.1 *Simulating Long-Term Aging of Asphalt Binder*

The objective of this part of the study is to quantify the potential of antioxidant additives in retarding oxidative aging by reducing the carbonyl content present in the binder after long-term aging. The experimental plan consisted of testing control binders and antioxidant modified binders using an FTIR to obtain the IR absorbance spectra of each of the binder type. Based on the results of the previous work of quantifying the effect of antioxidants on aging characteristics, the asphalt binder selected for testing were PG 64-22 and the antioxidant additives were Redicote AP and Solprene, since both Redicote and Solprene had favorable effects on the fatigue parameter (G*sinδ) after 20 hours of PAV aging. The PG 64-22 binder was obtained from Qatar and the antioxidant additives and copolymers were provided by AkzoNobel and Dynasol Elastomers, respectively.

The antioxidant additives were mixed with PG 64-22 binder in quarter gallon cans with a high shear mixer (Model: Silverson L5M-A). The binders were long-term aged in a PAV (Figure 4.1) for 20, 40 and 60 hours as per AASHTO R28.

Figure 4.1 ATS PAV for long term aging of binder

Table 4.1 represents the testing matrix for the FTIR test. The aged and unaged control binder (no modifier) and binders mixed with 1% Redicote and 3% Solprene were tested in the Thermo Scientific Nicolet iS5 FT-IR spectrometer (Figures 4.2a and 4.2b). This spectrometer model of Thermos Scientific is lightweight, small in size, easy to maintain and has multiple crystal options such as diamond laminate, zinc selenide (ZnSe), germanium (Ge), silicon (Si) and AMTIR. ZnSe (transmission range 52600-650 cm^{-1}) was used for all the tests which is an Attenuated Total Reflectance (ATR) crystal. In the ATR method, a small amount of sample (approx. 10-15 g) is placed in intimate contact of the crystal with a spatula (Figure 4.2c). It requires minimal sample preparation and is a non-destructive test technique. However, to obtain a good spectrum in this method, the angle of incidence must exceed the critical angle and it can only measure the spectra of the surface of the sample.

Table 4.1 Testing matrix for laboratory aged binders

Binder Grade	**Aging Condition**	**Asphalt Modifier/Polymers**
PG 64-22	Unaged	Control (No modifier)
	20 hours PAV aged	1% Redicote by weight
	40 hours PAV aged	3% Solprene by weight
	60 hours PAV aged	

All tests were carried with the OMNIC software version 8.2.0.387 of Thermo Scientific and the spectral data was analyzed accordingly. The spectrometer was calibrated by cleaning the crystal with toluene and collecting background data before testing.

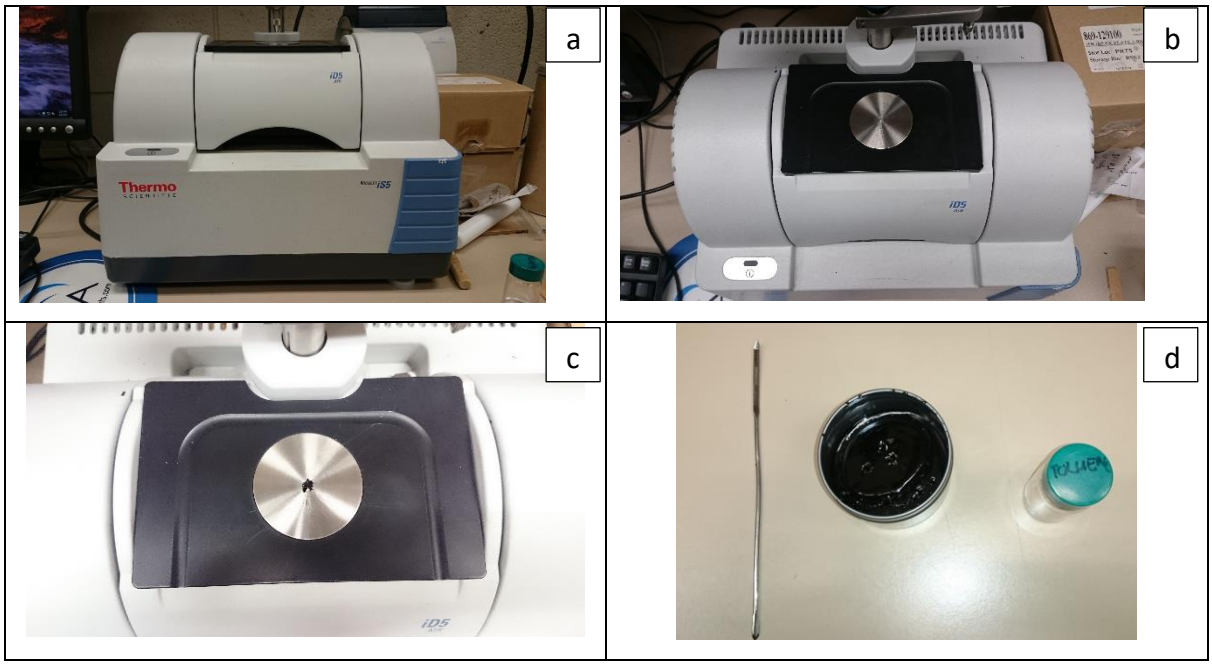

Figure 4.2 FTIR testing procedure with a Thermo Scientific Nicolet iS5 FT-IR Spectrometer

Three to five replicates were tested and their spectra were averaged and the baseline was corrected. In addition, the area under the peak of certain bands of chemical functional group based on the literature was calculated using OMNIC software.

4.2.2 *Aged Binder Extracted from Field Cores*

The test sections selected in this study are located in Qatar. Details of the pavement location and construction history is described in the paper of Sirin et al. (2017b). Figure 4.4 shows the layout of the test sections and information on layer thickness, mix design and materials used in each section. Gabbro was used as major aggregate in all the layers except base course of Section 3 where limestone was used. The wearing and base course of Section 5 differ in both mix design and asphalt type. Two different mix designs were used; Qatar Construction Specifications (QCS) or the Marshall Mix Design method and the percentage refusal density (PRD) design method.

	Section 1	Section 2	Section 3	Section 4	Section 5	Section 6
Wearing course 60mm	PRD Gabbro & Pen 40/50	PRD Gabbro & Pen 60/70	PRD Gabbro & Pen 60/70	QCS Gabbro & Pen 60/70	PRD Gabbro & Pen 60/70	PRD Gabbro & PMB
Base Course 270 mm	PRD Gabbro & Pen 40/50	PRD Gabbro & Pen 60/70	PRD Limestone & Pen 60/70	QCS Gabbro & Pen 60/70	QCS Gabbro & Shell Thiopave	PRD Gabbro & PMB
Subbase 200 mm	Unbound sub-base (Crushed stone)					
Subgrade	Sand					

Figure 4.3 Layers and materials properties of test sections (Sirin *et al.* 2017b)

Asphalt binders were extracted and recovered from field cores obtained from these test sites in accordance with ASTM D2172 (Method A). Methylene chloride was used as a solvent. Details of the extraction and recovery procedure is provided by Sirin et al. (2017b). A total number of 60 binder test samples were obtained; 10 asphalt binder samples were obtained from each test section (five from wheel path and five from the shoulder). The asphalt binders were extracted from wearing and base course at different depths (Figure 4.4). The test matrix is presented in Table 4.2. Similar to the laboratory-aged binders, three replicates were characterized by FTIR spectroscopy using the Thermo Nicolet iS5 spectrometer. The absorbance spectra were averaged and baseline corrected using OMNIC v8.0 software.

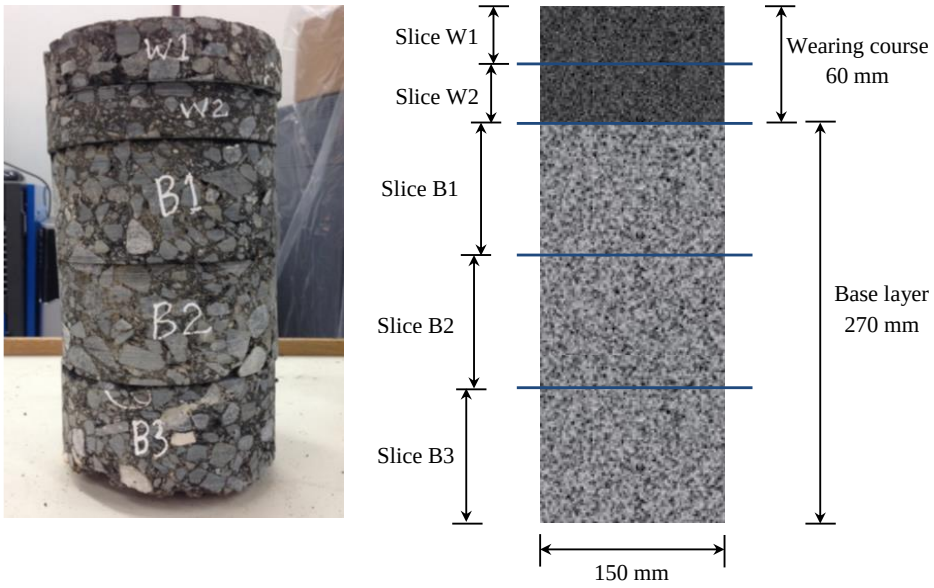

Figure 4.4 Schematic of slices from field cores after cutting (Sirin *et al.* 2017b)

Table 4.2 Testing matrix for extracted binders

Test Section	Location on the Pavement	Layer
Section 1	Wheel Path (WP)	Wearing course 1 (W1)
Section 2	Shoulder Path (SP)	Wearing course 2 (W2)
Section 3		Base course 1 (B1)
Section 4		Base course 2 (B2)
Section 5		Base course 3 (B3)
Section 6		

4.3 Experimental Results, Quantitative Analysis with FTIR and Discussion

4.3.1 *Impact of Antioxidant Additives on Chemical Growth of Carbonyl Components*

The Fourier Transform Infrared (FTIR) Spectroscopy is a widely used material-based analysis technique to identify unknown components of a compound and their quantity by passing an infrared (IR) radiation through the test sample (Thermo Nicolet 2001). Since part of the IR radiation gets absorbed by the specimen, the resulting spectrum outlines the amount of IR absorbance. Since each chemical compound displays a particular IR spectrum due to the unique combination of bonds among atoms and molecules, it works as a fingerprint of that compound. The size of each of the absorption peaks in the spectrum indicates the quantity of components present in a test specimen. To quantify the effect of oxidative aging on asphalt binder, many researchers (Lamontagne et al. 2001; Zhang et al. 2011; Yao et al. 2013; Han 2011) used FTIR spectroscopy and confirmed Carbonyl functional group as an indicator of oxidative aging which is usually centered on wavenumber of 1700 cm^{-1}.

In this first section, the FTIR was used to investigate the impact of using antioxidant additives on the growth of Carbonyl components. For the quantitative analysis, four band area ratios were identified based on the literature and their indices were calculated. The area of each band was calculated directly from the baseline corrected spectra using the peak area tool of OMNIC software. The valley to valley approach was used while measuring area under each of the peaks as per Lamontagne et al. (2001) since several vibrations of the same type of functional groups were taken into account. For example, there are six functional groups containing the carbonyl group, i.e., carboxylic acid, ketone, amide etc. and each of them have their own specific band but the overall band range for carbonyl group (C=O) was found to be

within wavenumber of 1650 cm^{-1} to 1820 cm^{-1} or 1850 cm^{-1} with the peak centered on 1697 cm^{-1} while the sulfoxide group (S=O) was centered on 1032 cm^{-1} from the spectra. The aliphatic branched and index band peak was found to be centered on wavenumber of 1376 cm^{-1} and 1456 cm^{-1}, respectively whereas the aromatic band was centered around 1600 cm^{-1}. The indices can be calculated from following formulas:

- Carbonyl index, $I_{C=O} = \frac{Area\ of\ the\ carbonyl\ band\ centered\ around\ 1697\ cm^{-1}\ (A_{1697})}{\sum A}$
- Sulfoxide index, $I_{S=O} = \frac{Area\ of\ the\ sulfoxide\ band\ centered\ around\ 1030\ cm^{-1}\ (A_{1030})}{\sum A}$
- Aliphatic index, $I_{C-H} = \frac{\sum I_{C-H\ of\ CH_3} + I_{C-H\ of -(CH_2)n-}}{\sum A}$
- Aromatic index, $I_{C=C} = \frac{Area\ of\ the\ aromatic\ band\ centered\ around\ 1600\ cm^{-1}\ (A_{1600})}{\sum A}$

where, $I_{C-H\ of\ CH_3} = \frac{Area\ of\ the\ aliphatic\ branched\ band\ centered\ around\ 1376\ cm^{-1}\ (A_{1376})}{\sum A}$;

$I_{C-H\ of -(CH_2)n-} = \frac{Area\ of\ the\ aliphatic\ index\ band\ centered\ around\ 1456\ cm^{-1}\ (A_{1456})}{\sum A}$;

∑A = Summation of area of the following spectral bands

$= A_{1697} + A_{1600} + A_{1456} + A_{1376} + A_{1032} + A_{864} + A_{814} + A_{743} + A_{724} + A_{(2923,2852)}$

Based on these formulas, the four indices were calculated from each of the spectra. Figure 4.5 shows the spectral comparison of control unaged PG 64-22 binder, PAV-aged control binder, and PAV-aged binder modified with 1% Redicote and 3% Solprene. Graphically, the difference in the area under the peak of 1696 cm^{-1} is visible in the spectra as the 60 hours PAV aged control binder has the highest peak. No peak centered at the wavenumber of 1696 cm^{-1} in the control unaged binder which confirms that the functional groups containing carbonyl compound forms through oxidation after aging.

Based on the literature, change in the growth of carbonyl compound is considered as an indicator of aging. The carbonyl indices were calculated from the absorbance spectra of the control and antioxidant modified binders at different long-term aging hours, i.e. 20, 40 and 60 hours. Figure 4.6 demonstrates the growth in carbonyl content with increased PAV aging

durations. For example, 3%S 60 means it is PG 64-22 binder modified with 3% Solprene and aged up to 60 hours in PAV. Similarly, 1%R 20 means the binder is modified with 1% Redicote and aged up to 20 hours in PAV. The results showed that the growth in carbonyl content is not linear with PAV aging (Figure 4.6). In addition, there was no presence of carbonyl compound in the unaged binders. This confirms that the presence of carbonyl compounds in asphalt binder is due to oxidative aging, the process in which aliphatic hydrocarbons react with the oxygen of air and produce various carbonyl functional groups, such as ketone, aldehyde, amide, ester etc.

Asphalt binder is traditionally considered as a dynamic colloidal system of the following four main chemical components: asphaltenes, resins, aromatics, saturates. It is considered that the high molecular weight asphaltene micelles are dispersed in a lower molecular weight maltenes (Loeber et al. 1998). Several possible oxidation reactions might occur during the aging of asphalt. During the oxidation process, asphalt molecules degenerate to form free radicals. It is suggested that these free radicals further react with oxygen and form unstable hydroperoxide (R-O-O-H) which decompose to carbonyl and sulfoxide functional groups (Ouyang et al. 2006a). The antioxidant additives retard the chemical growth of carbonyl components in asphalt binder by inhibiting the growth of peroxides or by radical scavenging (Ouyang et al. 2006a). Antioxidant additives act as peroxide inhibitor and react with hydroperoxides by reducing the growth of peroxy radicals and thus inhibiting the spread of free radical chain. This prevents further oxidation of asphalt molecules. Another suggestion on the antioxidation mechanism of copolymer is that the copolymer molecules trap the asphalt molecules within their polymeric network, created through the reaction between polymeric free radicals and C=C double bonds, and prevent oxidation (Cortizo *et al.* 2004; and Ouyang *et al.* 2006a).

Either the inhibition of free radical chain or less exposure to oxygen because of the linkage between asphalt molecules and polymeric free radicals, both the additives (Redicote and Solprene) used in this part of study have successfully retarded further carbonyl growth in asphalt binder (PG 64-22). There is no significant difference in the performance of 3% Solprene and 1% Redicote. Both are equally viable in retarding carbonyl growth.

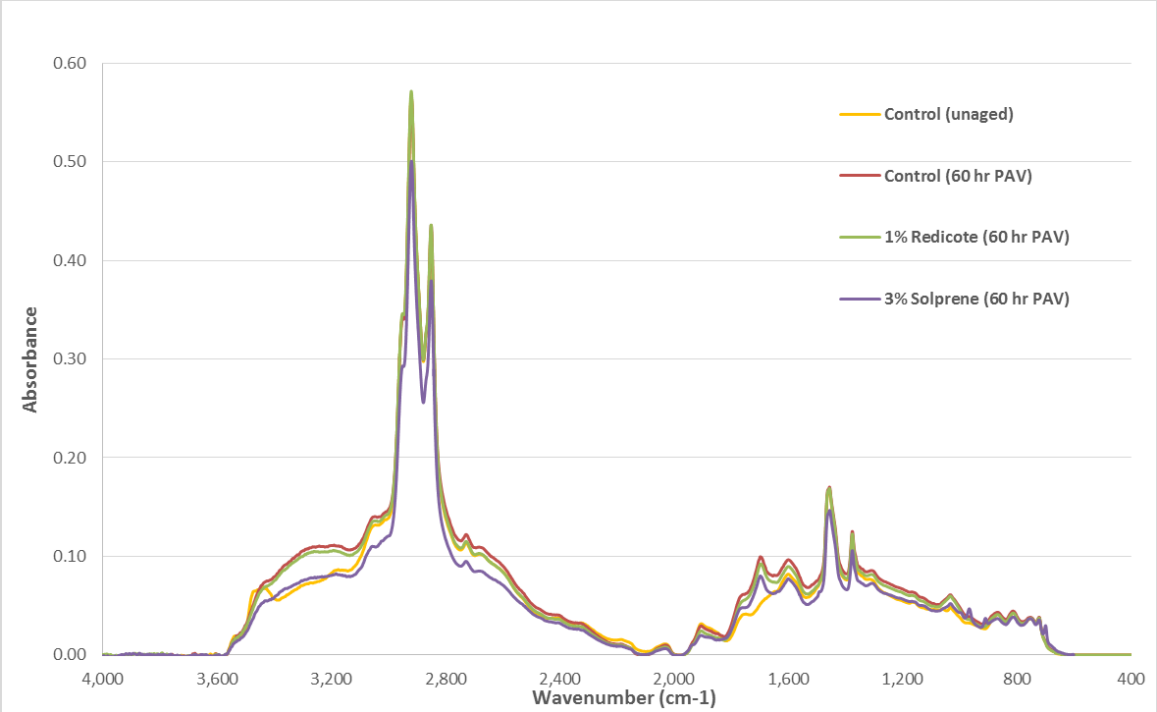

Figure 4.5 FTIR spectra of lab-aged binders

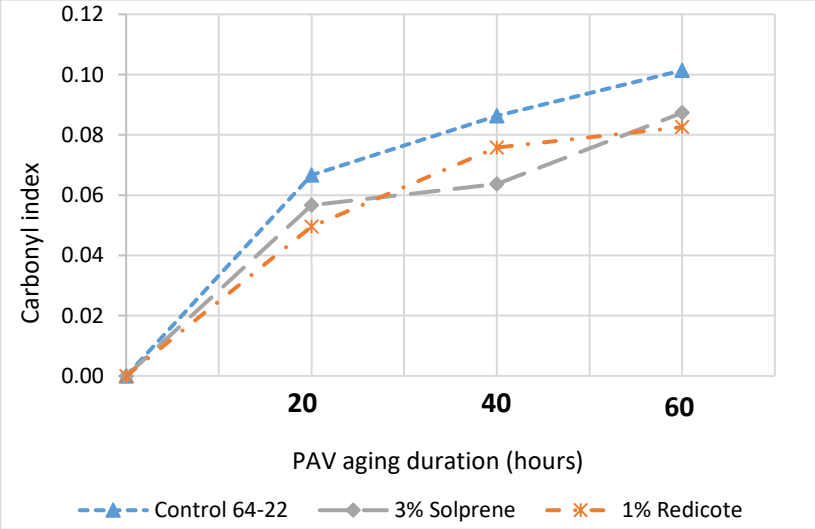

Figure 4.6 Impact of Antioxidant Additives on Retarding Carbonyl Growth by FTIR Spectrometry

4.3.2 *Aging Characteristics of Field-Aged Binder*

FTIR spectral analysis was performed on field-aged binders extracted from field cores obtained from six test sections at Qatar (Figures 4.3 and 4.4). The FTIR spectrometry was conducted to assess the relationship between the functional groups present in asphalt including Carbonyl, Sulfoxide, Aromatic and Aliphatic group and the rheological properties of the binders such as viscosity.

Figures 4.7 and 4.8 represent a typical FTIR spectra of asphalt binder samples extracted from the shoulder of Section 1 for base and wearing courses, respectively. 'SP' refers to shoulder path whereas B1, B2, B3 indicate Base 1, Base 2 and Base 3, respectively. It should be noted that the base was divided into three parts (see Figure 4.4). Similarly, the wearing course was divided into two parts referred as W1 and W2 (Figure 4.4). The spectra analysis confirmed that all of test samples had some extent of carbonyl and sulfoxide component at the peak around 1696 cm^{-1} and 1032 cm^{-1}.

To define the amount quantitatively, respective indices of functional groups were determined as presented in Figure 4.9. In addition to the change in carbonyl and sulfoxide group, the changes in concentration of aliphatic and aromatic hydrocarbon groups were also determined. Over time, the long chained aliphatic hydrocarbons react with oxygen through the aging process and their concentration decrease. Previous research found a decrease in aliphatic index ratio and an increase in aromatic index ratio after aging in the asphalt binder modified with carbon microfiber in comparison to the control binder (Yao et al. 2013) which is due to the hydrogenation of asphaltene into aromatic hydrocarbon and thus increasing the aromatic index.

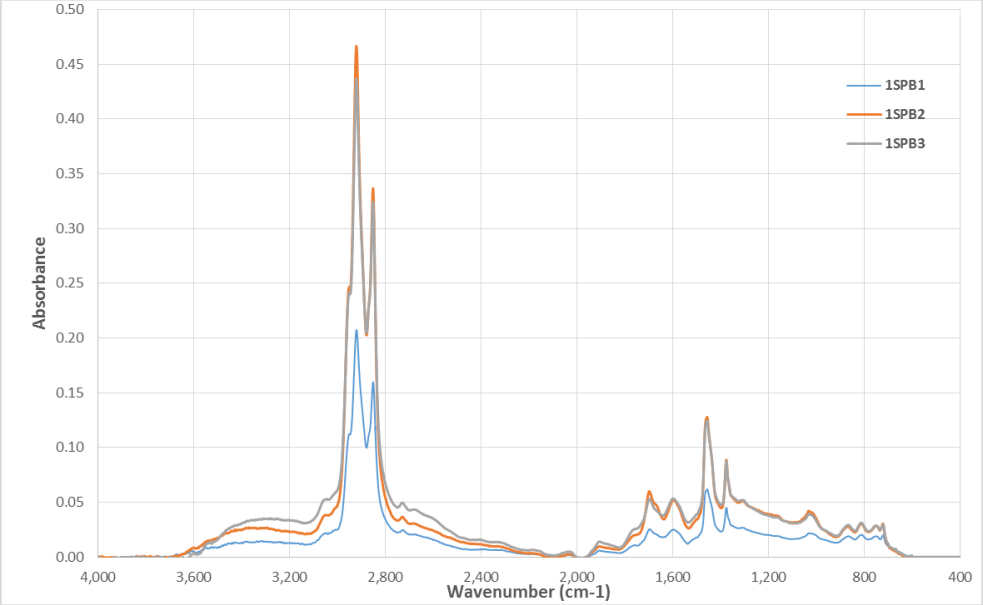

Figure 4.7 FTIR Spectral for asphalt binder samples extracted from of the base course of the shoulder path

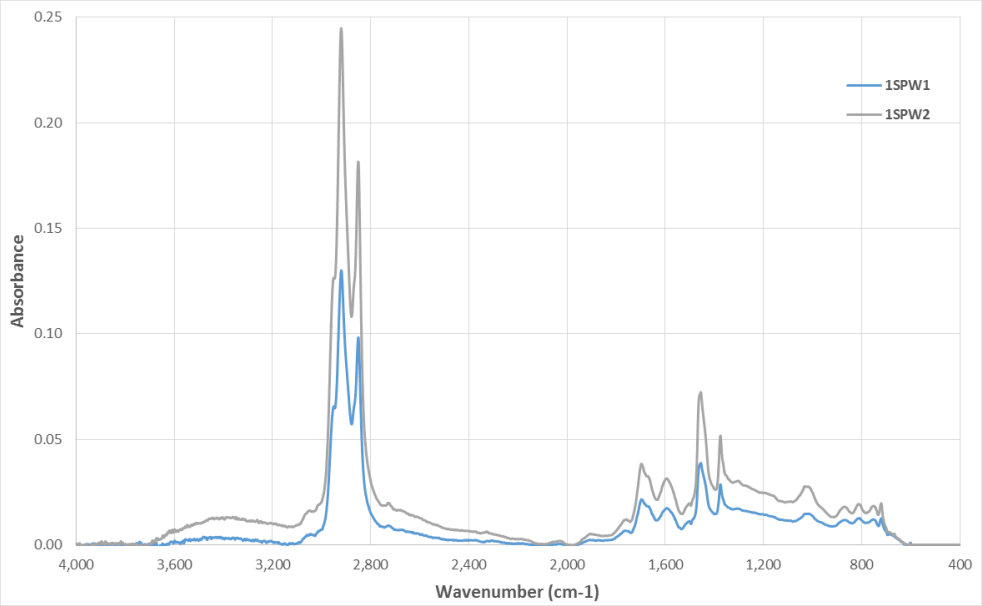

Figure 4.8 FTIR Spectral for asphalt binder samples extracted from of the wearing course of the shoulder path

Figure 4.9 shows the wearing course has more carbonyl content compared to the base course in all test sections. This is because that the wearing course is subjected to more oxidative aging compared to the base course. Regarding sulfoxide index, it was found higher in the wearing courses of Section 1 (shoulder path) and Section 4 (wheel path) but the opposite in Section 3

and 6. Section 5 also provided contradictory results whereas Section 2 failed to provide any correlation of sulfoxide content with depth. This mixed pattern of change of sulfoxide index due to aging was observed by many other researchers (Zhang et al. 2011; Ouyang et al. 2006a; Yao et al. 2013) and thus not considered as an indicator of oxidative aging.

Figure 4.9 also shows the change in the aromatic and aliphatic indices with pavement depth for wearing and base course. In all the sections, aromatic index is slightly higher in wearing course than the base course except Section 5 whereas the aliphatic index is lower in wearing courses compared to base section. This is due to the high rate of oxidation reaction of long chain hydrocarbons present in the asphalt binder of the wearing courses compared to the base sections (Zhang et al. 2011; Xu and Huang 2010; Ouyang et al. 2006b). Due to the natural process of oxygen diffusion throughout the depth of pavement, binders at the top layer are more exposed to the oxidation process. Due to oxidation, the maltenes of aliphatic hydrocarbon form asphaltene and the natural resins and asphaltenes hydrogenate into aromatic hydrocarbons (Yao et al. 2013). The presence of planar structured aromatics is confirmed by the peak centered around 1600 cm^{-1} due to the C=C double bond (stretching vibration) in the spectrum of field-aged asphalt binder. This phenomenon of the decrease in aliphatic index ratio with associated increase in aromatic index ratio was confirmed by the findings of Yao et al. (2013). Hence, aromatic index was higher at the wearing courses of all test sections whereas aliphatic index was lower in wearing courses compared to the base course.

Section 1 (Penetration grade 40/50) had the highest aliphatic index (Figure 4.9) compared to other test sections. The SBS polymer modified binder (PG 76-22) of section 6 was found to have the highest carbonyl content and least aliphatic index, along with Section 4 (PG 64-22).

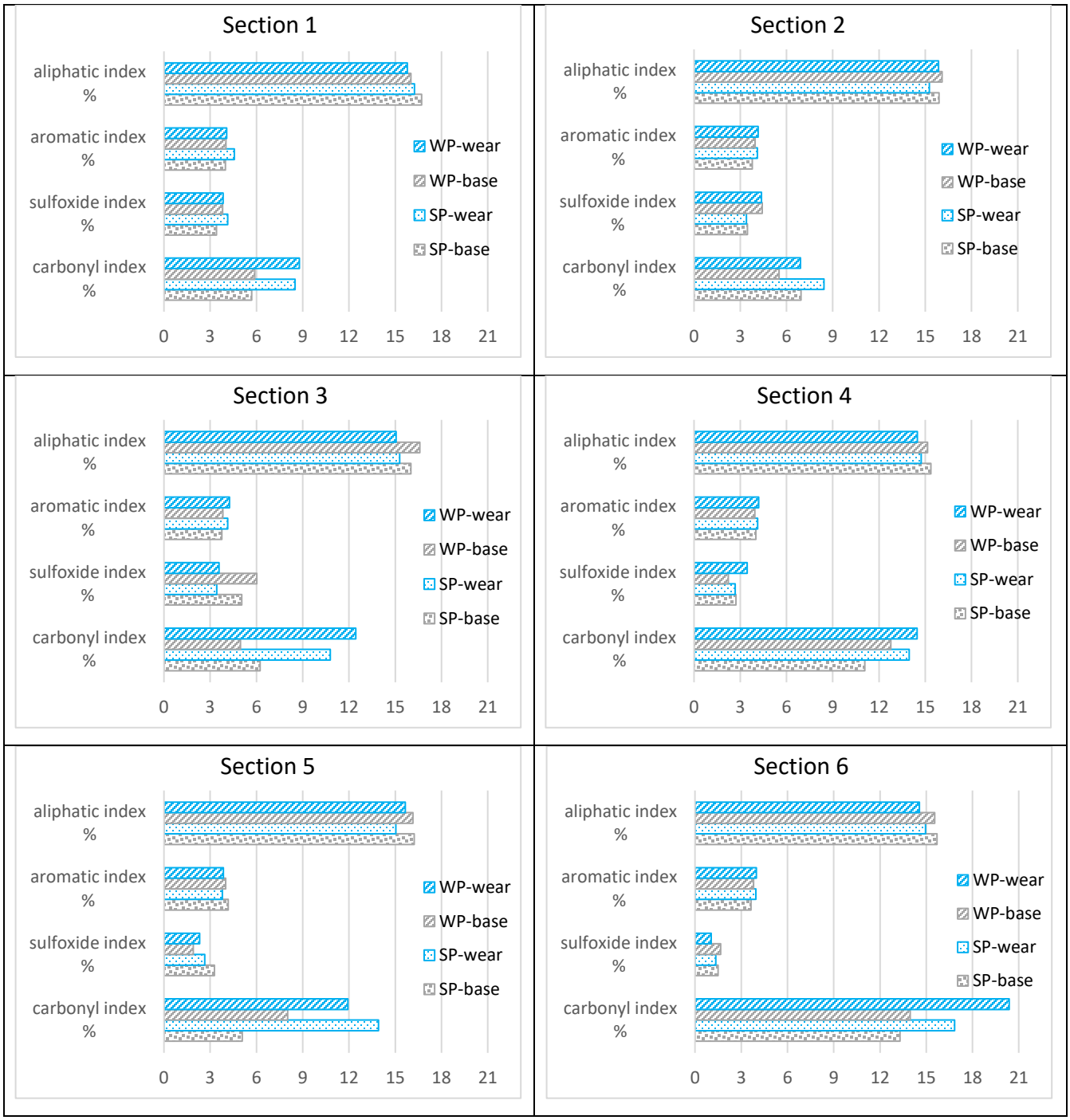

Figure 4.9 Change of carbonyl, sulfoxide, aromatic and aliphatic indices determined by FTIR spectrometry with different test sections and layers

Based on the previous findings, carbonyl content was considered for further analysis. The carbonyl index showed a good correlation with rheological properties such as apparent viscosity at 135 °C and 165°C (as per ASTM D4402-06) as presented in Figures 4.10 and 4.11. The carbonyl index increased with the viscosity of asphalt binder in all test sections at both

135°C and 165°C. In addition, the wearing course had higher viscosity and carbonyl index compared to the based course confirming that the wearing course is subjected to more oxidative aging.

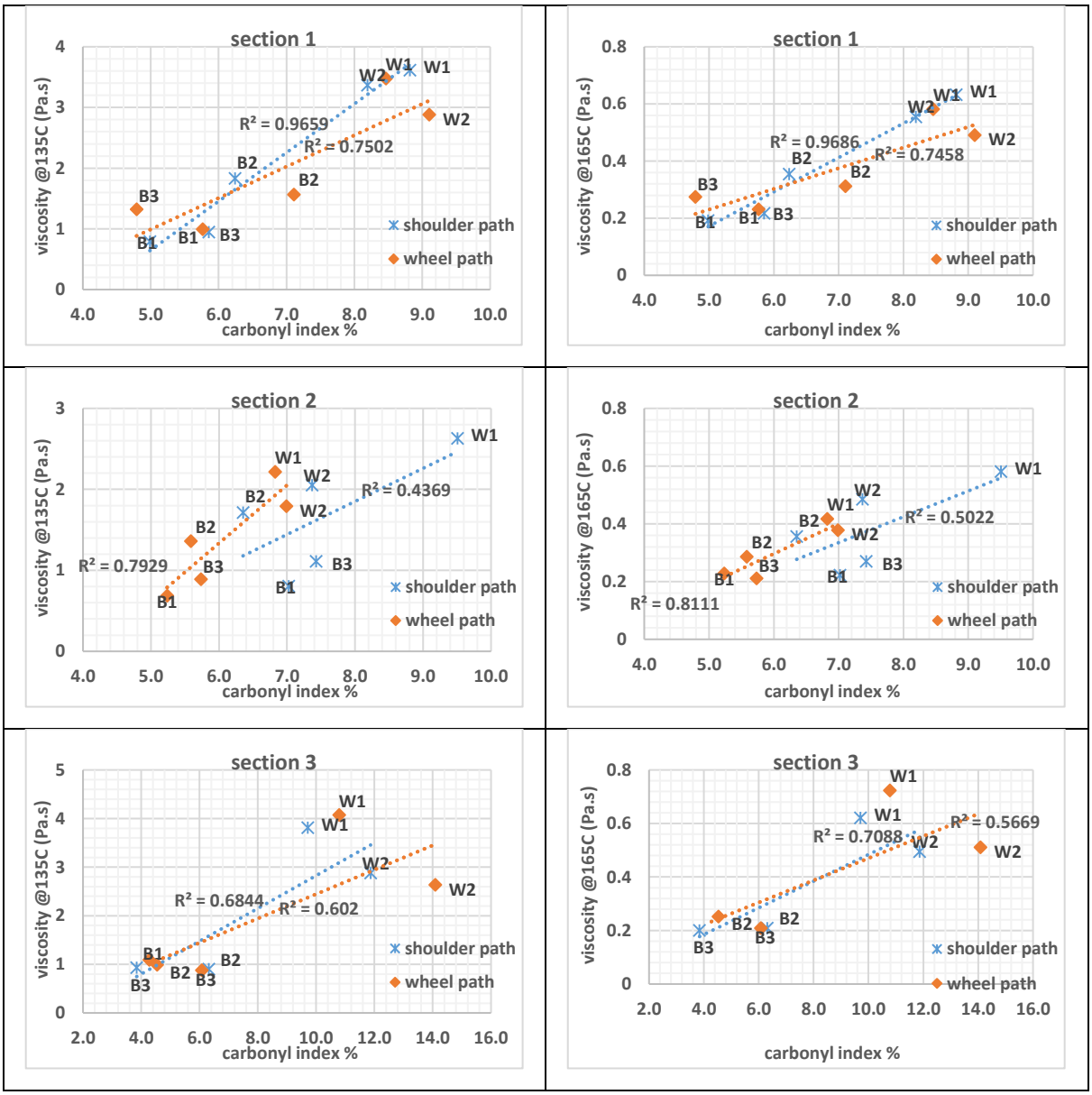

Figure 4.10 Correlation between Carbonyl index by FTIR spectrometry and viscosity of extracted binders (Section 1-3)

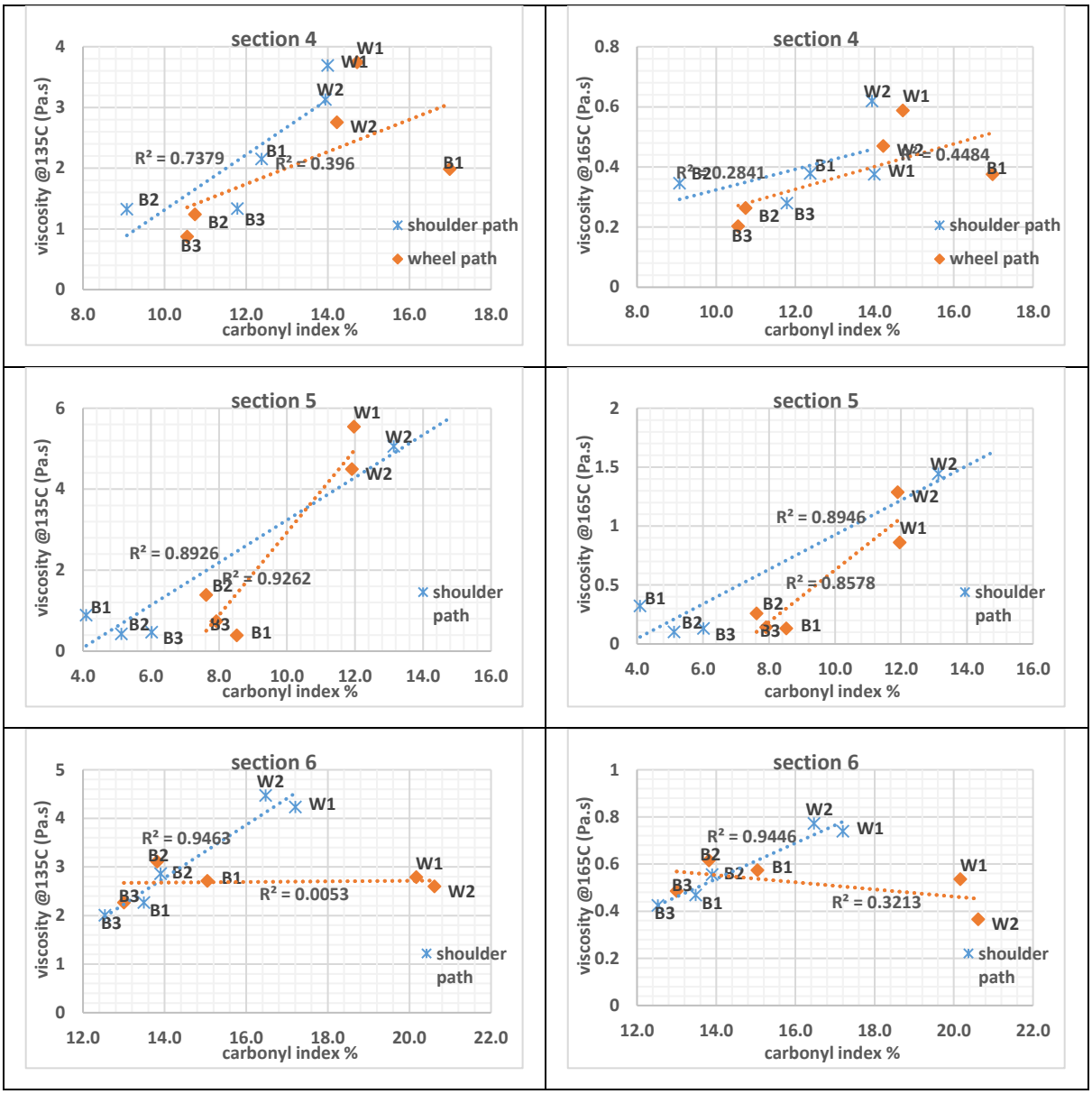

Figure 4.11 Correlation between Carbonyl index by FTIR spectrometry and viscosity of extracted binders (Section 4-6)

The highest amount of carbonyl index found in PRD was 14% whereas it was 17% in QCS, which was slightly higher than PRD. In respect to aggregate type, limestone was used in the base of Section 3 which had carbonyl index of 6% with a viscosity of less than 1 Pa.s whereas gabbro in Section 2 had 7.5% of carbonyl index with a viscosity greater than 1 Pa.s. These results show that aggregate type could affect the rate of binder aging which is consistent with the findings by Sirin et al. 2017b.

4.4 Comparative Characterization of Laboratory and Field-Aged Asphalt Binder with GPC

Several studies showed that the LMS(%) derived from the chromatograms affects the mechanical properties of asphalt binder such as viscosity, stiffness, brittleness etc. (Jennings 1980; Kim and Burati 1993; Kim et al. 2004). Higher LMS due to long-term aging was associated with higher stiffness and vice versa. This part of study examine the correlation between the LMS(%) and aging of asphalt binders. The LMS(%) was defined as the percentage of area under the chromatogram with molecules greater than 3000 Dalton (or g/mol) (Sheng et al. 201*6)* (Figure 4.12).

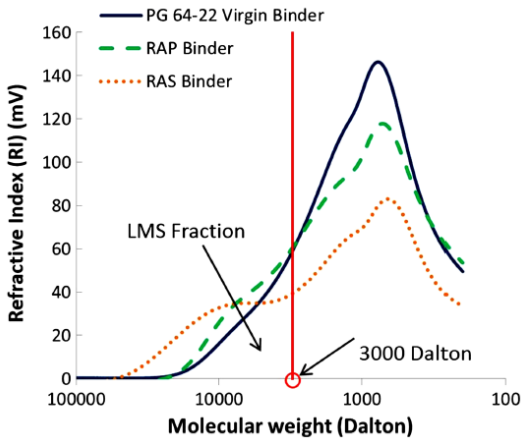

Figure 4.12 Determination of LMS(%) based on molecular weight (Sheng et al. 2016)

GPC tests were performed on both laboratory-aged binder and binders extracted from field cores. In the laboratory, the aging was performed up to 60 hours in PAV according to the AASHTO R28. The test samples included both unmodified PG 64-22 binder and binders modified with 1% Redicote and 3% Solprene. The field-aged binders were extracted from both wheel and shoulder path from six different test sections in Qatar (as discussed in Section 4.2.2). Specific samples were selected from the field-aged sample pool of six test sections and lab-aged binders. Control unmodified PG 64-22 was tested and compared with field-aged binders of wheel path from Section 2 (Figure 4.3). Section 2 was constructed using PG 64-22. Binders extracted from the top portion of surface course and bottom of base course were tested and compared with GPC results of control PG 64-22. In addition, PG 64-22 binders modified with antioxidant additives and copolymers (1% Redicote and 3% Solprene) and

subjected to 60 hours of PAV aging was also tested and compared to control PG 64-22. Since Section 6 was constructed using PG 76-22, the LMS results of field-aged binders extracted from the surface and base courses of Section 6 were compared to Control PG 76-22. Table 4.3 presents the test matrix for the GPC testing.

A Waters Breeze HPLC system with refractive index detector and GPC column was used for the chromatographic analysis (Figure 4.13a). Samples were prepared by dissolving asphalt binder in HPLC grade chloroform ($CHCl_3$) solvent. Each time, an amount of 10 to 11 mg of binder was placed into vials and 5 ml of chloroform was added with a volumetric pipette. To properly dissolve the binder in chloroform, the vials were mechanically swirled with a benchtop orbital shaker for 24 hours. All binders were dissolved within a similar concentration range of 2 to 2.2 mg/mL. Then about 100µL of asphalt solution was injected into a 2 mL autosampler vial filtering through a 0.45 µm syringe filter. To ensure consistency, the injection syringe and associated equipment were cleaned every time with chloroform using a Pasteur pipet dropper. After injection, the autosampler vials were put in to the removable trays and placed inside the AS3000 autosampler for running the tests. The system was calibrated using a range of narrow polystyrene standards (M_w of 2,000,000; 240,000; 98,900; 50,000; 13,000; 2,200; and 1,300 g/mol) and Benzil (210 g/mol) before testing the samples. The molecular weights (M_n and M_w) were determined using the principle of size exclusion chromatography (SEC). Molecular separation was achieved using a Jordi DVB linear mixed bed column (7.8 mm x 300 mm). The system temperature was maintained at 30°C and the flow rate was kept at 0.5 mL/min. Two types of detectors were used with the system; Waters model 2414 refractive index detector and a PostNova PN3609 multi-angle light scattering (MALS) detector. The NovaSEC v1.5.0.1 software was used to analyze the data. The peaks of the refractive indices in each chromatogram were integrated based on following criteria:

- For molecules with M_w greater than 3000 g/mol: between the elution time of 8.0 to 18.1 minute,
- For molecules with M_w less than 3000 g/mol: between 18.1 to 22.0 min.

Two replicates of each binder type were tested and the average LMS(%) results were reported.

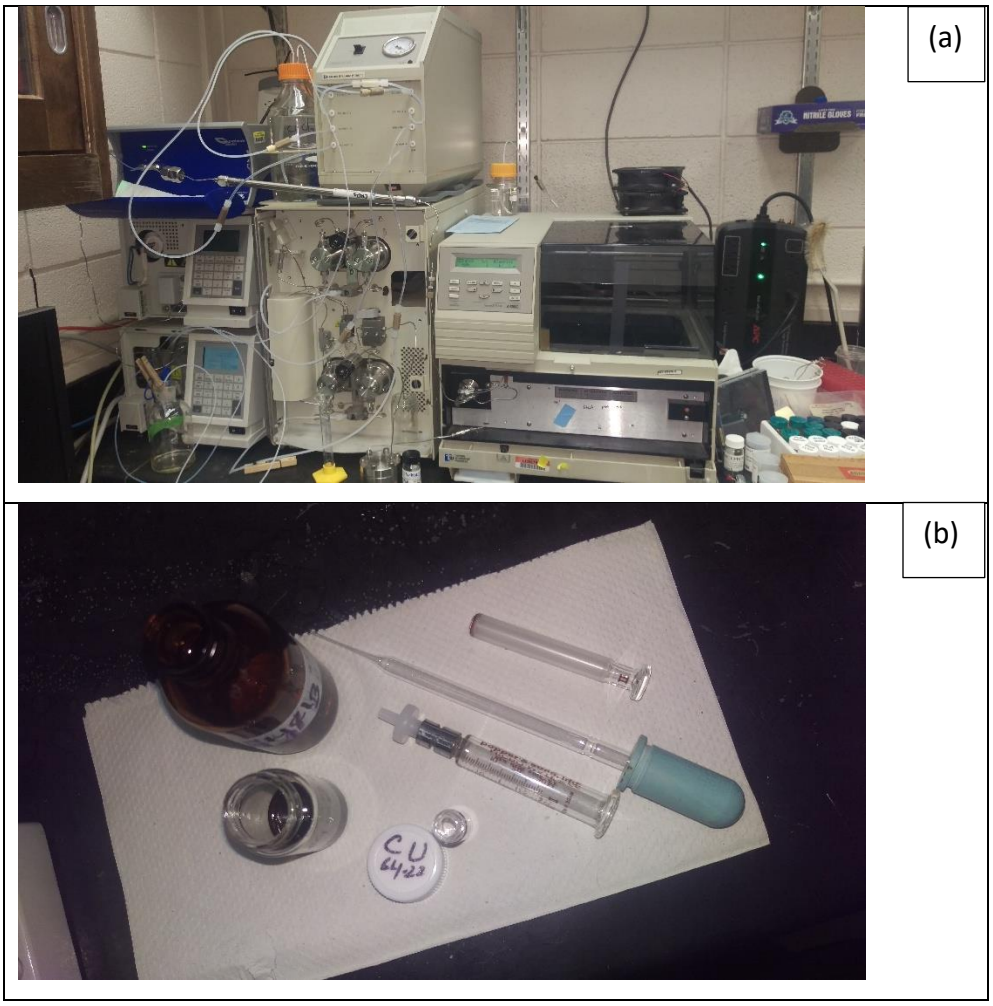

Figure 4.13 (a) Waters Breeze™ HPLC System, (b) sample preparation.

The testing matrix with concentration of each of the test samples is presented in Table 4.3.

Table 4.3 Testing Matrix for GPC

Sample ID	Description	Weight (mg)	Concentration (mg/ml)
Control PG 64-22	Control unaged unmodified PG 64-22	11.1	2.22
2WP W1	Top of section 2 wearing course (PG 64-22)	11.2	2.24
2WP B3	Bottom of section 2 base course (PG 64-22)	11.2	2.24
1%R CU	Unaged PG 64-22 mixed with Redicote (1% by weight of binder)	10.3	2.06
1%R 60	PG 64-22 mixed with Redicote (1% by weight of binder) and PAV aged up to 60 hours	10.8	2.16
3%S CU	Unaged PG 64-22 mixed with Solprene (3% by weight of binder)	10.8	2.16
3%S 60	PG 64-22 mixed with Solprene (3% by weight of binder) and PAV aged up to 60 hours	10.2	2.04
Control PG 76-22	Control unaged unmodified PG 76-22	10.6	2.12
6WP W1	Top of section 6 wearing course (PG 76-22)	10.7	2.14
6WP B3	Bottom of section 6 base course (PG 76-22)	10.6	2.12

4.5 Experimental Results, Quantitative Analysis with GPC and Discussion

The concentration of asphalt molecules (g/mol) eluting from the column through the pores of the beads was recorded. The resulting plot of refractive index versus elution time is called chromatogram. A typical chromatogram of unaged and unmodified asphalt binder (PG 76-22) is shown in Figure 4.14. The chromatograms of each sample tested are illustrated in Figure 4.15.

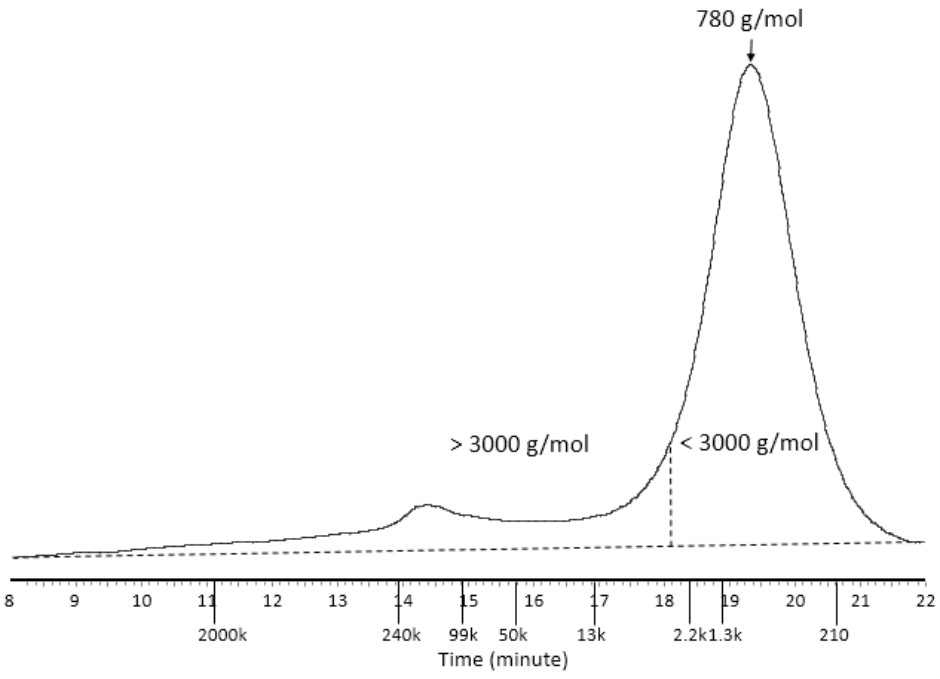

Figure 4.14 A typical chromatogram of control unaged binder (PG 76-22)

The abscissa in Figure 4.14 denotes the elution time (min). It can be seen from Figure 4.14 that the elution started approximately 8 minutes from injection and ended approximately after 22 minutes. The baseline of each of the chromatogram is corrected with the NovaSEC v1.5.0.1 software. The corrected baseline is also scaled in respect to the molecular weights of the narrow polystyrene standards and Benzil (from M_w of 2,000,000 to 210 g/mol) used for calibration, to specify the location of 3000 g/mol. From this location, a perpendicular line is drawn that divides the chromatogram into two distinct areas. Since the total area of the chromatogram denotes the total amount of asphalt molecules injected into the column (Kim et al. 2004), the area under the curve greater than 3000 g/mol provides with the LMS(%) in respect to the whole area. These areas greater than 3000 g/mol from each of the chromatogram were converted into molecular weight distribution and presented in Table 4.4 along with the rate of increase in LMS(%). From the LMS(%) value of each samples, the LMS ratio was calculated and presented in Figure 4.16. The LMS ratio is the ratio between LMS value after long-term aging to the LMS value of unaged samples of the same binder type (Lee et al. 2009). The LMS(%) value of each sample is also graphically represented in Figure 4.17.

Table 4.4 Molecular weight distribution of samples tested

Sample ID	Elution Time (min)	MW peak	SMS + MMS (<3000 g/mol) (in %)	LMS (>3000 g/mol) (in %)	Rate of increase in LMS(%)
Control PG 64-22	19.45	780	83.3	16.7	-
2WP W1	19.42	780	76	24	43.7%
2WP B3	19.44	780	77	23	37.7%
1%R CU	19.44	780	83.6	16.4	-
1%R 60	19.41	780	77.6	22.4	36.6%
3%S CU	19.46	780	79.9	20.1	-
3%S 60	19.43	780	73.4	26.6	32.3%
Control PG 76-22	19.4	780	80	20	-
6WP W1	19.43	780	70.8	29.2	46.0%
6WP B3	19.45	780	77.3	22.7	13.5%

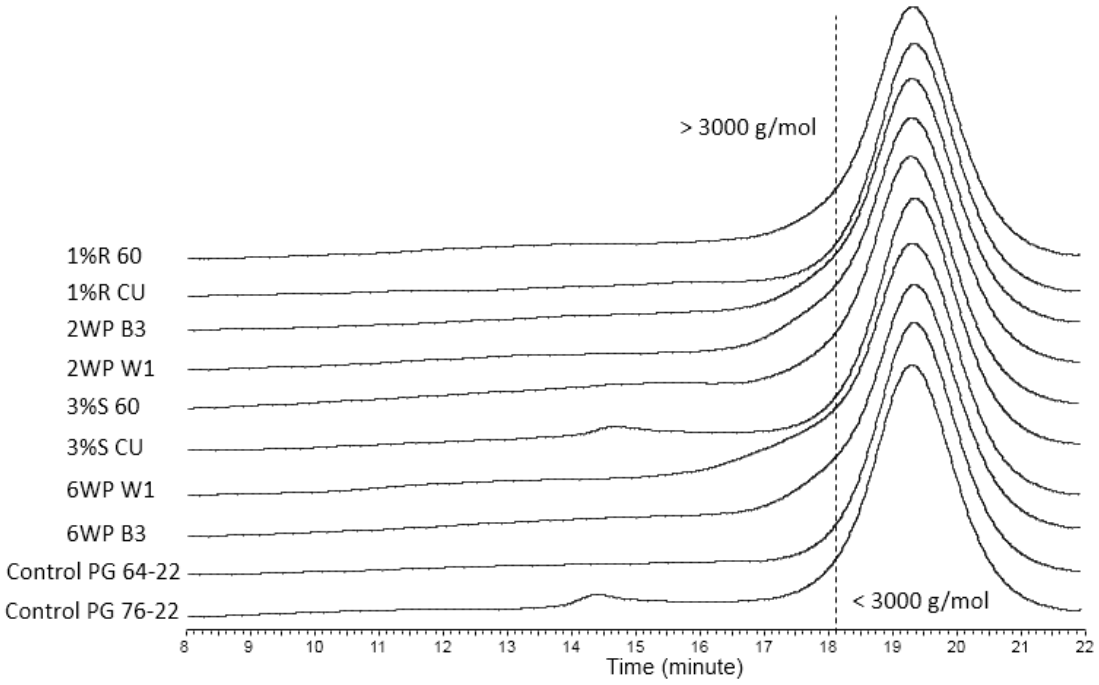

Figure 4.15 All the chromatograms of samples tested in GPC

The results showed that the wearing course had higher LMS(%) compared to the base course in both Sections 2 and 6. Section 2 was constructed using gabbro aggregate and PG 64-22 binder while Section 6 was constructed using gabbro aggregate and PG 76-22 binder.

In Section 2, the LMS(%) at the top of the wearing course (2WPW1) was found to be 24% whereas at it was 23% at the bottom of the base course (2WPB3). Similarly, in Section 6, the LMS(%) at the top of the wearing course (6WPW1) was 29.2% while it was 22.7% at the bottom of the base course (6WPB3). This higher percentage of LMS in the wearing course indicates more aging at the top layer of pavement compared to the bottom layer which is consistent with the findings from the FTIR analysis (Figures 4.9 and 4.10).

The LMS ratio was used to evaluate the rate of aging. As discussed earlier, the LMS ratio is the ratio of the LMS(%) of the aged test sample to that of the unaged one. Figures 4.16 and 4.17 show the LMS ratio and LMS(%) of the test samples, respectively. The results showed that both Redicote and Solprene additives provided favorable effect in terms of LMS ratio with values of 1.37 and 1.32, respectively compared to LMS ratio of the field-aged binder (PG 64-22). The LMS ratio of both surface and base courses of Section 2, which is constructed using PG 64-22 binder, were 1.44 and 1.38, respectively.

In addition, the results showed that the unaged PG 64-22 modified with Solprene (3%S CU) had higher LMS% value compared to Redicote (1%R CU). This increase in the large molecular weight percentage of unaged Solprene-modified PG 64-22 binder is due to the high molecular weight of Solprene 1205 [158.244 g/mol (PubChem 2017)]. Although Solprene performed slightly better in terms of decreasing LMS% growth rate compared to Redicote, both the additives were found viable alternative in retarding oxidative aging. As presented in Table 4.4, the growth rate of LMS% of Redicote and Solprene were 36.6% and 32.3%, respectively, which is lower than that of the base course and wearing course of Section 2 (i.e., 43.7% and 37.7%, respectively).

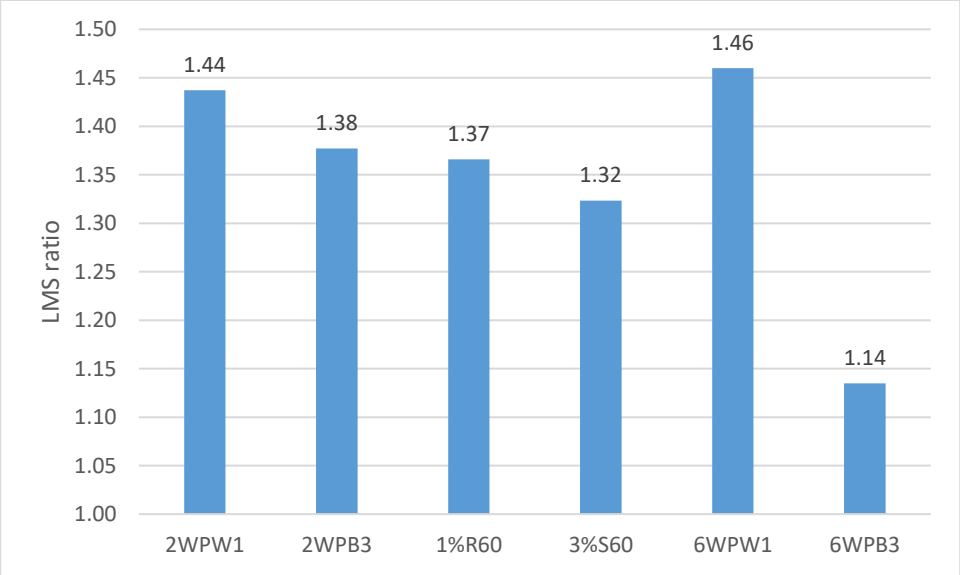

Figure 4.16 LMS ratio of the test samples

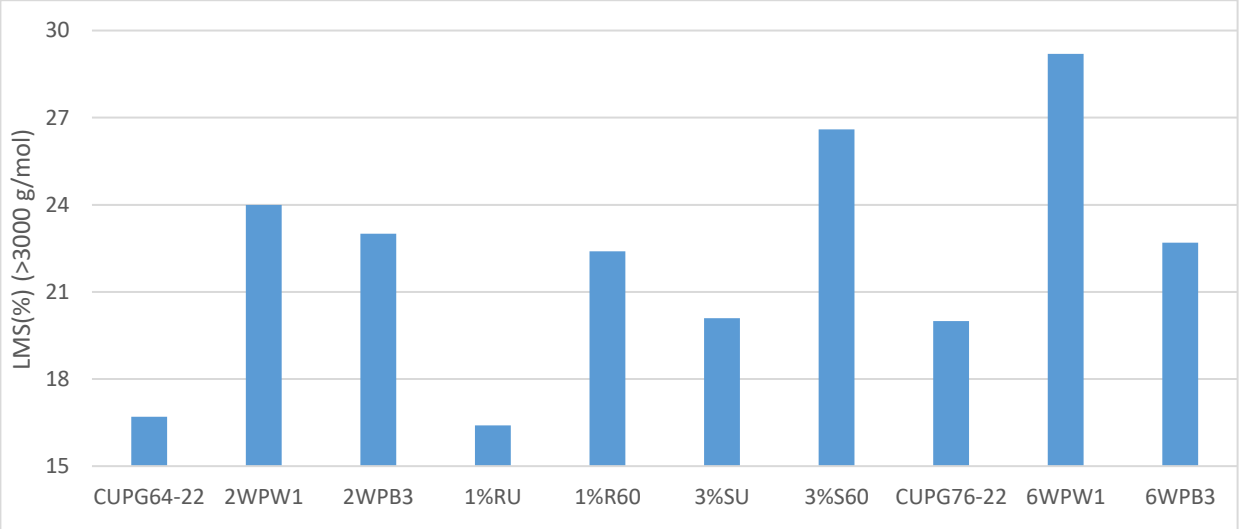

Figure 4.17 LMS(%) of test samples

4.6 Comparative Characterization of Laboratory and Field-Aged Asphalt Binder using AFM

In this section, the AFM was used to evaluate the effect of aging on the micro-mechanical properties of asphalt binders. The same set of test samples used in the GPC analysis was also tested using the AFM as presented in Table 4.3. The test asphalt binders were selected to cover number of parameters including aging conditions (unaged versus aged), aging method (field versus laboratory), type of modification (antioxidant additives and copolymers), performance grade (PG 64-22 and PG 76-22), and viscoelastic characteristics (G*sinδ as presented in Chapter 3). In addition, the test samples include binders exacted from the wearing course and base course from two field test sections (Section 2 and Section 6). The description of test sections was provided in Section 4.2.2. Figure 4.18 summaries the testing matrix used in AFM testing and sample ID.

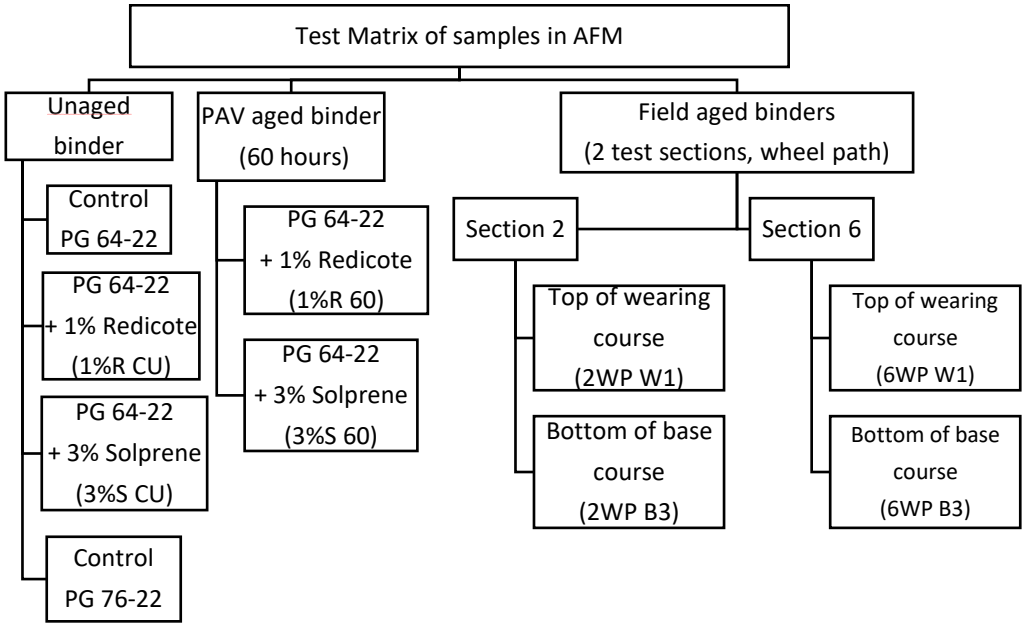

Figure 4.18 AFM Test Matrix

The WITec alpha300A Atomic Force Microscope was used for imaging of asphalt microstructure. The alpha300A system uses a precise "capacitive-feedback controlled scan-stage" with a scan range of 100 x 100 x 20 µm (WITec 2003a). This AFM system is capable of high-speed data acquisition and includes a programmable modulation generator and data evaluation module to process the force curves in real-time. However, the AFM is controlled through a computer where all the data visualization, storage and post-processing is done with

the associated software of the WITec system known as Project FOUR v4.1.15.36. The AFM was operated in Digital Pulse Force Mode (DPFM) to obtain information on the local mechanical properties of sample surface. The DPFM is an intermittent contact mode, especially suitable for soft and sticky materials (e.g., asphalt), that provides information on stiffness and adhesion in addition to the topographic image. With the programmable modulation generator, the z-piezo of the AFM can be programmed between 10 to 10,000 Hz. Usually a frequency of 1000 Hz is used and the amplitude of the signal is adjusted while scanning, to complete the cycle of force-distance curve. This frequency is usually lower than the resonance frequency of the cantilever tip. Figure 4.19 represents a typical force-distance curve between the tip and sample surface with the location of the measurements taken for each of the parameters. At the beginning, the baseline is set for the cantilever tip and it is moved towards the sample surface with the piezoelectric transducer. The attractive (negative) force between the sample surface and the tip makes them come in contact with each other. When the tip moves more towards the sample surface (downward), the repulsive (positive) force becomes dominant and reaches its maximum which is the F_{max}. After that, the piezo moves upward and force signal becomes attractive from repulsive again due to the increasing distance between the AFM tip and the sample surface. When the piezo moves upward further, the tip is detached from the sample surface. The adhesion peak value between the probe tip and the sample surface is found just before the tip loses its contact. After that, a new cycle begins and the whole process gets repeated. The measured gradient of the rising slope of the repulsive force in a cycle is denoted as the stiffness of a sample.

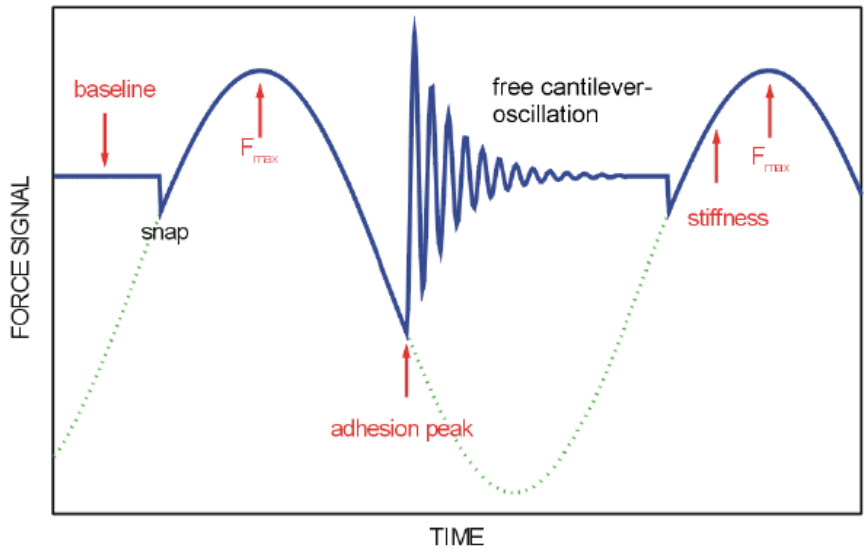

Figure 4.19 A complete modulation period. Dotted line is the modulation voltage and straight line is the force signal. Arrows show the position of baseline, F_{max}, adhesion and stiffness measurements respectively (WITec 2003b)

While working in DPFM mode, the modulation factor, photodetector and the cantilever tip of the AFM are required to be calibrated before taking any measurement (Schindelin et al. 2015). The modulation factor is the proportional constant between the oscilloscope amplitude and the force signal. It is calculated by measuring the oscilloscope amplitude at different values of amplitude set in DPFM control and averaging the ratios. The sensitivity of the photodetector is calibrated so that it can detect the tip deflection. A smooth sample (i.e., glass) surface is at first imaged with the tip and the force-distance curve is generated. The inverse value of the slope of the ascending and descending curves provide the sensitivity of the photodetector. Lastly, the spring constant of the AFM cantilever tip is calibrated by determining the quality factor (Q) obtained from a frequency sweep of the cantilever vibration at its resonance frequency. With the known value of the cantilever tip dimensions, frequency and quality factor, the tip spring constant was calibrated using the Sader method (Sader et al. 1999).

Due to the complexity of the spin-casting method, the heat-casting method used by Jahangir et al. (2015) was used in sample preparation. The binders were heated in a forced-draft oven at 150°C for 1 hour and a single drop of hot asphalt liquid was carefully poured on a 50 mm X 15 mm X 3 mm glass slide. Then the binders were allowed to cool slowly to ambient temperature (about 25°C). The glass slide was covered with steel container cap and the

wrapped with aluminium foil to prevent dust pick-up. The surface of the binder should be fairly smooth for testing. Then the glass slides containing the binders were tested in AFM. To maintain consistency, the same tip was used for all the samples. A nano-sensors cantilever tip (part no. PPP-ZEILR-10) with a calibrated force constant (C) of 1.8 N/m and resonant frequency (f) of 28 kHz was used in this study. The length, width and thickness of the cantilever tip are 449, 61 and 4 microns, respectively. Figure 4.20 represents the WITec alpha300A microscope with test setup, cantilever tip and the asphalt slides. Each of the scanned image is of 20 X 20 µm size (256 X 256 pixel). The default driving frequency of 1000 Hz was used with a scan speed of 0.4 s/Line. The base of the alpha300A comes with an active vibration isolation system (WITec 2003c) and environmental enclosure. The vibration isolation system helps obtain quality image by minimizing all the vibrations in the floor. Usually 3 to 5 scans were performed for each sample unless a good scan with minimal noise was obtained.

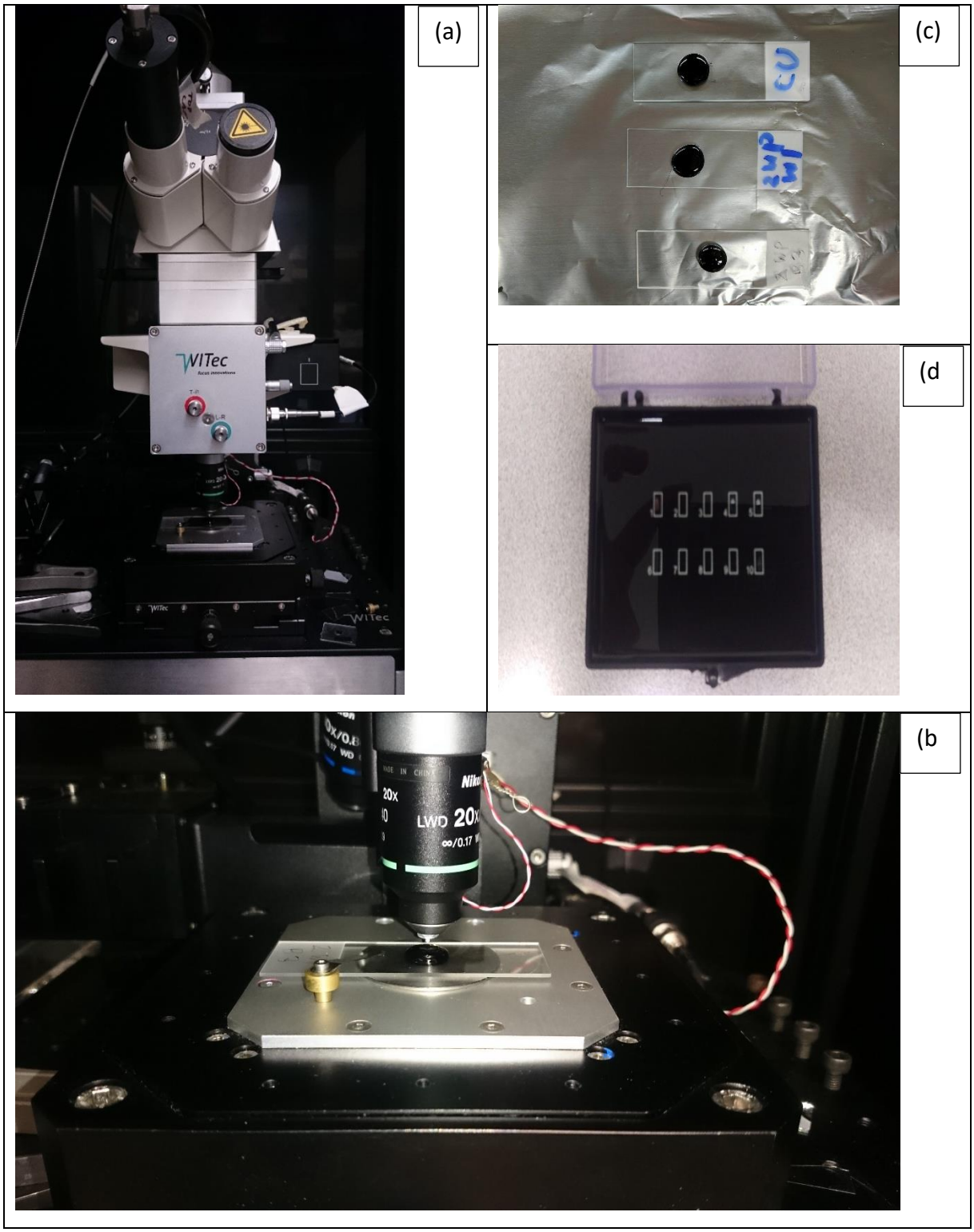

Figure 4.20 (a) WITec alpha300A microscope, (b) AFM test setup (zoomed), (c) glass slides with binder, (d) cantilever tips.

4.7 Binder Morphology, Experimental Results, Quantitative Analysis with AFM and Discussion

Based on the literature, the following parameters were considered for the AFM analysis:

- Phase identification from adhesion image
- Microstructural analysis based on change in % area of higher adhesion
- Line profile of the bee structures from topographic image
- Topography image statistics and roughness parameters (histogram and statistical data)
- Micro-mechanical properties such as adhesion and stiffness

As described earlier, four types of images were taken during each scan: surface topography, F_{max}, stiffness and adhesion. The topographic image provided information on surface roughness parameters and different phases of the surface microstructure. The F_{max} data was discarded due to irrelevancy to the objective of this study. The stiffness images gave valuable insights on the micro-rheology of the sample surface. The different microstructural phases in the asphalt binder and their subsequent changes with aging were clearly visible in the adhesion images. Similar to the terminology used by Jahangir (Jahangir *et al.* 2015), the term 'phase' is used to designate the microstructural domains noticed in the adhesion images and it does not imply to the physical state of any chemical substance. The term 'asphalt microstructure' implies the spatial distribution of these distinct phases on the sample surface. This section follows the same nomenclature used in the analysis with FTIR and same set of samples used in GPC test.

In the AFM analysis, two distinctive phases were observed in all the adhesion and topography images. These two phases were more prominent in the adhesion images of the DPFM mode and their distribution was completely random. Similar to the previous pattern observed by Allen (2010), the comparatively darker region was identified as Phase 1 and named as dispersing phase whereas the brighter region was identified as Phase 2 and subsequently named as dispersed phase. It was considered that Phase 2 is dispersed in the matrix of Phase 1. However, a third distinctive phase known as the 'bee' structures was observed in all the image types, i.e. adhesion, stiffness and topography, and identified as Phase 3. These

randomly distributed 'bees' or Phase 3 were surrounded by the matrix of Phase 1. A large difference in height distribution was observed in the topographic data of the bees when compared to the surrounding matrix of Phase 1. The findings on topographic analysis are described in detail in the later parts. Adhesion images with all the distinctive phases of a sample subjected to laboratory aging are shown in Figure 4.21. The left image portrays an unaged sample whereas the right one is the long-term laboratory-aged version of the same specimen. The increase in the percent area of the brighter region (Phase 2) is prominent after 60 hours of PAV aging. The darker regions indicate areas with lower adhesion (lower voltage values) and brighter regions have higher adhesion in the adhesion images.

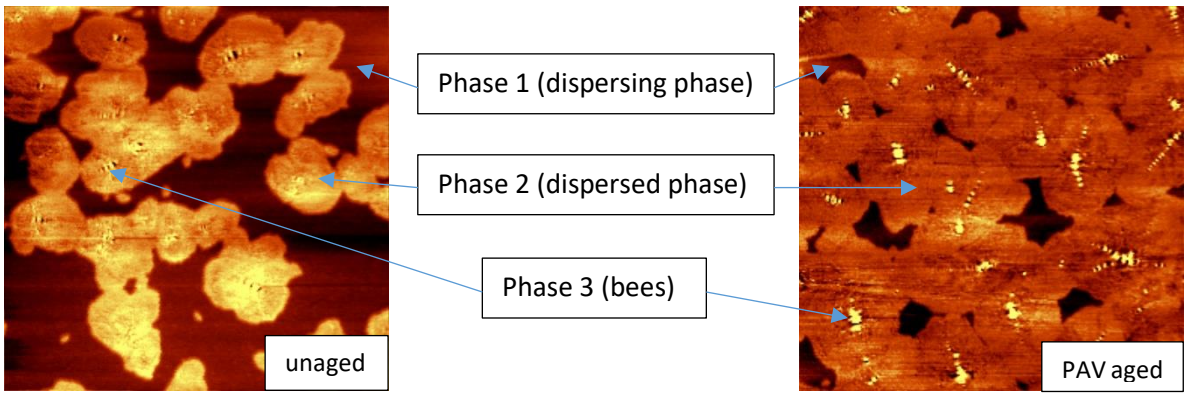

Figure 4.21 Identification of different phases in unaged and PAV aged binder (adhesion image)

The correlations of adhesion with surface topography and stiffness for all the samples are illustrated visually in Figures 4.22 and 4.23, respectively. These figures are presented in a scatterplot orientation with the X-axis as the image type (adhesion, stiffness and topography) and the Y-axis as distinct binder specimens. Both Figures 4.23 and 4.24 are divided into two blocks; Block A and Block B. In Figure 4.22, the first block (Block A) represents the comparison of the three image types with control unaged PG 64-22 (Control PG 64-22) to field-aged binders of Section 2 (2WP W1 and 2WP B3). The binder sample (2WP W1) was extracted from the wearing surface of Section 2 while binder sample (2WP B3) was extracted from the base course of the same section. The microstructural change due to field-aging with increased depth of pavement was observed in the wheel-path of Section 2. The effectiveness of antioxidant additives in retarding the oxidative aging in the microstructural level was observed

in the Block B of Figure 4.22 (1% R CU and 1% R 60) and Block A of Figure 4.23 (3%S CU and 3%S 60). PG 64-22 modified with 1% Redicote and 3% Solprene were aged in PAV for 60 hours (1%R 60 and 3%S 60) and the images were compared with that of the unaged ones (1%R CU and 3%S CU). In the second block of Figure 4.23, the field-aged binders from different depths of Section 6 wheel-path (top of HMA, i.e., 6WP W1 and bottom of base, i.e.,6WP B3) was compared with PG 76-22 (Control PG 76-22) since Section 6 was constructed using the same binder.

When the adhesion images are compared to the topographic images, in all cases, the brighter regions with higher adhesion correspond to the darker region in topography. This demonstrates that the changes in topography are usually accompanied by phase changes in adhesion of asphalt microstructure. Similar correlation of topography with phase images was observed by Allen 2010. However, a mixed correlation was observed between adhesion and stiffness images. Overall, the brighter regions indicate higher stiffness and vice versa. For some test samples (e.g., Control PG 64-22, 2WP W1, 2WP B3, 1%R CU, 3%S CU, Control PG 76-22 and 6WP B3), the brighter regions with higher adhesion correspond to brighter regions with higher stiffness. However, for three test samples (e.g., 1%R 60, 3%S 60 and 6WP W1), it was found that the brighter regions with higher adhesion correspond to darker regions of lower stiffness. This could be due to image artifact and the effect of surface slope during scanning.

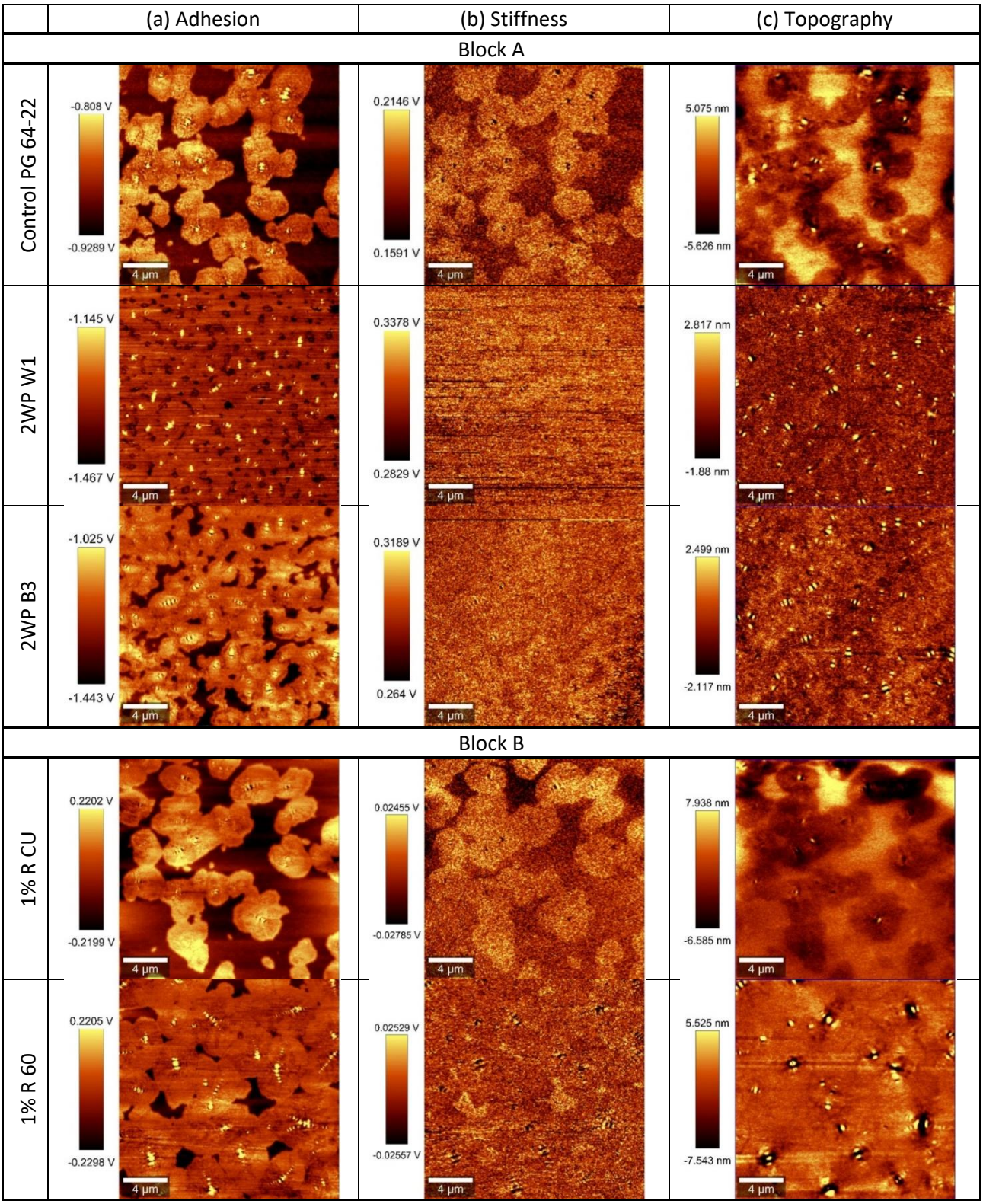

Figure 4.22 (a) Adhesion, (b) Stiffness and (c) Topography images of Control unmodified PG 64-22, 2WP W1, 2WP B3, 1% R CU and 1% R 60 binders (20 µm X 20 µm)

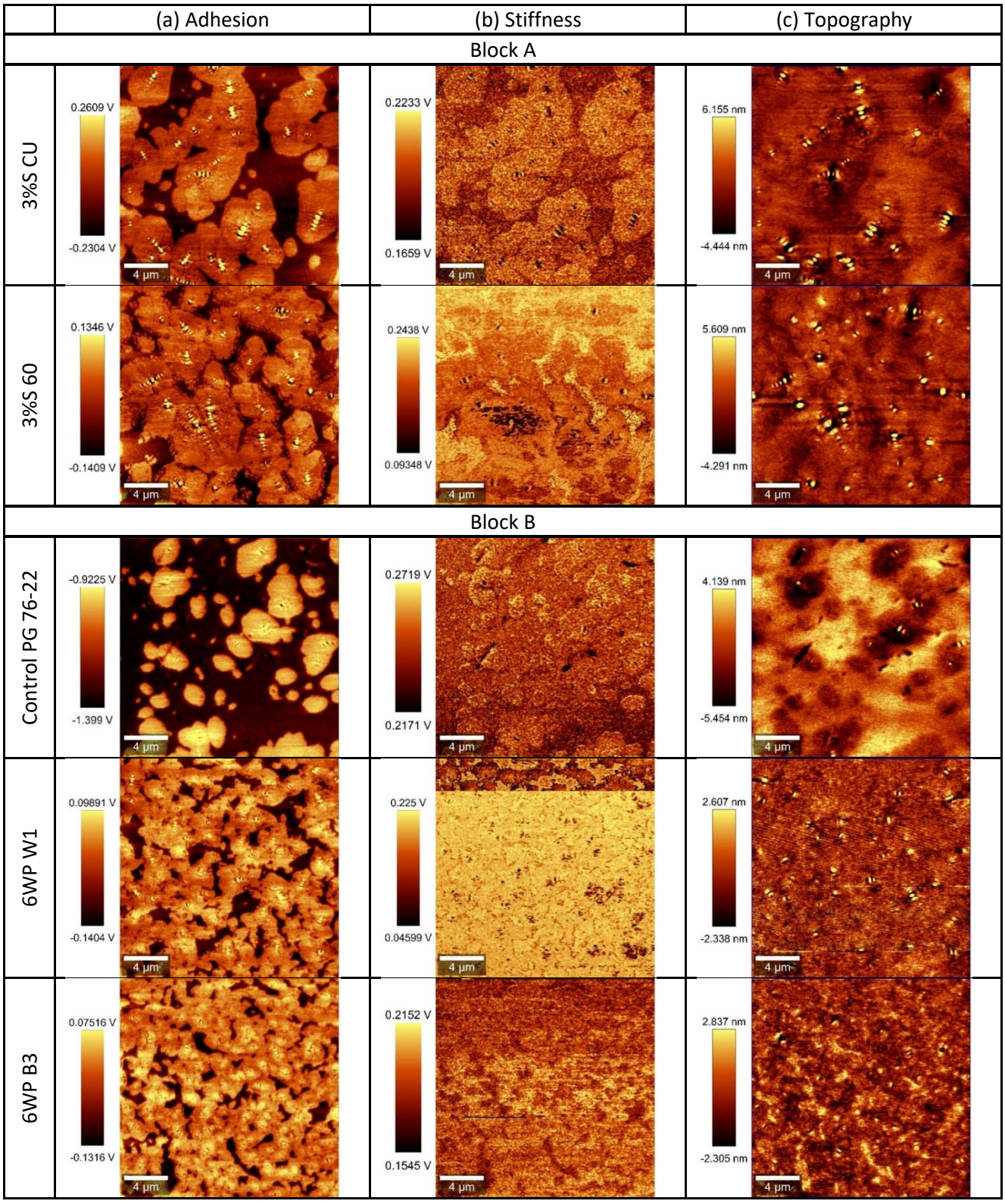

Figure 4.23 (a) Adhesion, (b) Stiffness and (c) Topography images of 3%S CU, 3%S 60, Control unmodified PG 76-22, 6WP W1 and 6WP B3 binders (20 µm X 20 µm)

To quantitatively assess the microstructural changes in asphalt surface properties due to the effect of aging, image analysis technique using the ImageJ software (Schindelin et al. 2015) was performed on all the adhesion images. Figure 4.24 presents an example of image analysis using the ImageJ tool. The images were converted to 8-bit color and a threshold was adjusted to separate two distinctive phases (Phase 1 and Phase 2). The brighter region with higher adhesion correspond to bright yellowish portion in the 8-bit color image (Figure 4.24) and vice versa. Then the percent of higher adhesion area (bright color) was calculated for all analyzed images. The findings are presented in Table 4.5 along with number of bees observed within the image (area of 400 μm^2). In all cases, the percent area of higher adhesion or the dispersive phase (Phase 2) increased after long-term aging for both laboratory and field-aged binders along with associated increase in the number of bees as expected. The percent area of higher adhesion at top of HMA of Section 2 was found to be 373.50 μm^2 (2WP W1) whereas it was 352.84 μm^2 at the bottom of the base course (2WP B3), compared to that of the control unaged PG 64-22 (305.13 μm^2). The top of HMA is more oxidized compared to the bottom of base course. Similar observations were made by Allen 2010 using the phase images where they noted that Phase 2 (corresponding higher adhesion area in this study) increased with aging.

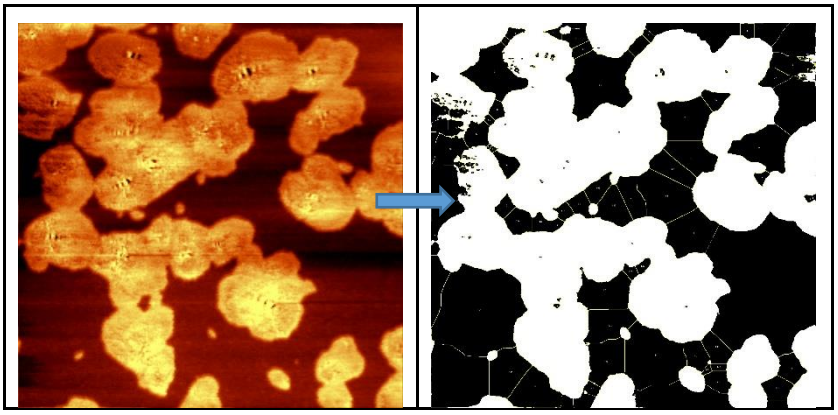

Figure 4.24 Adhesion image converted to Binary Watershed image in ImageJ

Table 4.5 Change in percent area of higher adhesion (brighter area) or Phase 2

Sample ID	Total ImageJ area count	Bright area (μm^2)	% Area	Bee count
Control PG 64-22	426	305.13	76.28	11
2WP W1	876	373.50	93.38	48
2WP B3	289	352.84	88.21	27
1%R CU	148	279.96	69.99	9
1%R 60	333	377.47	94.37	22
3%S CU	734	299.27	74.82	18
3%S 60	1062	339.72	84.93	23
Control PG 76-22	95	197.46	49.37	9
6WP W1	710	319.52	79.88	27
6WP B3	522	330.60	82.65	17

The dispersed phase (Phase 2) of Redicote-modified PG 64-22 binder increased from 279.96 μm^2 (1%R CU) to 377.47 μm^2 (1%R 60) after 60 hours of PAV aging which is almost 1.35 times greater than the area of 1%R CU. In the Solprene-modified PG 64-22 binder, the increase in higher adhesion area (Phase 2) of the PAV aged binder (339.72 μm^2 in 3%S 60) was 1.13 times when compared to the unaged one (299.27 μm^2 in 3%S CU). The number of bees increased 2.5 times in aged Redicote-modified PG 64-22 binder (1%R 60) whereas in the aged Solprene-modified PG 64-22 binder (3%S 60), it was 1.3 times. The results demonstrated that Solprene (3%S CU) provided better results compared to Redicote (1%R CU). However, a slightly opposite trend was found in Section 6 top (6WP W1) and bottom (6WP B3) layer when compared to similar layers of Section 2. The base layer of Section 6 (6WP B3) was found to age more with greater area of higher adhesion (330.6 μm^2) compared to the top layer (319.52 μm^2 in 6WP W1). Poor compaction and presence of air voids could be an explanation of this aggravated aging in the base layer of Section 6 (Figure 4.25).

Figure 4.25 Poor compaction in the middle of base layer (Sirin *et al.* 2017a)

The image analysis (Table 4.5) showed that Phase 2 with the higher adhesion areas become more dispersed in Phase 1 with aging (i.e., the area of the Phase 2 increases with aging). This phenomenon is confirmed by the histogram of adhesion distributions of all the samples as presented in Figure 4.26. The presence of both the phases (Phase 1 and Phase 2) are imminent in the bimodal histogram of the Control PG 64-22. The distribution of lower adhesion values is centered on -0.91V and the higher adhesion values are centered on -0.84V. After field-aging, slightly negatively-skewed unimodal distribution was observed for binders from both top and bottom layers of Section 2 (2WP W1 and 2WP B3). Similar conversion from bimodal to unimodal distribution was observed for antioxidant modified binders (1%R CU and 3%S CU) and binders from Section 6 (6WP W1 and 6WP B3) when subjected to long-term aging. This quantitative analysis of the distribution of adhesion confirmed the increase in percent area of higher adhesion (brighter region) with long-term aging of asphalt.

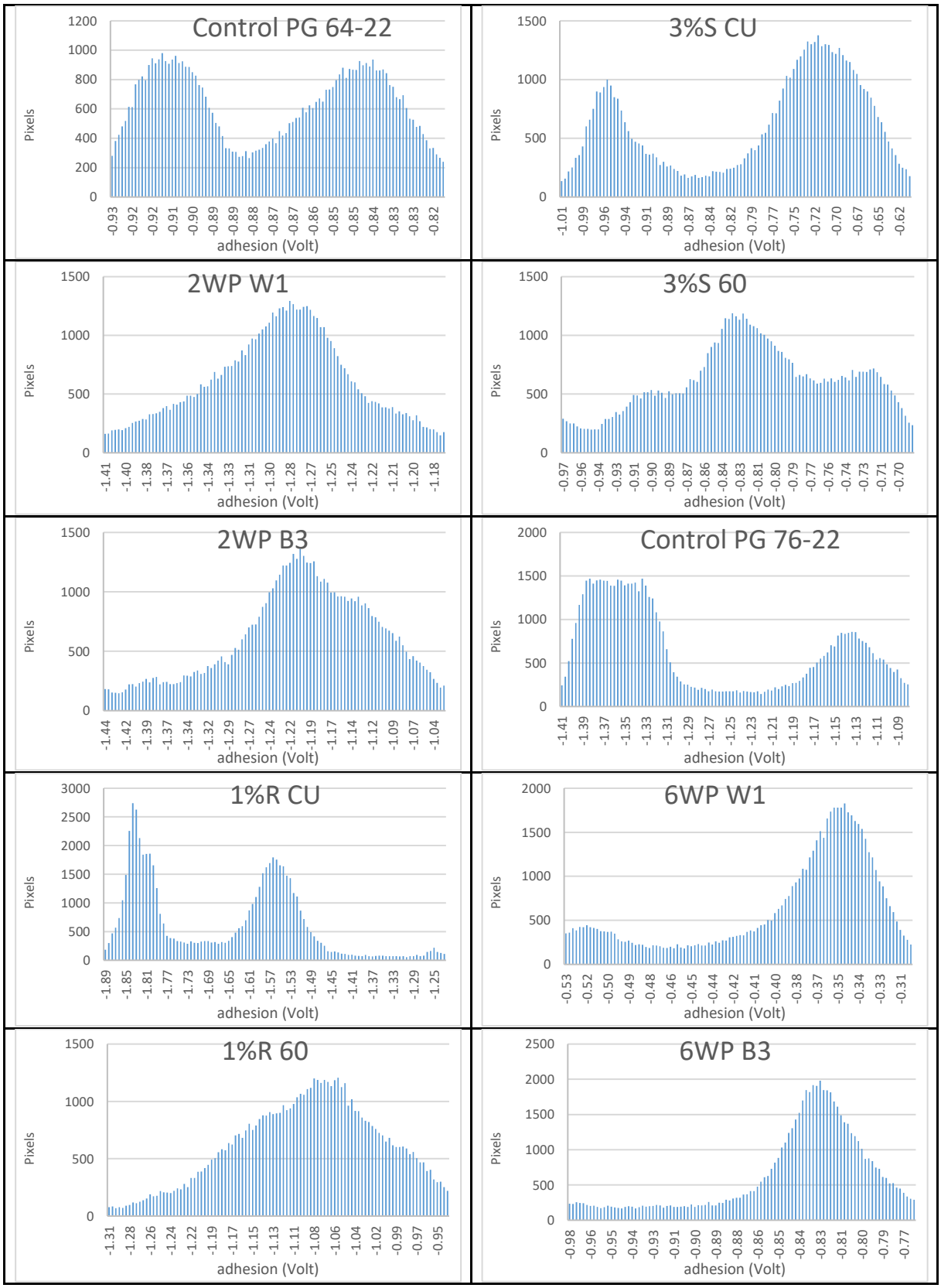

Figure 4.26 Distribution of adhesion of asphalt binder samples (Histograms)

The topographic images provided detail insight on the surface roughness condition. Similar to the experimental results provided by other researchers (Loeber et al. 1996; Jäger et al. 2004; Masson et al. 2006), the classic 'bee' structures were observed in all of the asphalt samples in a randomly distributed pattern. 'Bees' are alternating peaks and valleys in the surface topography of asphalt, usually with much higher heights than rest of the distribution. The topographic image gives characteristic dimensions of the bee structures in terms of *ΔH* and *d*, if a line profile is plotted on the bee as presented in the line profile of Figure 4.27. *ΔH* is the maximum height and *d* is the maximum spacing of two adjacent peaks in a bee structure.

The surface height distribution of the test samples exhibited Gaussian distribution in almost all cases (Figure 4.28). From the topographic image of each test samples, ten bee structures were randomly selected for analysis. The *ΔH* and *d* values were measured and the average values were reported in Table 4.6. Similar to the conclusion of Jäger et al. (2004), no correlation was found with the change in the characteristic dimensions of bee structures and the effect of aging. The bee-structures from the field-aged binders of Section 2 (2WP W1 and 2WP B3) were found to have lower height (12.7 and 13.6 nm) when compared to Control PG 64-22 (28.5 nm). Similarly, the bees of Section 6 wearing (6WP W1) and base (6WP B3) course have shorter height (15 and 10.2 nm) compared to that of Control PG 76-22 (17.3 nm). However, the bee height increased in Redicote-modified PG 64-22 binder (1%R CU) from 18.5 to 44.4 nm after 60 hours of PAV aging (3%S 60). In Solprene-modified PG 64-22 binder, the age-induced increase in bee height is around 6 nm only, i.e., from 32.3 nm (3%S CU) to 38.2 nm (3%S 60). Although long-term aging increased the height and spacing of bee structures in the lab-aged binders, opposite pattern was observed in the field-aged binders when compared to the corresponding control unaged binder.

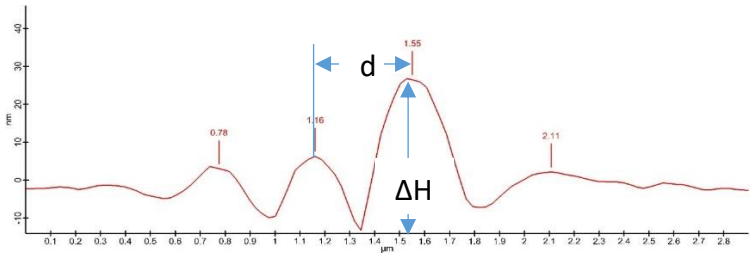

Figure 4.27 Line profile of a bee structure (Control PG 64-22)

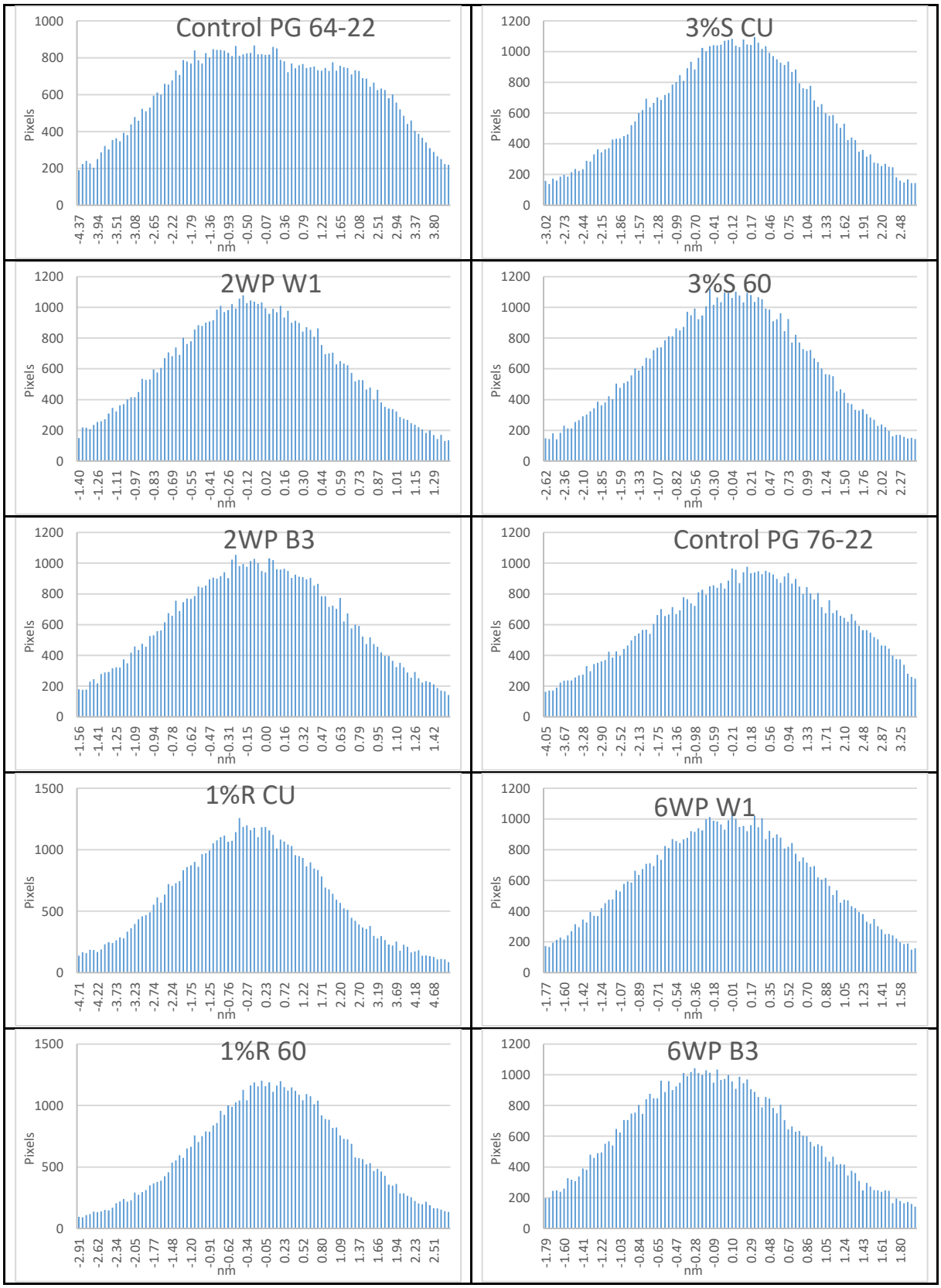

Figure 4.28 Distribution of surface topography of asphalt binder samples (Histograms)

Table 4.6 Characteristics of bee structure in the asphalt binders from line profiling

Sample ID	Shape	Height (nm)	Std. dev. of height (nm)	Spacing (μm)	Std. dev. of spacing (μm)
Control PG 64-22	bee-like	28.5	9.8	0.47	0.096
2WP W1	bee-like	12.7	5.8	0.44	0.069
2WP B3	bee-like	13.6	3.8	0.43	0.035
1%R CU	bee-like	18.5	6.1	0.45	0.032
1%R 60	bee-like	44.4	16.4	0.49	0.057
3%S CU	bee-like	32.3	10.7	0.48	0.103
3%S 60	bee-like	38.2	13.0	0.59	0.216
Control PG 76-22	bee-like	17.3	6.3	0.45	0.037
6WP W1	bee-like	15.0	5.1	0.41	0.060
6WP B3	bee-like	10.2	2.4	0.34	0.017

The statistical analysis of the surface roughness parameters of the entire image area (400 μm^2) captured the effect of aging on the microstructural properties of asphalt binder surface. The AFM software, Project FOUR 4.1, provides a set of seven amplitude and three hybrid parameters to study the surface roughness characteristics. Since certain parameters from this set are of higher interest due to their ability of characterizing the surface topography more efficiently, the relevant parameters are reported in Table 4.7. The reported parameters include maximum peak height (SP), maximum valley/pit height (SV), maximum height (SZ), arithmetic mean height (SA), root mean squared height (SQ), skewness (SSK) and kurtosis (SSU). Maximum peak (SP) and pit height (SV) are the absolute value of the distance of the highest peak and largest pit from a reference mean plane respectively. Maximum height (SZ) is the sum of SP and SV. Arithmetic mean height (SA) is the mean of all the heights and pits of the sample surface about a mean plane and SQ is the standard deviation of the mean plane (Figure 4.29a). SQ parameter identifies any substantial deviation of the phases present in sample surface and whether it is influencing the mean plane. Skewness (SSK) describes the height distribution of the topography. If the distribution is symmetrical around the mean plane (Figure 4.29b), the surface is Gaussian with zero skewness. A distribution with a longer tail in the lower side means negative skewness whereas in the upper side means positive skewness.

Positive skewness refers to more peaks and spiked surface whereas negative skewness means there are more valleys/pits in the distribution. Kurtosis (SSU) also describes the sharpness of the surface roughness. A kurtosis value of 3 indicates a Gaussian surface where sharp and indented portions exist in parallel (Figure 4.29c). A value greater than 3 indicates a spiked distribution and the opposite means flat tops and deep valleys.

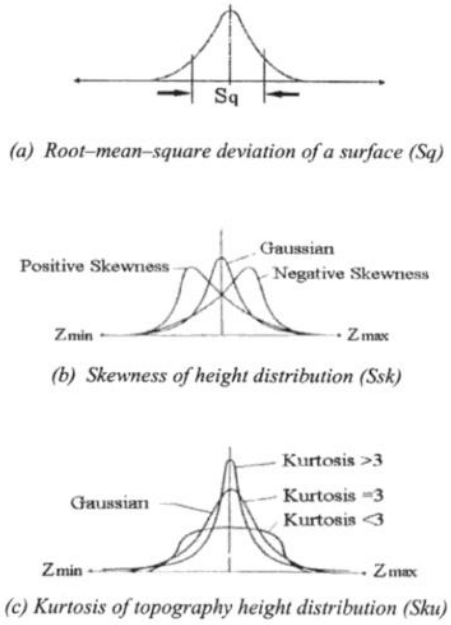

Figure 4.29 Height distribution (Blunt and Jiang 2003)

Table 4.7 presents the statistical data of the associated roughness parameters of the topographic images presented in Figures 4.22 and 4.23. The arithmetic mean height (SA) of the wearing course (2WP W1) and base course (2WP B3) of Section 2 was found to be 0.64 nm and 0.7 nm, respectively which is almost one-third of Control PG 64-22 (2.01 nm). Similarly, the SA of Control PG 76-22 reduced from 1.72 nm to 0.79 and 0.82 nm in the wearing course (6WP W1) and base course (6WP B3) of Section 6, respectively. In the lab-aged Redicote-modified PG 64-22 binder (1%R 60), it is 1.35 nm which is lower than SA of the unaged one (2.01 nm for 1%R CU). In Solprene-modified PG 64-22 binder, aging reduced the SA from 1.34 (3%S CU) to 1.21 nm (3%S 60).

The root mean squared height (SQ) of the wearing and base course of Section 2 was found 0.94 nm (2WP W1) and 1.01 nm (2WP B3), respectively which less than half of Control PG 64-

22 (2.56 nm). Similarly, the SQ of Control PG 76-22 reduced from 2.18 nm to 1.1 and 1.07 nm in the wearing course (6WP W1) and base course (6WP B3) of Section 6, respectively. In the lab-aged Redicote-modified PG 64-22 binder (1%R 60), it is 2.46 nm which is lower than SQ of the unaged one (2.7 nm for 1%R CU). In Solprene-modified PG 64-22 binder, the aging reduced the SQ from 2.19 (3%S CU) to 2.14 nm (3%S 60). Similar to the conclusions of Allen (2010), it was found that both SA and SQ reduced in all laboratory- and field-aged binders.

As stated earlier, the skewness (SSK) parameter provides insight on the degree of biasness of the surface sharpness. The field-aged PG 64-22 binders from both top (2WP W1) and bottom layers (2WP B3) of Section 2 are positively skewed at higher extent compared to the unaged control one (Control PG 64-22). Aging increased skewness of Section 2 from 0.73 (Control PG 64-22) to 2.24 (2WP W1) and 2.02 (2WP B3). Similar pattern of skewness was observed for the PG 76-22 since the height distribution of field-aged binders from Section 6 (6WP W1 and 6WP B3) transformed to positively skewed (1.42 and 0.32) distribution when compared to the negatively skewed distribution of Control PG 76-22 binder (-0.55). It implies that due to the effect of long term-aging, the honed surface (valley/pit) transformed into more spiked surface. The sharpness is more severe on the top of HMA (2WP W1 and 6WP W1) as expected. The antioxidant and copolymer modified binders were able to reduce the surface sharpness in terms of skewness compared to the field-aged binder. In the Redicote-modified laboratory-aged binder (1%R 60), the height distribution is negatively skewed (-0.12) which confirms the presence of more valleys than spikes even after 60 hours of PAV aging. Aged Solprene-modified binder (3%S 60) could retard the spike formation further by holding the same value of skewness (3.38) after aging. The statistical results on kurtosis (SSU) followed the same pattern of skewness in all cases except Redicote modified binder. It is evident from the statistical analysis that long-term oxidative aging makes microstructural changes in the asphalt surface, which is also supported by the findings from Allen (2010). Similar to the results of bee dimensions reported in Table 4.6, SP, SV and SZ of Table 4.7 provided mixed notion on the effect of aging on the overall topographic texture statistics. According to these three parameters, aging caused an increase in overall roughness in lab-aged binders but with an opposite trend in the field-aged binders, which is inconclusive.

Table 4.7 Statistical Analysis of Surface Roughness Parameters

Sample	SP (nm) maxi-mum peak height	SV (nm) maximum valley/pit height	SZ (nm) maxi-mum height	SA (nm) arith-metic mean height	SQ (nm) root mean squared height (std. dev.)	SSK skew-ness	SSU kurto-sis
Control PG 64-22	37.63	-14.82	52.45	2.01	2.56	0.73	11.19
2WP W1	15.01	-9.33	24.34	0.64	0.94	2.24	24.69
2WP B3	15.32	-9.32	24.64	0.70	1.01	2.02	25.52
1%R CU	14.75	-18.27	33.02	2.01	2.70	0.31	4.53
1%R 60	40.60	-34.95	75.55	1.35	2.46	-0.12	43.98
3%S CU	35.03	-20.51	55.54	1.34	2.19	3.38	42.65
3%S 60	39.31	-25.95	65.26	1.21	2.14	3.38	59.16
Control PG 76-22	16.08	-16.03	32.10	1.72	2.18	-0.55	4.53
6WP W1	17.29	-13.41	30.70	0.79	1.10	1.42	19.10
6WP B3	10.33	-11.72	22.05	0.82	1.07	0.32	5.79

In addition to the morphological characterization of asphalt binder in nanoscale, the AFM is capable of capturing the information on local stiffness when operated in DPFM mode (Schmidt et al. 2005). Being a significant material property, change in stiffness is directly associated with asphalt hardening and thus formation of cracking in the binder. Proper characterization of asphalt binder stiffness would help to understand the failure mechanism. Allen (2013) hypothesized bee structures as the 'crack initiation sites' and proposed the incompatibility in asphalt microstructure due to the fractional growth of either asphaltenes or saturates as a probable cause of the appearance of bees. As stated earlier, despite the three cases where opposite correlation was observed due to image artifacts, in seven cases of the stiffness images presented in Figures 4.22 and 4.23, the bee structure was found to be surrounded by higher stiffness region with brighter color. This phenomenon was also cited by Jäger et al. (2004) and Allen et al. (2012).

Table 4.8 shows the variation of microstructural stiffness of the test binders. The distribution of stiffness over the entire scan area of 20 µm X 20 µm is presented in Figure 4.30. Since the distribution is Gaussian in almost all cases except three cases where unimodal negatively

skewed distribution was observed, the average value of the entire stiffness distribution was reported in Table 4.8 with standard deviation. Similar to Jäger et al. (2004), a relative stiffness was developed from the ratio of unaged binder type to the field or lab-aged binder of the same. Figure 4.31 presents the relative stiffness of lab-aged antioxidant modified binders and field-aged binders from Sections 2 and 6. The microstructural stiffness of the wearing course (2WP W1) and base course (2WP B3) of Section 2 was found 0.314 Volt and 0.295 Volt, respectively which is almost double of Control PG 64-22 (0.187 Volt). However, the stiffness of Control PG 76-22 (0.245 Volt) was found to be slightly higher than that of the wearing course (0.185 Volt) and base course (0.189 Volt) of Section 6, respectively. In the lab-aged Redicote-modified PG 64-22 binder (1%R 60), it is 0.28 Volt which is lower than the stiffness of the unaged one (0.352 Volt for 1%R CU). In Solprene-modified PG 64-22 binder, mixing the copolymer retarded the increase in age-induced stiffness of 0.181 Volt (3%S 60) when compared to the unaged one (0.198 Volt for 3%S CU). This study captured the effect of aging on the microstructural stiffness of asphalt binder and the efficiency of antioxidant additives in retarding aging by reducing the age induced stiffness. When compared to Section 2, both Redicote and Solprene provided viable performance in reducing microstructural stiffness.

Table 4.8 Microstructural stiffness of asphalt sample surface

Sample ID	**Stiffness (Volt)**	**Std. Dev. (Volt)**
Control PG 64-22	0.187	0.0137
2WP W1	0.314	0.0117
2WP B3	0.295	0.0134
1%R CU	0.352	0.0335
1%R 60	0.280	0.0119
3%S CU	0.198	0.0127
3%S 60	0.181	0.0418
Control PG 76-22	0.245	0.0118
6WP W1	0.185	0.0370
6WP B3	0.189	0.0124

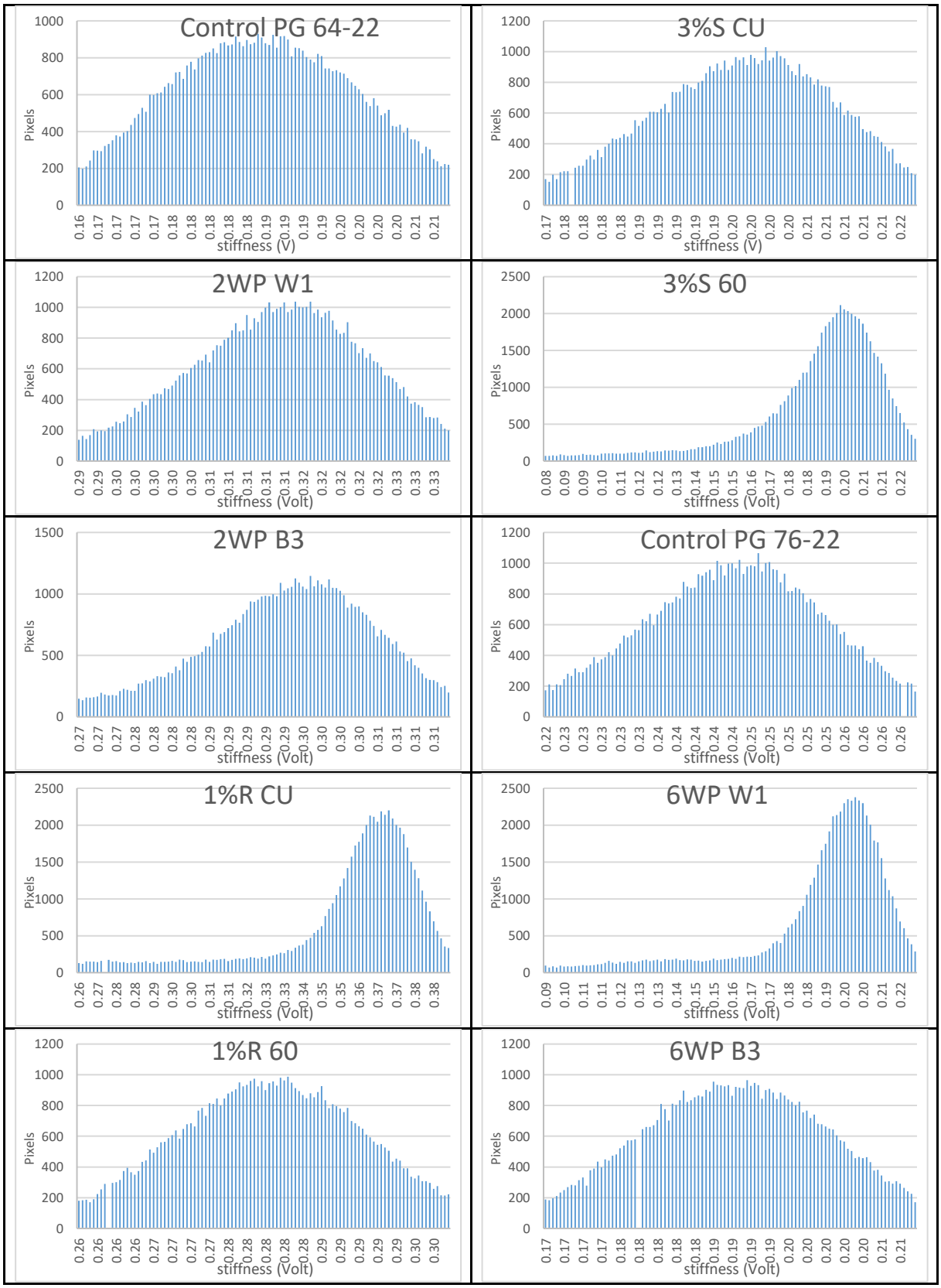

Figure 4.30 Distribution of microstructural stiffness of asphalt sample surface (Histograms)

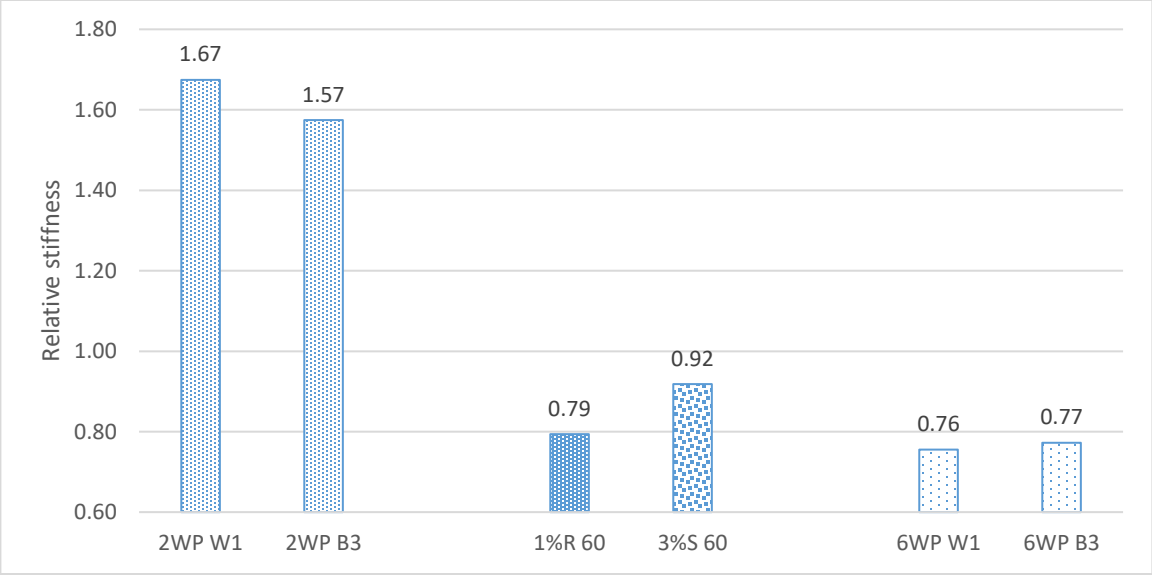

Figure 4.31 Relative stiffness of the binders tested in AFM

CHAPTER 5 EVALUATION OF THE EFFECT OF AGING ON VISCOELASTIC PROPERTIES OF ASPHALT MIXTURES USING THE PRONY SERIES

5.1 Introduction

The rheological property of asphalt is a complex phenomenon. Due to its viscoelastic nature, the mechanical response is nonlinear and depends on several factors such as time, temperature and rate of loading (Rahmani et al. 2017). Typically, the elastic part is modeled with a spring and described with the Hooke's law ($\sigma = E\varepsilon$) where E is the elastic modulus. While a dashpot represents the viscous component by considering a stress-strain rate proportionality constant known as viscosity (η) (Roylance 2001) (Equation 5.1).

$$\sigma = \eta \frac{d\epsilon}{dt} \tag{5.1}$$

There are several constitutive models used to describe the viscoelastic behavior of asphalt binder when subjected to varying loading conditions including the Maxwell model, the Kelvin-Voigt model, the Standard Linear Model and the Generalized Maxwell model (Kim 2009).

Among these models, the generalized Maxwell model or the Maxwell-Wiechert model (Figure 5.1) can consider stress-relaxation over a varying time distribution whereas the generalized Kelvin-Voigt model can characterize the creep compliance more realistically (Park and Schapery 1999).

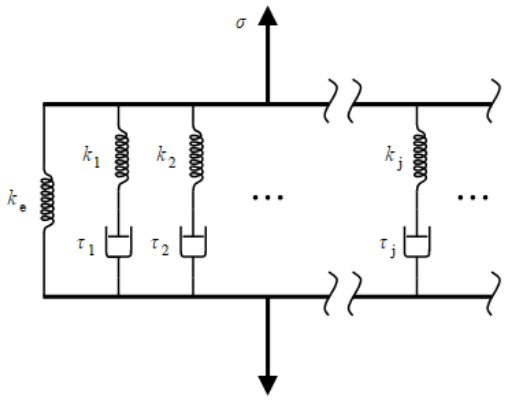

Figure 5.1 Generalized Maxwell model or Wiechert material model (Mottahedi et al. 2011)

In a purely elastic material, the deformation occurs instantly if the stress is removed. But in a viscoelastic material, the elastic recovery is time dependent. When a viscoelastic material is subjected to constant stress (creep test) (Figure 5.2a), the creep compliance (*D*), is defined as the time-dependent strain divided by the applied stress and the delayed response to an applied stress is known as the retardation time (*λ*). The retardation time portraits the delay of elasticity (Mezger 2011). On the other hand, when a viscoelastic material is subjected to a constant strain, the stress required to maintain the strain decreases over time in the recovery phase (Figure 5.2b), right after the instantaneous recovery. This phenomenon is known as 'stress relaxation' and the time required for the delayed recovery is relaxation time (*ρ*).

The Prony series coefficients of the Prony's method, initially developed by Gaspard Riche de Prony in 1795, can be used to fit the creep compliance versus time data of a creep-recovery test in order to analyze the viscoelastic properties of a material subjected to constant stress. Thus, the strain-recovery function can be interpreted as a mechanical element model similar to the generalized Maxwell or Kelvin-Voigt model with the Prony series.

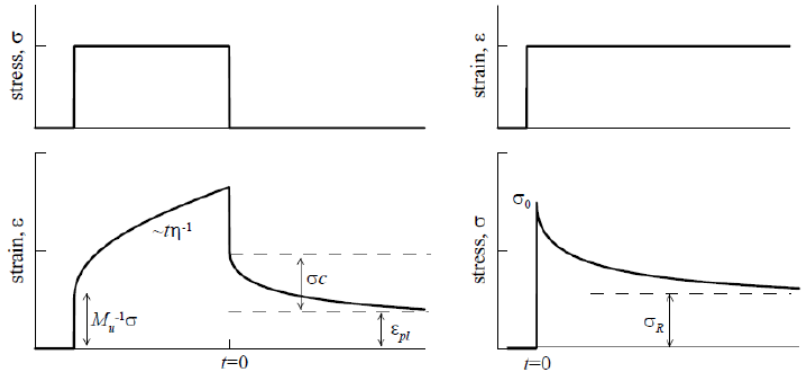

(a) (b)

Figure 5.2 Typical behavior of (a) creep-recovery, (b) stress-relaxation of linear viscoelastic material (Liu *et al.* 2015)

Prony's method is a widely popular function to fit the viscoelastic creep-recovery behavior of asphalt binder. Several researchers (Rahmani et al. 2013; Rahmani et al. 2017; Park and Kim 2001; Kim et al. 2007; Huang et al. 2007; and You et al. 2014) used the Prony representation of transient creep compliance (*ΔD*) in a creep test as shown in Equation 5.2.

$$\Delta D = \sum_{n-1}^{N} D_n[1 - e^{-\lambda_n \psi^t}] \quad (5.2)$$

where, N = no. of Prony series coefficients

λ_n = *n*th retardation time

D_n = *n*th compliance associated with the *n*th retardation time

ψ^t = reduced time

The application of Prony series coefficients reduces the requirement of analyzing huge data amount of all the time steps. According to Kim et al. (2007), *"Among many curve fitting techniques, the Prony series representation has been frequently adopted because the Prony series fits the data quite precisely and is more efficient for use in mathematical operations."*

5.2 Experimental Design

The Prony series analysis was conducted on the dynamic modulus test results that were previously collected as part of studying the effect of time and temperature on short-term aging of asphalt mixtures (Sirin et al. 2018). The study was undertaken to develop improved protocols for asphalt mixture aging in the laboratory. The aim was to simulate asphalt mixture aging due to the climate conditions in the State of Qatar. Extensive laboratory testing was carried out on typical asphalt mixtures in Qatar. The test specimens were conditioned at different temperatures and time durations. The dynamic modulus test was used to evaluate the effect of short and long-term aging on the mechanical properties of test specimens (Sirin et al. 2018).

Gabbro aggregate and Pen 60-70 asphalt binder were used in preparing asphalt mixtures test samples. The optimum binder content used was 4.3% and the samples were compacted to have 7% air voids. The compacted specimens had a height of 178 mm and diameter of 150 mm. The mixing and compaction temperatures used were 143°C and 135°C, respectively. All the test specimens were cored and cut to 100 mm diameter and 150 mm height. These final cored full mixtures were at first short-term aged in forced-draft oven at aging temperatures of 125, 135 and 145°C and short-term aging duration of 2, 4, 6 and 8 hours. Then they were subjected to long-term aging with varying aging temperatures (75, 85 and 95°C) and long-term aging duration (0, 2, 4, 6, 8 and 10 days). The '0' day aging means the test samples were not

subjected to long-term aging. After each of the long-term aging duration, the dynamic modulus test was conducted on the test samples using the asphalt mixture performance tester (AMPT). The test was conducted at different frequencies (10, 1 and 0.1 Hz) and temperatures (4, 20 and 40°C) according to AASHTO TP 62. From each combination, two replicates were tested, the results averaged and the master curves constructed from the averaged dynamic modulus data at a reference temperature of 20°C. Table 5.1 presents typical sample dynamic modulus test results (Sirin et al. 2018).

In Table 5.1, 'S125T2L75' is the specimen ID which represents information about aging time and duration. For example, 'S125T2L75' refers to following attributes: S = short-term aging, 125 = short term aging temperature of 125°C, T2 = short-term aging duration (time) of 2 hours, and L = long-term aging, 75 = long-term aging temperature of 75°C.

Table 5.1 Typical Dynamic modulus data of Asphalt Mixtures subjected to short and long-term aging (Sirin *et al.* 2018)

		S125T2L75		S125T2L85		S125T2L95	
		Dynamic Modulus (MPa)	Phase angle (degree)	Dynamic Modulus (MPa)	Phase angle (degree)	Dynamic Modulus (MPa)	Phase angle (degree)
Temperature	Frequency (Hz)	**0 day**		**0 day**		**0 day**	
4°C	0.1	7741	24.05				
	1	12385	16.54				
	10	17242	11.33				
20°C	0.1	1259	39.78				
	1	3399	35.34				
	10	7147	26.29				
40°C	0.1	112	27.06				
	1	331	36.30				
	10	1236	39.09				
		2 days		**2 days**		**2 days**	
4°C	0.1	9477	21.19	10809	21.59	10200	21.48
	1	14528	14.79	16866	14.92	16173	15.03
	10	19617	10.25	23121	11.57	22077	10.29
20°C	0.1	1685	36.64	2116	36.78	2198	35.83
	1	4212	32.00	5034	31.65	5177	31.00
	10	8284	24.00	9742	23.46	9832	23.14
40°C	0.1	199	30.15	275	29.29	208	28.12
	1	631	38.30	829	36.40	606	35.45
	10	2123	37.15	2589	36.73	2007	37.36
		4 days		**4 days**		**4 days**	
4°C	0.1	9951	20.88	11570	19.98	11658	19.71
	1	15158	14.69	17462	13.97	17407	13.77
	10	20473	10.18	23437	09.55	22880	09.41
20°C	0.1	1946	35.57	2466	36.07	2576	33.65
	1	4710	30.72	5604	29.32	5798	28.98
	10	9060	22.99	10309	21.92	10620	21.81
40°C	0.1	159	28.24	291	30.17	224	28.64
	1	460	35.92	901	35.90	656	34.83
	10	1596	37.38	2739	35.12	2109	36.13

The dynamic modulus (*E**) and phase angle (*δ*) data of each of the samples were used to obtain the Prony series coefficients. The dynamic compliance (*D**) is inverse of dynamic modulus. From the dynamic compliance test data, the experimental storage (*D'*) and loss compliance (*D''*) were calculated based on following equations:

$$D' = D^* \cos(\delta) \tag{5.7}$$

$$D'' = D^* \sin(\delta) \tag{5.8}$$

The time-temperature shift factors were identified using the sigmoidal function to construct the master curves of storage and loss compliance. A built-in 'Prony' function of MATLAB (Rahmani et al. 2017) was implemented to fit the experimental storage and loss compliance master curve using the following Prony series representation of storage (D') and loss modulus (D'') with respect to reduced frequency and the Prony parameters were obtained accordingly (Rahmani *et al.* 2017; Park and Schapery 1999; Christensen 1982):

$$D'(\omega) = D_0 + \sum_{i=1}^{N} \frac{D_n}{(\omega/\lambda_n)^2+1} \tag{5.9}$$

$$D''(\omega) = \sum_{i=1}^{N} \frac{(D_n)(\omega/\lambda_n)}{(\omega/\lambda_n)^2+1} \tag{5.10}$$

where, *ω* is the reduced angular frequency.

Compared to seven Prony parameters used by Rahmani at al. (2017), nine Prony parameters were used in this study to increase the accuracy of the analysis. In addition, the first compliance term (D_0) known as the instantaneous creep compliance was also identified. Table 5.2 represents Prony coefficients; compliance terms (D_n) and retardation times (λ_n) of some short-term aged test specimens (i.e., 0 days long-term aged).

Table 5.2 Prony series coefficients of unaged (short-term aged only) samples

n	S125T2L75		S135T2L75		S135T6L75		S145T2L75	
	D_n (1/MPa)	λ_n (1/s)	D_n (1/MPa)	λ_n (1/s)	D_n (1/MPa)	λ_n (1/s)	D_n (1/MPa)	λ_n (1/s)
1	4.90E-05	6.11E+03	4.67E-05	7.02E+03	4.20E-05	7.35E+03	4.95E-05	4.59E+03
2	1.59E-05	9.22E+02	1.47E-05	1.01E+03	1.65E-05	1.05E+03	2.11E-05	6.67E+02
3	2.16E-05	1.39E+02	1.97E-05	1.46E+02	1.74E-05	1.50E+02	2.17E-05	9.70E+01
4	3.57E-05	2.10E+01	3.31E-05	2.11E+01	2.64E-05	2.15E+01	4.44E-05	1.41E+01
5	8.82E-05	3.16E+00	8.34E-05	3.04E+00	7.82E-05	3.07E+00	9.84E-05	2.05E+00
6	2.37E-04	4.76E-01	2.09E-04	4.38E-01	1.40E-04	4.39E-01	2.83E-04	2.98E-01
7	3.52E-04	7.18E-02	3.20E-04	6.33E-02	2.75E-04	6.28E-02	4.40E-04	4.34E-02
8	1.73E-03	1.08E-02	1.62E-03	9.12E-03	9.31E-04	8.98E-03	2.08E-03	6.31E-03
9	5.07E-03	1.63E-03	4.34E-03	1.32E-03	2.68E-03	1.28E-03	5.31E-03	9.18E-04
D_0	6.59E-03		6.94E-03		5.04E-03		6.71E-03	

5.3 Analysis and Discussion of Test Results

The effect of long-term aging on the Prony parameters was investigated by comparing the compliance terms and retardation times at different aging durations (e.g., 2, 4, 6, 8, 10 days). Figures 5.3 and 5.4 represent the comparison of aged (at different durations) and unaged compliance terms and retardation, respectively for a test specimen. It can be seen that the decrease in both the parameters is not uniform with increase in aging duration. The difference of the same Prony parameter (i.e., 1^{st}, 2^{nd}, 3^{rd} … 9^{th} parameter) over different aging time is not significant. In addition, due to the overlapping, it is difficult to evaluate the effect of aging on the parameters of Prony series. Meanwhile, this could be due to the variation in the test results of the dynamic modulus test.

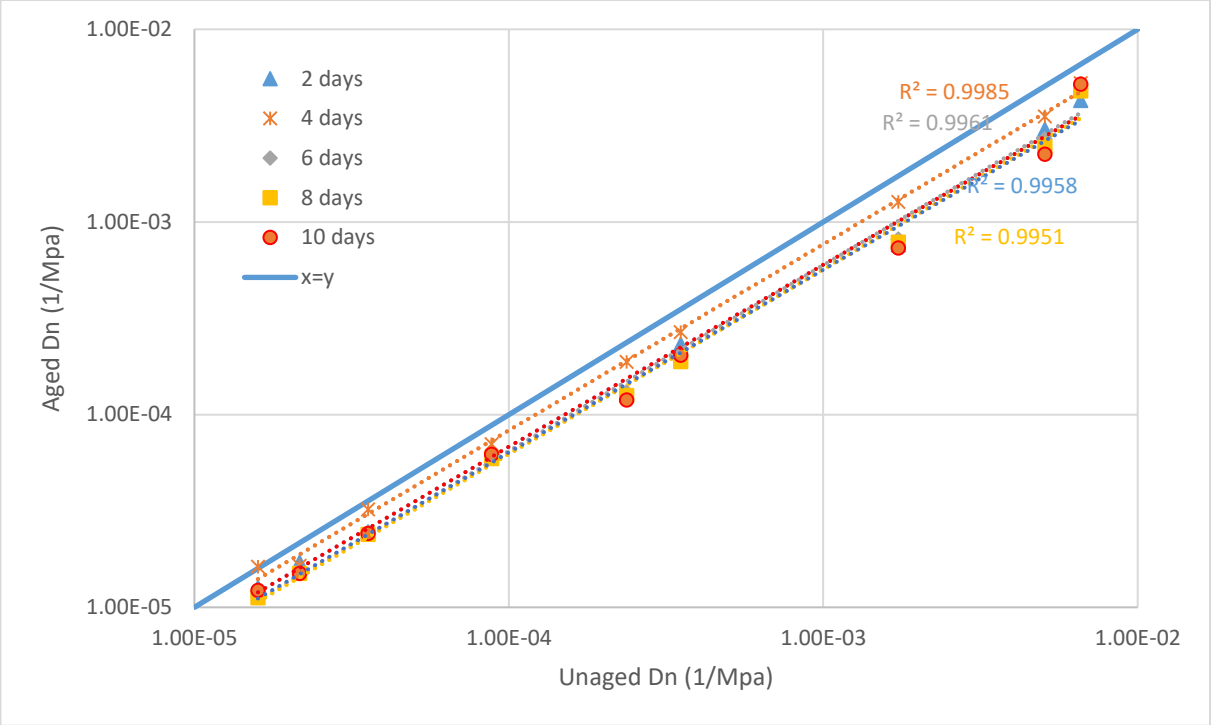

Figure 5.3 Effect of long-term aging duration on the compliance terms of Prony parameters derived from the Dynamic Modulus test data

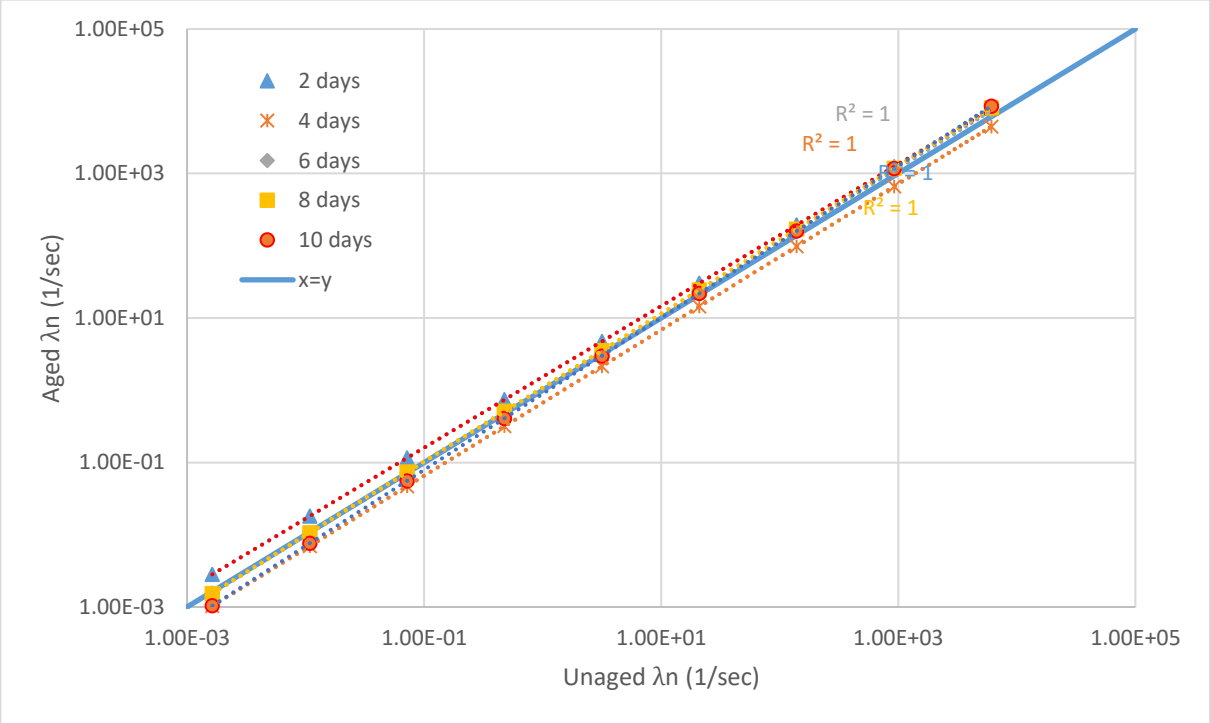

Figure 5.4 Effect of long-term aging duration on the retardation times of Prony parameters derived from the Dynamic Modulus test data

The researchers investigated the efficiency of a newly proposed parameter called aging state variable '*A*' by Rahmani et al. (2017), in describing the effect of long-term aging on the viscoelastic behavior of asphalt binder. Based on Equations (5.6), (5.9) and (5.10), Rahmani et al. (2017) developed following relationships of aged storage and loss compliance to that of the unaged ones by relating with the Prony parameters using the aging state variable '*A*' as given in Equations 5.11 and 5.12.

$$D'^{,A}(\omega) = D_0 + \sum_{i=1}^{N} \frac{(1-A)^k D_n}{[\omega/(1-A)^k \lambda_n]^2+1} \quad (5.11)$$

$$D''^{,A}(\omega) = \sum_{i=1}^{N} \frac{(1-A)^k (D_n)[\omega/(1-A)^k \lambda_n]}{[\omega/(1-A)^k \lambda_n]^2+1} \quad (5.12)$$

In Equations (5.11) and (5.12), the Prony parameters are derived from the unaged asphalt mixtures whereas the storage and loss compliances are of the aged asphalt mixtures. Both Equations (5.11) and (5.12) were used to determine the aging state variable '*A*'. The experimental storage and loss compliances of each of the long-term aged samples were derived directly from the dynamic modulus and phase angle data. The predicted storage and loss compliances of each of the long-term aged specimens were determined using equations (5.11) and (5.12) by using unaged compliance and retardation time as inputs. At each of the long-term aging duration, the aging state variable '*A*' was fitted by minimizing the sum of squares of error (SSE) between the predicted and experimental storage and loss compliances. The value of aging-susceptibility parameter *k* was considered to be 1 as recommend by Rahmani et al. (2017).

Figure 5.5 represents the effect of long-term aging on the aging state variable '*A*' of asphalt mixtures derived using Prony parameters. It can be seen that the aging state variable '*A*' increased with the increase of long-term aging duration but the increase was not linear. A similar trend was observed by Rahmani et al. (2017). The increase in the aging state variable *'A'* with long-term aging duration demonstrate the increase in stiffness of asphalt mixtures due to age induced hardening. This also confirms the validity of the parameter '*A*' as an indicator of age-induced viscoelastic response of asphalt binder. Figure 5.5 also presents the

effect of temperature on the long-term viscoelastic response of asphalt. Higher temperature was found to induce more oxidative aging compared to lower temperature as expected.

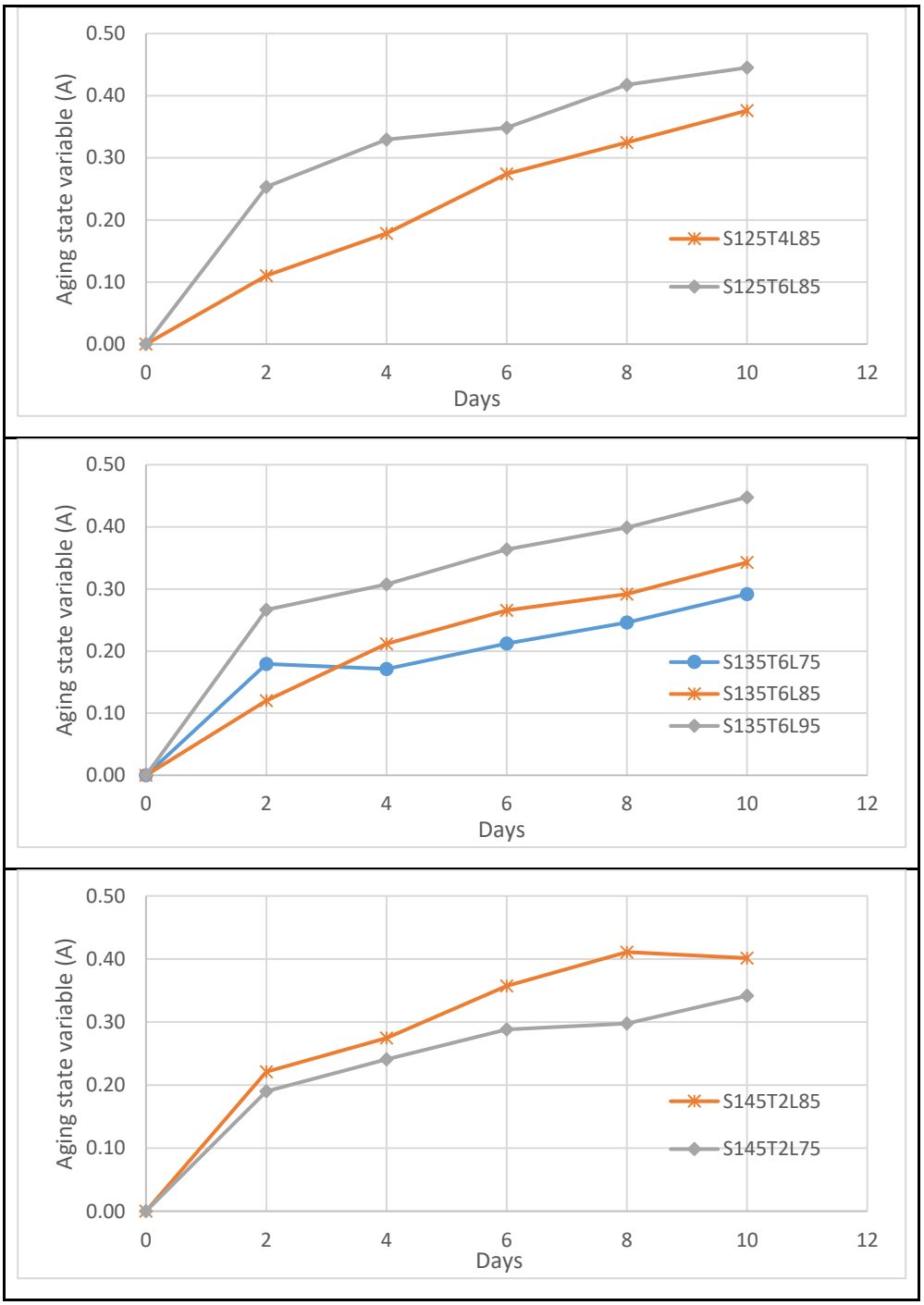

Figure 5.5 Effect of long-term aging on the aging state variable *'A'*, an indicator of age induced viscoelastic response of asphalt binder

CHAPTER 6 CONCLUSIONS AND RECOMMENDATIONS

6.1 Conclusions

This chapter summarizes the main findings of this study and presents recommendations for future research.

6.1.1 *Summary of Findings and Conclusions of Chapter 3*

This chapter investigated the feasibility of antioxidant additives and copolymers to retard the aging of asphalt binders. At first the effect of various antioxidant additives and copolymers with antioxidant agents was examined using long-term aging index as a screening tool. The physical forms of the additives varied from oil, liquid, powder and pellets. Then, selected additives were used to modify asphalt binders and prepare the fine asphalt mixtures. The effect of antioxidants was evaluated at the binder and mastic levels. The conclusions of this part of study were:

- Copolymers such as Solprene and Calprene used in the study showed a very high reduction in aging index. Using these copolymers showed improvements in the intermediate temperature stiffness of the test binders. They also provided improved stiffness at high temperatures compared to the control binders.
- The Redicote AP additive was found to be a viable additive to retard aging. The results showed that it provided better performance with PG 67-22 binder compared to PG 64-22 binder which was also confirmed from the frequency sweep tests.
- A few antioxidants such as Irganox 201 and DLTDP tend to make the binder soft which may be a concern for rutting resistance. Therefore, it is recommended to combine these additives with other products if required.
- The antioxidants may show different performance with different binders. That means, an antioxidant which works well with one binder may not provide desired results with another binder.
- The frequency sweep test results showed that the polymers used in this study altered properties of the control binders mainly in the low-reduced frequency region (high

temperature). The overall performance of the binders was improved when modified with polymers and antioxidants.

- The newly developed rheological parameters (i.e., G'/(η'/G'), G-R fatigue parameter, Kandhal's ductility) were found to capture the effect of aging and conformed with the findings of the respective master curve. These parameters depicted and confirmed the decreasing rate of aging in binder when modified with antioxidants, in terms of both crack initiation and ductility.
- The FAM mixtures prepared using Redicote- and Solprene-modified binders provided higher fractured energy after aging compared to control FAM mixtures, which would indicate improved fatigue resistance. In addition, these two additives reduced the aging index compared to control FAM mixtures.
- The type of aggregate was found to influence of the rate of aging of asphalt mixtures. The gabbro fine asphalt mixtures had higher aging index compared to limestone fine asphalt mixtures. The basalt fine asphalt mixtures did not provide satisfactory results with the modified binders used in this study (i.e., 1% Redicote and 3% Solprene).

6.1.2 *Summary of Findings and Conclusions of Chapter 4*

The results of rheological properties of asphalt binders modified with different antioxidants and the mechanical properties of fine asphalt mixtures presented in Chapter 3 were further validated at spectroscopic, chemical and microstructural level using FTIR, GPC and AFM, respectively. The following are the main findings of this advanced analysis.

- The presence of carbonyl content was not found in any of the unaged binders.
- FTIR analysis verified the viability and performance of Redicote and Solprene in retarding oxidative aging by reducing the chemical growth of carbonyl components in the binder.
- From the spectroscopic analysis of field-aged binder, it was evident that the rate of oxidation was higher in wearing course when compared to base course.
- Positive correlation was found between viscosity and carbonyl index in asphalt binder. The carbonyl index increased as the viscosity increased due to binder aging.

- The aromatic index was found higher in the wearing courses of all test sections whereas aliphatic index was lower in wearing courses compared to the base course.
- Long-term aging caused an increase of the percent of large molecules of asphalt binders.
- The chemical analysis using GPC verified the findings of the performance of Redicote and Solprene in retarding aging. Both the chemicals retarded the growth of large molecules when mixed with PG 64-22.
- The microstructural analysis of both laboratory- and field-aged asphalt binders with AFM confirmed that long-term aging induces significant quantitative changes in the different phases (Phases 1, 2 and 3) of asphalt surface.
- Phase 2 or the dispersive phase (brighter region) is associated with higher adhesion and stiffness. The area of Phase 2 increases with aging.
- Asphalt surface roughness is affected by aging. The aging induces more spikiness/sharpness on the asphalt surface as well as increased concentration of bees which are hypothesized as the crack initiation locations.

6.1.3 *Summary of Findings and Conclusions of Chapter 5*

This chapter investigated the effect of aging on the viscoelastic response of asphalt mixture using the Prony series representation and a newly developed parameter called aging state variable *'A'* as an indicator of age-induced viscoelastic response of asphalt mixtures. The dynamic modulus and phase angle data were used to construct master curves, from which the time-temperature shift factors and associated storage and loss compliance were calculated. The Prony coefficients were identified by fitting the experimental storage and loss compliance master curves and the aging state variable 'A' was obtained for each of the mixtures to predict the age-induced viscoelastic response. The main findings of this part are summarized below.

- The aging state variable *'A'* was found to successfully capture the effect of long-term aging temperature and duration on the mechanical properties (i.e., dynamic modulus) of asphalt mixtures.
- The aging state variable '*A'* increased with increase in aging level and temperature thus it can be used an indicator of age-induced viscoelastic response of asphalt mixtures.

6.2 Future Recommendations

- It should be noted that this is a limited study and different antioxidants may show different performance with asphalt binders of different PG grades and crude sources. It is recommended to extend this study to evaluate additional asphalt binders and antioxidant additives.
- The FTIR testing performed in this study was quite extensive. The test was performed on 60 field-aged binder samples and 12 laboratory-aged samples (including both unmodified and antioxidant-modified binders). It is recommended to expand the GPC and AFM analysis and test more asphalt binders aged in the laboratory and extracted from the field.

REFERENCES

Abraham, H., 1960. *Asphalt and Allied Substances*. 6th ed. New York: D. Van Nostrand Company, Inc.

Airey, G.D., Rahimzadeh, B., and Collop, A.C., 2004. Linear Rheological Behavior of Bituminous Paving Materials. *Journal of Materials in Civil Engineering*, 16 (3), 212–220.

Al-Azri, N., Jung, S., Lunsford, K., Ferry, A., Bullin, J., Davison, R., and Glover, C., 2006. Binder Oxidative Aging in Texas Pavements: Hardening Rates, Hardening Susceptibilities, and Impact of Pavement Depth. *Transportation Research Record: Journal of the Transportation Research Board*, 1962, 12–20.

Al-Qadi, I.L., Ozer, H., Lambros, J., Khatib, A. El, Singhvi, P., Khan, T., and Doll, B., 2015. *Testing Protocols to Ensure Performance of High Asphalt Binder Replacement Mixes Using RAP and RAS, Report No. FHWA-ICT-15-017*. Illinois Center for Transportation, Urbana, IL 61801.

Ala, A., Baek, C.C., Eyad, M., and Tom, P., 2002. The influence of laboratory aging method on the rheological properties of Asphalt binders. *Journal of testing and evaluation*, 30 (2), 171–176.

Ali Mansoori, G., 1997. Modeling of asphaltene and other heavy organic depositions. *Journal of Petroleum Science and Engineering*, 17 (1–2), 101–111.

Allen, R.G., 2013. Microstructural Characterization of the Chemo-mechanical Behavior of Asphalt in Terms of Aging and Fatigue Performance Properties. Texas A&M University, College Station.

Allen, R.G., Little, D.N., and Bhasin, A., 2012. Structural Characterization of Micromechanical Properties in Asphalt Using Atomic Force Microscopy. *Journal of Materials in Civil Engineering*, 24 (10), 1317–1327.

Allen, R.G., Little, D.N., Bhasin, A., and Glover, C.J., 2014. The effects of chemical composition on asphalt microstructure and their association to pavement performance. *International Journal of Pavement Engineering*, 15 (1), 9–22.

An Introduction to Gel Permeation Chromatography and Size Exclusion Chromatography, 2016. Agilent Technologies.

Anderson, D.A., Christensen, D.W., Bahia, H.U., Dongre, R., Sharma, M.G., Antle, C.E., and Button, J., 1994. *Binder Characterization and Evaluation. Volume 3: Physical Characterization*. Strategic Highway Research Program, National Research Council, Washington, D. C.

Anderson, R.M., King, G.N., Hanson, D.I., and Blankenship, P.B., 2011. Evaluation of the Relationship between Asphalt Binder Properties and Non-Load Related Cracking. *Asphalt Paving Technology*, 80, 615–663.

Apeagyei, A.K., 2008. Development of Antioxidant Treatments for Asphalt Binders and Mixtures. PhD Dissertation, University of Illinois at Urbana-Champaign, USA.

Apeagyei, A.K., 2011. Laboratory evaluation of antioxidants for asphalt binders. *Construction and Building Materials*, 25 (1), 47–53.

Apeagyei, A.K., Buttlar, W.G., and Dempsey, B.J., 2008. Antioxidant treatment of asphalt binders.

Baek, C., Underwood, S.B., and Kim, Y.R., 2012. Effects of Oxidative Aging on Asphalt Mixture Properties. *Transportation Research Record: Journal of the Transportation Research Board*, 2296, 77–85.

Barth, E.J., 1962. *Asphalt*. Gordon& Breach, New York.

Beitchman, B.D., 1960. Effects of antioxidants on asphalt durability. *JOURNAL OF RESEARCH of the National Bureau of Standards C. - Engineering and Instrumentation*, 64C (1), 13–17.

Bell, C.A., 1989. *Summary Report on Aging of Asphalt-Aggregate Systems. Research Report No. SR-OCU-A-003A-89-2, SHRP-A-305*. Strategic Highway Research Program, National Research Council, Washington, D.C.

Bell, C.A., Kliewer, J.E., and Sosnovke, D.A., 1995. *Investigation of the relationship between field performance and laboratory aging properties of asphalt mixtures*. Engineering properties of asphalt mixtures and the relationship with their performance, ASTM STP 1265. American Society for Testing and Materials, Philadelphia.

Bell, C.A., Wieder, A.J., and Fellin, M.J., 1994. *Laboratory Aging of Asphalt-Aggregate Mixtures: Field Validation, Research Report SHRP-A-390*. Oregon State University, Corvallis.

Blunt, L. and Jiang, X., 2003. *Advanced Techniques for Assessment Surface Topography Development of a Basis for 3D Surface Texture Standards 'SURFSTAND'*. Kogan Page Science.

Bower, N., Wen, H., Wu, S., Willoughby, K., Weston, J., and DeVol, J., 2016. Evaluation of the performance of warm mix asphalt in Washington state. *International Journal of Pavement Engineering*, 17 (5), 423–434.

Branthaver, J.F., 1993. Size Exclusion Chromatography Studies of Aged SHRP Asphalts. *Fuel Science and Technology International*, 11 (1), 123–139.

Christensen, D.W. and Anderson A, D., 1992. Interpretation of dynamic mechanical test data for paving grade asphalt cements (with discussion). *Journal of the Association of Asphalt Paving Technologists*, 61, 67–116.

Christensen, R.M., 1982. Theory of Viscoelasticity. *Journal of Applied Mechanics*, 38 (3), 720.

Cohen, J., 1988. *Statistical power analysis for the behavioral sciences*. 2nd ed. Cambridge, MA: Academic Press.

Cohen, J., 1992. A power primer. *Psychological Bulletin*, 112 (1), 155–159.

Corbett, L.W., 1969. Composition of asphalt based on generic fractionation, using solvent

deasphaltening, elution-adsorption chromatography, and densimetric characterization. *Analytical Chemistry*, 41 (4), 576–579.

Cortizo, M.S., Larsen, D.O., Bianchetto, H., and Alessandrini, J.L., 2004. Effect of the thermal degradation of SBS copolymers during the ageing of modified asphalts. *Polymer Degradation and Stability*, 86 (2), 275–282.

Dealy, J.M., 1979. Rheological properties of oil sand bitumens. *The Canadian Journal of Chemical Engineering*, 57 (6), 677–683.

Dempsey, B., 2006. AOXADUR Antioxidant Treatment for Increasing Service Life of Asphalt Mixtures [online]. Available from: http://otm.illinois.edu/technologies/aoxadur-antioxidant-treatment-increasing-servitf06037 [Accessed 1 Jul 2015].

Derjaguin, B. V., Muller, V.M., and Toporov, Y.P., 1975. Effect of contact deformations on the adhesion of particles. *Journal of Colloid And Interface Science*, 53 (2), 314–326.

Dessouky, S. and Diaz, M., 2015. Improving asphalt mixtures performance by mitigating oxidation using anti-oxidants additives. *In*: I. Karaman, R. Arroyave, and E. Masad, eds. *Proceedings of the TMS Middle East - Mediterranean Materials Congress on Energy and Infrastructure Systems, MEMA 2015*. Doha, Qatar: John Wiley & Sons, Inc., Hoboken, New Jersey, 45–54.

Ding, Y., Huang, B., and Shu, X., 2016. Evaluation of intermolecular interaction between virgin and aged asphalt binders using GPC. *In*: *Functional Pavement Design*. CRC Press, 39.

Dukatz, E.L., Anderson, D.A., and Rosenberger, J.L., 1984. Relationship between Asphalt Flow Properties and Asphalt Composition. *Association of Asphalt Paving Technologists Proceedings*, 53, 160–185.

Farcas, F., 1996. Etude d'une methode de simulation du vieillissement sur route des bitumes.

Fernández-Gómez, W., 2013. A review of asphalt and asphalt mixture aging. *Ingeniería e Investigación*, 33 (1), 5–12.

Ghavibazoo, A., Abdelrahman, M., and Ragab, M., 2015. *Evaluation of oxidization of crumb rubber-modified asphalt during short-term aging*. Transportation Research Record.

Glover, C.J., Davison, R.R., Domke, C.H., Ruan, Y., Juristyarini, P., Knorr, D.B., and H., J.S., 2005. *Development of New Method for Assessing Asphalt Binder Durability with Field Validation, Report FHWA/TX-05/1872-2*. Texas Transportation Institute, College Station, Texas.

Glover, C.J., Martin, E., Chowdhury, A., Han, R., Prapaitrakul, N., Jin, X., and Lawrence, J., 2009. *Evaluation of Binder Aging and Its Influence in Aging of Hot Mix Asphalt Concrete: Literature Review and Experimental Design, Research Report No. FHWA/TX-08/0-6009-1*. Texas Transportation Institute, College Station, Texas.

Gray, M.R., Tykwinski, R.R., Stryker, J.M., and Tan, X., 2011. Supramolecular Assembly Model for Aggregation of Petroleum Asphaltenes. *Energy & Fuels*, 25 (7), 3125–3134.

Griffiths, P.R., 1983. Fourier transform infrared spectrometry. *Science*, 222 (4621), 297–302.

Han, R., 2011. Improvements to a Transport Model of Asphalt Binder Oxidation in Pavements. Texas A&M University.

Hattingh, M.M., 1984. The Fractionation of Asphalt. *Association of Asphalt Paving Technologists Proceedings*, 53, 197–215.

Herrington, P.R. and Ball, G.F.A., 1996. Temperature dependence of asphalt oxidation mechanism. *Fuel*, 75 (9), 1129–1131.

Houston, W.N., Mirza, M.W., Zapata, C.E., and Raghavendra, S., 2005. *Environmental Effects in Pavement Mix and Structural Design Systems, Part 1 of Contractor's Final Report for NCHRP Project 9-23*. Arizona State University, Phoenix, Arizona.

How Molecular Weight Averages are Calculated [online], 2016. *PolyAnalytik*. Available from: www.polyanalytik.com/basic-concepts/how-to-calculate-molecular-weight-and-molecular-weight-distribution/ [Accessed 1 Jan 2016].

Huang, C.W., Masad, E., Muliana, A.H., and Bahia, H., 2007. Nonlinearly viscoelastic analysis of asphalt mixes subjected to shear loading. *Mechanics of Time-Dependent Materials*, 11 (2), 91–110.

Hveem, F.N., Zube, E., and Skog, J., 1959. *Progress Report on the ZACA-Wigmore Experimental Asphalt Test Project*. Symposium on Road and Paving Materials, ASTM International.

Introduction to Fourier Transform Infrared Spectrometry, 2001. Thermo Nicolet Corporation. 5225 Verona Road, Madison, WI 53711-4495, U.S.A.

Jager, A., Lackner, R., Eisenmenger-Sittner, C., and Blab, R., 2004. Identification of Microstructural Components of Bitumen by Means of Atomic Force Microscopy (AFM). *Proceedings in Applied Mathematics and Mechanics*, 4 (1), 400–401.

Jahangir, R., Little, D., and Bhasin, A., 2015. Evolution of asphalt binder microstructure due to tensile loading determined using AFM and image analysis techniques. *International Journal of Pavement Engineering*, 16 (4), 337–349.

Januszke, R.M., 1971. Paving Asphalt Additives in Durability Determination. *Industrial & Engineering Chemistry Product Research and Development*, 10 (2), 209–214.

Jennings, P.W., 1980. *High pressure liquid chromatography as a method of measuring asphalt composition, Publication No. FHWA-MT-7930*. FHWA, U.S. Department of Transportation.

Kandhal, P.S., 1977. Low-Temperature Ductility in Relation to Pavement Performance, STP628. *ASTM International*, 95–106.

Kandhal, P.S. and Chakraborty, S., 1996. Effect of asphalt film thickness on short-and long-term aging of asphalt paving mixtures. *Transportation Research Record: Journal of the Transportation Research Board*, 1535 (1), 83–90.

Kim, K.W. and Burati, J.L., 1993. Use of GPC Chromatograms to Characterize Aged Asphalt Cements. *Journal of Materials in Civil Engineering*, 5 (1), 41–52.

Kim, K.W., Doh, Y.S., and Amerkhanian, S.N., 2004. Evaluation of aging characteristics of selected PMA using HP-GPC. *International Journal of Highway Engineering*, 6 (2), 15–24.

Kim, K.W., Doh, Y.S., and Amirkhanian, S., 2004. Effect of polymers on aging of asphalt binder. *Journal of the Korean Society of Pavement Engineers*, 6 (2), 15–24.

Kim, M., Buttlar, W., Baek, J., and Al-Qadi, I., 2009. Field and Laboratory Evaluation of Fracture Resistance of Illinois Hot-Mix Asphalt Overlay Mixtures. *Transportation Research Record: Journal of the Transportation Research Board*, 2127, 146–154.

Kim, Y.-. R., Allen, D.H., and Little, D.N., 2007. Computational constitutive model for predicting nonlinear viscoelastic damage and fracture failure of asphalt concrete mixtures. *International Journal of Geomechanics*, 7 (2), 102–110.

Kim, Y.R., 2009. *Modeling of Asphalt Concrete*. Modeling of Asphalt Concrete.

Kim, Y.R. and Wen, H., 2002. Fracture energy from indirect tension testing. *Asphalt Paving Technology 2002, March 18, 2002 - March 20, 2002*, 71 (August), 779–793.

King, G., Anderson, M., Hanson, D., and Blankenship, P., 2012. Using Black Space Diagrams to Predict Age-Induced Cracking. *7th RILEM International Conference on Cracking in Pavements*, 453–463.

King, P.L., Ramsey, M.S., McMillan, P.F., and Swayze, G., 2004. Laboratory fourier transform infrared spectroscopy methods for geologic samples. *In*: *Infrared Spectroscopy in Geochemistry, Exploration Geochemistry and Remote Sensing*. 57–91.

Kronenberger, A., 2006. Atomic Force Microscopy - Basics and Applications [online]. *School of Engineering and Science, Duke University*. Available from: https://users.cs.duke.edu/~reif/courses/molcomplectures/MolecularImaging/AFM/Atomic Force Microscopy(AFM) (Kronenberger).pdf.

Lamontagne, J., Dumas, P., Mouillet, V., and Kister, J., 2001. Comparison by Fourier transform infrared (FTIR) spectroscopy of different ageing techniques: Application to road bitumens. *Fuel*, 80 (4), 483–488.

Larsen, D.O., Alessandrini, J.L., Bosch, A., and Cortizo, M.S., 2009. Micro-structural and rheological characteristics of SBS-asphalt blends during their manufacturing. *Construction and Building Materials*, 23 (8), 2769–2774.

Lau, C.K., Lunsford, K.M., Glover, C.J., Davison, R.R., and Bullin, J., 1992. Reaction Rates and Hardening Susceptibilities as Determined from Pressure Oxygen Vessel Aging of Asphalts. *Transportation Research Record*, 1342, 50–57.

Lee, D., 1973. Asphalt durability correlation in Iowa. *Transportation Research Record*, 468, 43–60.

Lee, S.-J., Amirkhanian, S.N., and Kim, K.W., 2009. Laboratory evaluation of the effects of short-term oven aging on asphalt binders in asphalt mixtures using HP-GPC. *Construction and Building Materials*, 23 (9), 3087–3093.

Lee, S.J., Amirkhanian, S.N., Shatanawi, K., and Kim, K.W., 2008. Short-term aging characterization of asphalt binders using gel permeation chromatography and selected Superpave binder tests. *Construction and Building Materials*, 22 (11), 2220–2227.

Leontaritis, K.J. and Ali Mansoori, G., 1988. Asphaltene deposition: a survey of field experiences and research approaches. *Journal of Petroleum Science and Engineering*, 1 (3), 229–239.

Lesueur, D., 2009. The colloidal structure of bitumen: Consequences on the rheology and on the mechanisms of bitumen modification. *Advances in Colloid and Interface Science*.

Lin, F. and Meier, D.J., 1995. A Study of Latex Film Formation by Atomic Force Microscopy. 1. A Comparison of Wet and Dry Conditions. *Langmuir*, 11 (7), 2726–2733.

Liu, C., Pineda, E., and Crespo, D., 2015. Mechanical Relaxation of Metallic Glasses: An Overview of Experimental Data and Theoretical Models. *Metals*, (June), 1074–1111.

Liu, M., Ferry, M. a., Davison, R.R., Glover, C.J., and Bullin, J. a., 1998. Oxygen Uptake As Correlated to Carbonyl Growth in Aged Asphalts and Asphalt Corbett Fractions. *Industrial & Engineering Chemistry Research*, 37 (12), 4669–4674.

Loeber, L., Muller, G., Morel, J., and Sutton, O., 1998. Bitumen in colloid science: a chemical, structural and rheological approach. *Fuel*, 77 (13), 1443–1450.

Loeber, L., Sutton, O., Morel, J., Valleton, J.-M., and Muller, G., 1996. New direct observations of asphalts and asphalt binders by scanning electron microscopy and atomic force microscopy. *Journal of Microscopy*, 182 (1), 32–39.

Lü, J.-M., Lin, P.H., Yao, Q., and Chen, C., 2010. Chemical and molecular mechanisms of antioxidants: experimental approaches and model systems. *Journal of Cellular and Molecular Medicine*, 14 (4), 840–860.

Lu, X. and Isacsson, U., 2002. Effect of ageing on bitumen chemistry and rheology. *Construction and Building Materials*, 16 (1), 15–22.

Marasteanu, M.O. and Anderson, D.A., 1999. Improved model for bitumen rheological characterization. *Proceedings of the Eurobitume Workshop on Performance Related Properties for Bituminous Binders, Luxembourg*, (133), 1–4.

Martin, K.G., 1968. Laboratory Evaluation of Antioxidants for Bitumen. *In*: *Proceedings of the Fourth conference of the Australian Road Research Board*. Vermont South, Victoria, Australia: ARRB Group Limited, 1477–1494.

Masad, E., Castelo Branco, V.T.F., Little, D.N., and Lytton, R., 2006. *An Improved Method for the Dynamic Mechanical Analysis of Fatigue Failure of Sand Asphalt Mixtures, FHWA/473630*. Texas Transportation Institute, College Station, Texas.

Masad, E., Castelo Branco, V.T.F., Little, D.N., and Lytton, R., 2008. A unified method for the analysis of controlled-strain and controlled-stress fatigue testing. *International Journal of Pavement Engineering*, 9 (4), 233–246.

Masson, J.F., Collins, P., and Polomark, G., 2005. Steric hardening and the ordering of asphaltenes in bitumen. *Energy and Fuels*, 19 (1), 120–122.

Masson, J.F., Leblond, V., and Margeson, J., 2006. Bitumen morphologies by phase-detection atomic force microscopy. *Journal of Microscopy*, 221 (1), 17–29.

Mayzo Antioxidants, BNX 1010 Antioxidant and Thermal Stabilizer [online], 2016. Available from: www.mayzo.com/pdf/BNX1010TF.pdf [Accessed 13 Aug 2016].

Mezger, T.G., 2011. *The Rheology Handbook: For Users of Rotational and Oscillatory Rheometers*. 3rd revise. Vincentz Network, Hanover, Germany.

Michalica, P., Kazatchkov, I.B., Stastna, J., and Zanzotto, L., 2008. Relationship between chemical and rheological properties of two asphalts of different origins. *Fuel*, 87 (15–16), 3247–3253.

Mohamed, A.A., 2007. A Study on the Physical and Mechanical Properties of Asphaltic Concrete Incorporating Crumb Rubber Produced through Dry Process. Universiti Sains Malaysia.

Morian, N., Hajj, E.Y., and Sebaaly, P.E., 2013. Significance of Mixture Parameters on Binder Aging in HMA Mixtures. *Transportation Research Record*, 2370, 116–127.

Mortazavi, M. and Moulthrop, J.S., 1993. *SHRP Materials Reference Library, SHRP Report A-646*. National Research Council, Washington, D.C.

Mottahedi, M., Dadalau, A., Hafla, A., and Verl, A., 2011. Numerical Analysis of Relaxation Test Based on Prony Series Material Model. *Integrated Systems, Design and Technology 2010*, 79–91.

NAPA-EAPA, 2011. *The Asphalt Paving Industry: A Global Perspective*. 2nd ed. National Asphalt Pavement Association (NAPA) and Europeanl Asphalt Pavement Association (EAPA).

Ouyang, C., Wang, S., Zhang, Y., and Zhang, Y., 2006a. Improving the aging resistance of styrene-butadiene-styrene tri-block copolymer modified asphalt by addition of antioxidants. *Polymer Degradation and Stability*, 91 (4), 795–804.

Ouyang, C., Wang, S., Zhang, Y., and Zhang, Y., 2006b. Improving the aging resistance of asphalt by addition of Zinc dialkyldithiophosphate. *Fuel*, 85 (7–8), 1060–1066.

Pan, J. and Tarefder, R.A., 2016. Investigation of asphalt aging behaviour due to oxidation using molecular dynamics simulation. *Molecular Simulation*, 42 (8), 667–678.

Pan, T., Sun, L., and Yu, Q., 2012. An atomistic-based chemophysical environment for evaluating asphalt oxidation and antioxidants. *Journal of Molecular Modeling*, 18 (12), 5113–5126.

Park, S.W. and Kim, Y.R., 2001. Fitting Prony-Series Viscoelastic Models with Power-Law Presmoothing. *Journal of Materials in Civil Engineering*, 13 (1), 26–32.

Park, S.W. and Schapery, R.A., 1999. Methods of interconversion between linear viscoelastic material functions. Part I—a numerical method based on Prony series. *International Journal of Solids and Structures*, 36 (11), 1653–1675.

Pauli, A.T., Branthaver, J.F., Robertson, R.E., Grimes, W., and Eggleston, C.M., 2001. Atomic force microscopy investigation of SHRP asphalts. *Prepr. - Am. Chem. Soc., Div. Pet. Chem.*, 46, 104–110.

Pauli, A.T., Grimes, R.W., Beemer, A.G., Turner, T.F., and Branthaver, J.F., 2011. Morphology of asphalts, asphalt fractions and model wax-doped asphalts studied by atomic force microscopy. *International Journal of Pavement Engineering*, 12 (4), 291–309.

Petersen, J.C., 1984a. Chemical Composition of Asphalt as Related to Asphalt Durability : State of the Art. *Transportation Research Record*, (999), 13–30.

Petersen, J.C., 1984b. Chemical Composition of Asphalt as related to Asphalt Durability: State of the Art. *Transportation Research Record*, (999), 13–30.

Petersen, J.C., 2009. *A Review of the Fundamentals of Asphalt Oxidation (E-C140)*. Transportation Research Record: Journal of the Transportation Research Board.

Petersen, J.C., Branthaver, J.F., Robertson, R. E., Harnsberger, P.M., Duvall, J.J., and Ensley, E.K., 1993. Effects of Physicochemical Factors on Asphalt Oxidation Kinetics. *Transportation Research Record*, 1391, 1–10.

Petersen, J.C. and Glaser, R., 2011. Asphalt Oxidation Mechanisms and the Role of Oxidation Products on Age Hardening Revisited. *Road Materials and Pavement Design*, 12 (4), 795–819.

PubChem, 2017. Styrene-butadiene copolymer [online]. Available from: https://pubchem.ncbi.nlm.nih.gov/compound/62697#section=Top [Accessed 19 Oct 2017].

Rahmani, E., Darabi, M.K., Abu Al-Rub, R.K., Kassem, E., Masad, E.A., and Little, D.N., 2013. Effect of confinement pressure on the nonlinear-viscoelastic response of asphalt concrete at high temperatures. *Construction and Building Materials*, 47, 779–788.

Rahmani, E., Darabi, M.K., Little, D.N., and Masad, E.A., 2017. Constitutive modeling of coupled aging-viscoelastic response of asphalt concrete. *Construction and Building Materials*, 131, 1–15.

Reyes, C.M., 2012. Influence of Anti-Oxidant Modifications in Asphalt Binder Phesio-Chemical Properties and Mixes Performance. M.S. Thesis, Department of Civil Engineering, The University of Texas at San Antonio, San Antonio, Texas.

Roberts, F.L., Kandhal, P.S., Brown, E.R., Lee, D.Y., and Kennedy, T.W., 1996. *Hot Mix Asphalt Materials, Mixture Design, and Constrution*. National Asphalt Pavement Association, Research and Education Foundation. Lanham, Maryland: National Asphalt Pavement Association, Research and Education Foundation.

Robertson, R.E., Branthaver, J.F., Plancher, H., Duvall, J.J., Ensley, E.K., Harnsberger, P.M., and Peterson, J.C., 1991. Chemical properties of asphalts and their relationships to pavement performance. *Asphalt Paving Technology: Association of Asphalt Paving Technologists-Proceedings of the Technical Sessions*, 60, 413–436.

Rojas, J.M., Amado, H., and Reyes, F. a, 2012. Efectos de la radiación ultravioleta en asfaltos colombianos. *Rervista científica: Ciencia e Ingenieria*, 15, 96–104.

Rowe, G.M., 2011. Prepared Discussion Following the Anderson AAPT Paper Cited Previously. *Association of Asphalt Paving Technologists*, 80, 649–662.

Rowe, G.M., King, G., and Anderson, M., 2014. The Influence of Binder Rheology on the Cracking of Asphalt Mixes in Airport and Highway Projects. *Journal of Testing and Evaluation*, 42 (5), 1063–1072.

Roylance, D., 2001. *Engineering Viscoelasticity*. Cambridge, MA 02139: Massachusetts Institute of Technology.

Sader, J.E., Chon, J.W.M., and Mulvaney, P., 1999. Normal spring constant calculated using the Sader method [online]. Available from: http://www.ampc.ms.unimelb.edu.au/afm/calibration.html [Accessed 17 Jul 2017].

Said, S., 2005. Aging Effect on Mechanical Characteristics of Bituminous Mixtures. *Transportation Research Record: Journal of the Transportation Research Board*, 1901 (1), 1–9.

Schapery, R., 1969. On the characterization of nonlinear viscoelastic materials. *Polymer Engineering & Science*, 9 (4), 295–310.

Schindelin, J., Rueden, C.T., Hiner, M.C., and Eliceiri, K.W., 2015. The ImageJ ecosystem: An open platform for biomedical image analysis. *Molecular Reproduction and Development*.

Schmidt, U., Hild, S., Ibach, W., and Hollricher, O., 2005. Characterization of thin polymer films on the nanometer scale with confocal Raman AFM. *In*: *Macromolecular Symposia*. 133–143.

Sebaaly, P., Little, D., and Epps, J., 2006. *The benefits of hydrated lime in hot mix asphalt*. National Lime Association, Virginia, USA.

Shea, J.J., 1998. Handbook of Instrumental Techniques for Analytical Chemistry. *IEEE Electrical Insulation Magazine*, 14 (6), 42–42.

Sheng, Z., Baoshan, H., Xiang, S., Jason, M., and Benjamin, B., 2016. Effects of WMA Technologies on Asphalt Binder Blending. *Journal of Materials in Civil Engineering*, 28 (2), 4015106.

Sheng, Z., Benjamin, B., Baoshan, H., and Xiang, S., 2014. Characterizing Rheological Properties of Binder and Blending Efficiency of Asphalt Paving Mixtures Containing RAS through GPC. *Journal of Materials in Civil Engineering*, 26 (5), 941–946.

Sias, D.J. and Richard, K.Y., 2001. Laboratory Evaluation of Fatigue Damage and Healing of Asphalt Mixtures. *Journal of Materials in Civil Engineering*, 13 (6), 434–440.

Siddiqui, M.N. and Ali, M.F., 1999. Investigation of chemical transformations by NMR and GPC during the laboratory aging of Arabian asphalt. *Fuel*, 78 (12), 1407–1416.

Sirin, O., Kassem, E., Paul, D.K., and Khan, M.S., 2018. Laboratory Evaluation and Prony Series Representation of the Effect of Aging on Dynamic Modulus of Asphalt Mixture (Work in progress).

Sirin, O., Paul, D.K., Kassem, E., and Ohiduzzaman, M., 2017a. Effect of ageing on asphalt binders in the State of Qatar: a case study. *Road Materials and Pavement Design*, 1–20.

Sirin, O., Paul, D.K., Kassem, E., and Ohiduzzaman, M., 2017b. Effect of Aging on Asphalt Binders in the State of Qatar: A Case Study (in press). *Association of Asphalt Paving Technologists*.

Standard Test Method for Effect of Heat and Air on a Moving Film of Asphalt (Rolling Thin-Film Oven Test), ASTM D2872, 2012. American Society for Testing and Materials, Annual Book of ASTM Standards, ASTM International, West Conshohocken, PA.

Stuart, B.H., 2004. *Infrared Spectroscopy: Fundamentals and Applications*. John Wiley & Sons.

Swiertz, D., 2010. Asphalt aging characteristics, rheological implications and laboratory techniques. University of Wisconsin-Madison.

Tang, B. and Isacsson, U., 2006. Chemical characterization of oil-based asphalt release agents and their emissions. *Fuel*, 85 (9), 1232–1241.

Thalheimer, W. and Cook, S., 2002. How to calculate effect sizes from published research: A simplified methodology. *Work-Learning Research*, (August), 1–9.

The Power of the Fourier Transform for Spectroscopists [online], 2014. Available from: https://chem.libretexts.org/Core/Physical_and_Theoretical_Chemistry/Spectroscopy/Fundamentals_of_Spectroscopy/The_Power_of_the_Fourier_Transform_for_Spectroscopists.

Traxler, R., 1963. Durability of asphalt cements. *Association of Asphalt Paving Technologist*, 32, 44–63.

Traxler, R.N., 1961. Relation between Asphalt Composition and Hardening by Volatilization and Oxidation. *American Association of Asphalt Paving Technologists Proceedings*, 30, 359–377.

Troy, P., Will, G., Alec, C., and Shin-Che, H., 2014. Adherence Energy of Asphalt Thin Films Measured by Force-Displacement Atomic Force Microscopy. *Journal of Materials in Civil Engineering*, 26 (12).

Vallerga, B.A., 1981. Pavement Deficiencies Related to Asphalt Durability. *Association of Asphalt Paving Technologists*, 50, 481–491.

Wei, B., Shull, J., Lee, Y.-J., and Hawley, M., 1996. Characterization of Asphalt Binders Based on Chemical and Physical Properties. *International Journal of Polymer Analysis and Characterization*, 3, 33–58.

West, P. and Starostina, N., 2009. *AFM Image Artifacts.* Pacific Nanotechnology, Inc., Lot-Oriel Gruppe Europa.

West, P.E., 2006. *Introduction to Atomic Force Microscopy: Theory, Practice, Applications*. Pacific Nanotechnology.

Williams, M.L., Landel, R.F., and Ferry, J.D., 1955. The Temperature Dependence of Relaxation Mechanisms in Amorphous Polymers and Other Glass-forming Liquids. *Journal of the American Chemical Society*, 77 (14), 3701–3707.

Williams, R.C., 2008. *Using Lignin as an Asphalt Antioxidant*. Tech Transfer Summaries. 10. http://lib.dr.iastate.edu/intrans_techtransfer/10.

WITec, 2003a. *Digital Pulse Force Mode AFM, a revolution in Atomic Force Microscopy!* Ulm, Germany.

WITec, 2003b. Digital Pulse Force Mode User Manual. Ulm, Germany.

WITec, 2003c. alpha300 A - Nanoscale Surface Characterization [online]. Available from: http://www.witec.de/products/alpha300-series/alpha300-a/ [Accessed 1 Oct 2017].

Xiao, F., Amirkhanian, S.N., Karakouzian, M., and Khalili, M., 2015. Rheology evaluations of WMA binders using ultraviolet and PAV aging procedures. *Construction and Building Materials*, 79, 56–64.

Xu, T. and Huang, X., 2010. Study on combustion mechanism of asphalt binder by using TG-FTIR technique. *Fuel*, 89 (9), 2185–2190.

Yao, H., Dai, Q., and You, Z., 2015. Fourier Transform Infrared Spectroscopy characterization of aging-related properties of original and nano-modified asphalt binders. *Construction and Building Materials*, 101, 1078–1087.

Yao, H., You, Z., Li, L., Goh, S.W., Lee, C.H., Yap, Y.K., and Shi, X., 2013. Rheological properties and chemical analysis of nanoclay and carbon microfiber modified asphalt with Fourier transform infrared spectroscopy. *Construction and Building Materials*, 38, 327–337.

You, T., Masad, E.A., Al-rub, R.K.A., Kassem, E., and Little, D.N., 2014. Calibration and Validation of a Comprehensive Constitutive Model for Asphalt Mixtures. *Transportation Research Record*, 2447 (2), 13–22.

Zang, L., 2016. Basics of Atomic Force Microscope (AFM) [online]. Available from: www.eng.utah.edu/~lzang/images/Lecture_10_AFM.pdf [Accessed 20 Jun 2012].

Zhang, F., Yu, J., and Han, J., 2011. Effects of thermal oxidative ageing on dynamic viscosity, TG/DTG, DTA and FTIR of SBS- and SBS/sulfur-modified asphalts. *Construction and Building Materials*, 25 (1), 129–137.

Zhang, H.L., Wang, H.C., and Yu, J.Y., 2011. Effect of aging on morphology of organo-montmorillonite modified bitumen by atomic force microscopy. *Journal of Microscopy*, 242 (1), 37–45.